 Copy Nº 20

APAE NO. 54
Supplement 1
AEC Research and
Development Report
UC-81, Reactors - Power
(Special Distribution)

EXTENDED

SM-2 CRITICAL EXPERIMENTS

CE-2

ALCO

ALCO PRODUCTS, INC.
NUCLEAR POWER ENGINEERING DEPARTMENT
P. O. BOX 414, SCHENECTADY 1, N. Y.

DISCLAIMER

APAE No. 54
SUPPLEMENT 1
AEC Research and
Development Report
UC-81, Reactors-Power
(Special Distribution)

EXTENDED SM-2 CRITICAL EXPERIMENTS
CE-2

By

W. J. McCool
R. A. Robinson
S. H. Weiss
T. M. Raby
E. W. Schrader
L. D. Walthousen

Approved by:
W. J. McCool, Supervisor, Critical Facility

Issued: June 30, 1961

Contract No. AT(30-3)-326
with U. S. Atomic Energy Commission
New York Operations Office

ALCO PRODUCTS, INC.
Nuclear Power Engineering Department
Post Office Box 414
Schenectady 1, N.Y.

AEC LEGAL NOTICE

This report was prepared as an account of Government sponsored work. Neither the United States, nor the Commission, nor any person acting on behalf of the commission:

A. Makes any warranty or representation, expressed or implied, with respect to the accuracy, completeness, or usefulness of the information contained in this report, or that the use of any information, apparatus, method, or process disclosed in this report may not infringe privately owned rights: or

B. Assumes any liabilities with respect to the use of, or for damages resulting from the use of any information, apparatus, method, or process disclosed in this report.

As used in the above, "person acting on behalf of the Commission" includes any employee or contractor of the Commission, or employee of such contractor, to the extent that such employee or contractor of the Commission, or employee of such contractor prepares, disseminates, or provides access to, any information pursuant to his employment or contract with the Commission, or his employment with such contractor.

ALCO LEGAL NOTICE

This report was prepared by Alco Products, Incorporated in the course of work under, or in connection with, Contract No. AT(30-3)-326, issued by U.S. Atomic Energy Commission, NYOO; and subject only to the rights of the United States, under the provisions of this contract, Alco Products, Incorporated makes no warranty or representation, express or implied, and shall have no liability with respect to this report or any of its contents or with respect to the use thereof or with respect to whether any such use will infringe the rights of others.

DISTRIBUTION

External Copies

1 - 2 New York Operations Office
U.S. Atomic Energy Commission
376 Hudson Street
New York, 14, New York

Attention: Chief, Army Reactors Staff
Reactor Division

3 - 5 U.S. Atomic Energy Commission
Washington 25, D.C.

Attention: Chief, Water Systems Project
Branch (Army Reactors)
Division of Reactor Development
Mail Station F-311

6 U.S. Atomic Energy Commission
Washington 25, D.C.

Attention: Chief, Evaluation and Planning Branch
Civilian Reactors, Division of
Reactor Development
Mail Station F-311

7 U.S. Atomic Energy Commission
Chief, New York Patent Group
Brookhaven National Laboratory
Upton, New York

Attention: Harman Potter

8 U.S. Atomic Energy Commission
Idaho Operations Office
P.O. Box 2108
Idaho Falls, Idaho

Attention: Director, Division of Military
Reactors

9 U.S. Atomic Energy Commission
Reports and Statistics Branch
Division of Reactor Development
Washington, 25, D.C.

10 - 11 Office of the Chief of Engineers
Department of the Army
Building T-7
Washington, 25, D.C.

Attention: Chief, Projects Branch
Nuclear Power Division

12 - 14 Nuclear Power Field Office
U.S. Army Engineer Reactors Group
Fort Belvoir, Virginia

Attention: Chief, Nuclear Power Field Office

15 Nuclear Power Field Office
U.S. Army Engineer Reactors Group
Fort Belvoir, Virginia

Attention: O.I.C. SM-1

16 Chief, U.S. Army Reactors Group
Fort Greeley, Alaska
APO 733
Seattle, Washington

Attention: O.I.C. SM-1A

17 Chief, USAPR&DC
Thule, Greenland
APO 23
New York, New York

Attention: O.I.C. PM-2A

18 - 20 Office of Technical Information Extension
P.O. Box 62
Oak Ridge, Tennessee

21 Union Carbide Nuclear Corporation
Oak Ridge National Laboratory
Y-12 Building 9704-1
P.O. Box "Y"
Oak Ridge, Tennessee

Attention: A. L. Boch

DISTRIBUTION (CONT'D)

22 The Martin Company
P.O. Box 5042
Middle River, Maryland

Attention: AEC Contract Document Custodian

23 Combustion Engineering, Incorporated
Nuclear Division
Windsor, Connecticut

Attention: Director, Nuclear Division

24 - 25 Alco Products, Inc.
P.O. Box 145
Fort Belvoir, Va.

Attention: W.K. Stromquist

Internal

26	K. Kasschau	40	M.A. Alford
27	J. Gronan	41	S.H. Weiss
28	E.B. Gunyou	42	E.W. Schrader
29	J.G. Gallagher	43	T.M. Raby
30	E.F. Phelps	44	L.D. Walthousen
31	P.E. Bobe	45	S.N. Kemp
32	W.T. Williams	46	A.N. Crouch
33	W.J. McCool	47	K.C. Sontheimer
34	R.A. Robinson	48	R.D. Robertson
35	D.H. Lee	49	P.V. Oby
36	B.E. Fried	50	W.S. Brown
37	J.P. Oggerino	51	R. H. Beam
38	S. Paluszkiewicz	52 - 54	Criticality Facility File
39	E.F. Clancy	55 - 62	NPED File
		63 - 64	Core Analysis File

ABSTRACT

This report contains a description and results of a second series of critical experiments performed on the SM-2 core mockup, as additional to the first series of experiments reported in APAE No. 54. The SM-2 core mockup contains 36.4 kg U-235 and an estimated 67.9 gm B-10. The equivalent diameter and the active height are about 22 in.; the metal-to-water volume ratio is 0.344. Data is presented on activation, reactivity, and stuck rod measurements. All measurements were conducted on the open seven control rod array employing 38 stationary fuel elements.

Activation measurements consisted of neutron flux measurements using uranium fission foils for relative power distribution studies, the effect of flux suppressors on reducing power peaks, blocked coolant channel measurements, and gamma ray dose distribution. Reactivity measurements were performed to determine the effect of flow divider, flux suppressors and simulated high temperature and pressure operation; B-10 loading in the SM-2 core; and core material coefficients. For the latter, the worth in cents per gm or cents per cc was determined at simulated temperature of 510°F for B-10, U-235, stainless steel, and void. Stuck rod measurements were made to obtain an indication of the criticality margin in the event one or more control rods should stick in the operating position.

ACKNOWLEDGEMENT

The authors gratefully acknowledge the contribution of F. L. Hess, Associated Nucleonics, Inc., in preparation of portions of this report.

THIS PAGE

WAS INTENTIONALLY

LEFT BLANK

TABLE OF CONTENTS

		Page
ABSTRACT		vii
SUMMARY		1
INTRODUCTION		3
1.0	SYSTEM DESCRIPTION	5
1.1	Introduction	5
1.2	Experimental Assembly	5
1.2.1	Core Support Assembly	5
1.2.2	Control Rod Assembly	5
1.2.3	Fuel Element Structure	5
1.2.4	Steel Reflector Assembly	6
1.2.5	Flow Divider	6
1.2.6	Neutron Source	6
1.3	Experimental Techniques	6
1.3.1	Reactivity Measurements	6
1.3.2	Boron Loading	7
1.4	Nomenclature and Explanations	7
1.4.1	Active Core	7
1.4.2	Control Rod Withdrawal	7
1.4.3	Control Rod Position	7
1.4.4	Control Rod Array	7
1.4.5	Data Point, Experimental	7
1.4.6	Temperature	7
2.0	REACTIVITY MEASUREMENTS	17
2.1	Introduction	17
2.2	B-10 Loading in the SM-2 Core Mockup from Core Reactivity Measurements	17
2.2.1	Introduction	17
2.2.2	Experimental Procedure and Results	18

TABLE OF CONTENTS (CONT'D)

		Page
2.3	Material Coefficients	25
2.3.1	Introduction	25
2.3.2	Procedure	25
2.3.3	Heterogeneity Effect	25
2.3.4	U-235 Worth	26
2.3.5	B-10 Worth	26
2.3.6	Stainless Steel Worth	30
2.3.7	Void Worth	30
2.4	Reactivity Measurements Using Flow Divider	31
2.5	Suppressor Reactivity	33
2.6	Additional Reactivity Measurements	33
2.6.1	Effect of Mockup Control Rod Suppressors	33
2.6.2	Worth of Side Plates	34
3.0	ACTIVATION MEASUREMENTS	37
3.1	Introduction	37
3.2	Core Mapping	37
3.2.1	Introduction	37
3.2.2	Procedure	37
3.2.3	Nomenclature	38
3.2.4	Data Processing	39
3.2.5	Core Average	39
3.2.6	Experimental Results Employing Laminated Steel Reflectors Without Flow Divider (SM-2 Preliminary Mockup Core)	40
3.2.7	Experimental Results Employing Laminated Steel Reflector, Flow Divider, and Flux Suppressors At the Top of the Active Meat of the Control Rod Fuel Elements (SM-2 Final Mockup Core)	41
3.2.8	Conclusions	91
3.3	Flux Suppressor Measurements	95
3.3.1	Introduction	95
3.3.2	Mockup Suppressors	95
3.3.3	Flux Suppressor Effectiveness	96
3.3.4	Integral Suppressors	96

TABLE OF CONTENTS (CONT'D)

Page

3.4 Blocked Channel Measurements ---------- 96

3.4.1 Introduction ---------- 96
3.4.2 Experimental Method ---------- 105
3.4.3 Water Reflected Core Measurements ---------- 105
3.4.4 Steel Reflected Core Measurements ---------- 105

4.0 MISCELLANEOUS MEASUREMENTS ---------- 115

4.1 Gamma Ray Dose Measurements ---------- 115

4.1.1 Experimental Techniques ---------- 115
4.1.2 Experimental Results ---------- 121

4.2 Seven Rod Bank Calibration at Simulated Elevated Temperature and Pressure ---------- 121

4.2.1 Introduction ---------- 121
4.2.2 Calibration Technique ---------- 121
4.2.3 Simulation of Operating Conditions ---------- 128
4.2.4 Reactivity Change Due to Operation at 510°F and 2000 psi ---------- 133

4.3 Stuck Rod Measurements ---------- 133

REFERENCES ---------- 135

APPENDIX A: Calculation Procedures Used to Determine B-10 Loading - A-1

A.1 Calibration of Standard Tapes ---------- A-1

A.2 Intercalibration of Tapes ---------- A-2

A.3 Intercalibration of SM-2 Mockup Fuel Plates ---------- A-2

A.4 Intercalibration of Elements ---------- A-3

A.5 B-10 Worth Calculation of Assembled Mockup Element ---------- A-4

A.6 Comparison of BMI Reference and Mockup Element ---------- A-4

TABLE OF CONTENTS (CONT'D)

	Page
APPENDIX B: Typical Calculation Procedure for Obtaining the Core Average	B-1
B.1 Experimental Data Obtained Using Preliminary Mockup as an Example	B-1
B.2 Calculation of Average Flux Across Plate "a" in Radial Direction Using Simpson's Rule	B-2
B.3 Calculation of Average Power Along Plate "a" in an Axial Direction	B-3
B.4 Calculation of Cell Average	B-3
B.5 Calculation of Core Average	B-4
B.6 Normalization of Data	B-5
APPENDIX C: Determination of B-10 Content of Boron Tapes	C-1

LIST OF FIGURES

Figure	Title	Page
1.1	Core Support Structure	9
1.2	Cross Section of SM-2 Core Mockup with Stainless Steel Reflector	10
1.3	SM-2 Core in Reactor Tank	11
1.4	Control Rod Assembly	12
1.5	Stationary Fuel Element	13
1.6	Control Rod Fuel Element	14
1.7	Flow Divider Location	15
1.8	Boron Tape Applicator	16
2.1	Heterogeneity Factor, Uranium Worth vs. No. of Stainless Steel Bundles, Element in Position 33	27
2.2	Composite Seven Rod Bank Calibration	35
3.1	Uranium Foil Locations on Element in Position 13	43
3.2	Fuel Plate Arrangement	44
3.3	Location of Radial Planes Without Flow Divider, Section of Core Through Center of Elements in Positions 41, 42, 43 and 44.	45
3.4	Relative Power Distribution in SM-2 Preliminary Mockup Core, Normalized to Core Average	46
3.5	Relative Power Distribution Along Axial Traverse on Centerline of Fuel Plate "j", Elements in Positions 12, 13 and 14, SM-2 Preliminary Mockup Core	60
3.6	Relative Power Distribution Along Axial Traverse on Centerline of Fuel Plate "j", Elements in Positions 21, 22 and 23, SM-2 Preliminary Mockup Core	61
3.7	Relative Power Distribution Along Axial Traverse on Centerline of Fuel Plate "j", Elements in Positions 31, 33 and 34, SM-2 Preliminary Mockup Core	62

LIST OF FIGURES (CONT'D)

Figure	Title	Page
3.8	Relative Power Distribution Along Axial Traverse on Centerline of Fuel Plate "j", Elements in Positions 41, 42 and 43, SM-2 Preliminary Mockup Core	63
3.9	Relative Power Distribution Along Axial Traverse on Centerline of Fuel Plate "i" of Control Rods A, C and F, SM-2 Preliminary Mockup Core	64
3.10	Relative Power Distribution Along Radial Traverse 5 in. Above Bottom of Active Core, SM-2 Preliminary Mockup Core	65
3.11	Relative Power Distribution in the SM-2 Final Mockup Core, Normalized to Core Average	69
3.12	Relative Power Distribution Along Axial Traverse on Centerline of Fuel Plate "j", Elements in Positions 12, 13 and 14, SM-2 Final Mockup Core	85
3.13	Relative Power Distribution Along Axial Traverse on Centerline of Fuel Plate "j", Elements in Positions 21, 22 and 23, SM-2 Final Mockup Core	86
3.14	Relative Power Distribution Along Axial Traverse on Centerline of Fuel Plate "j", Elements in Positions 31, 33 and 34, SM-2 Final Mockup Core	87
3.15	Relative Power Distribution Along Axial Traverse on Centerline of Fuel Plate "j", Elements in Positions 41, 42 and 43, SM-2 Final Mockup Core	88
3.16	Relative Power Distribution Along Axial Traverse on Centerline of Fuel Plate "i" of Control Rods A, C and F, SM-2 Final Mockup Core	89
3.17	Relative Power Distribution Along Radial Traverse 5 in. Above Bottom of Active Core, SM-2 Final Mockup Core	90
3.18	Relative Power Distribution Along Axial Traverse on Centerline of Fuel Plate "i", of Control Rod C, SM-2 Preliminary and Final Mockup Cores	93
3.19	Relative Power Distribution Along Radial Traverse at Top of the Active Core of Fuel Plate "i" of Control Rods A, C and F, SM-2 Preliminary and Final Mockup Cores	94

LIST OF FIGURES (CONT'D)

Figure	Title	Page
3.20	Relative Power Distribution Along Axial Traverse of Fuel Plate "j", Element in Position 41 Using Flux Suppressors, SM-2 Preliminary Mockup Core	101
3.21	Relative Power Distribution Along Axial Traverse of Fuel Plate "j", Element in Position 42 Using Flux Suppressors, SM-2 Preliminary Mockup Core	102
3.22	Relative Power Distribution Along Axial Traverse of Fuel Plate "j", Element in Position 43 Using Flux Suppressors, SM-2 Preliminary Mockup Core	103
3.23	Relative Power Distribution Along Axial Traverse at 1.78 in. W.R.P. of Fuel Plate "r", Element in Position 43 Using Flux Suppressors, SM-2 Preliminary Mockup Core	104
3.24	Thermocouple Plate, SM-2 Critical Facility Test	111
3.25	Blocked Channel Filler Position and Normal Fuel Plate Array	112
3.26	Relative Power Distribution Along Axial Traverse on Centerline of Fuel Plates "i" and "j" Blocked Channel Measurements made in SM-2 Core Mockup with Water Reflector, Without Flow Divider	113
3.27	Relative Power Distribution Along Axial Traverse on Centerline Between Fuel Plates "i" and "j", Elements in Positions 42 and 46, Blocked Channel Measurements Made in SM-2 Core Mockup with Steel Reflector Without Flow Divider	114
4.1	Location of Film Badges on Fuel Elements and Steel Reflector for Gamma Ray Dose Measurements	117
4.2	Location of Film Badges on Core Support Plate for Gamma Ray Dose Measurements	118
4.3	Gamma Ray Dose Measurements, SM-2 Preliminary Mockup Core	123
4.4	Gamma Ray Dose Measurements, SM-2 Preliminary Mockup Core	124

LIST OF FIGURES (CONT'D)

Figure	Title	Page
4.5	Gamma Ray Dose Measurements, SM-2 Preliminary Mockup Core	125
4.6	Seven Rod Bank Calibration Curve at Simulated 510°F and 2000 psi Conditions, SM-2 Mockup Core with Steel Reflector and Flow Divider	129
4.7	Density of Water vs. Temperature at 2000 psi	130
4.8	No. of Aluminum Strips per Fuel Element Required to Simulate Operating Temperature of the SM-2 Reactor at 2000 psi	131
4.9	Composite Seven Rod Bank Calibration Showing Calibration at 2000 psi and 510°F	132
A.1	Control Rod E Calibration Curve	A-5
A.2	B-10 Worth of Standards in Element Position 22 Plate "i"	A-6
A.3	Log N Slope vs. Reactivity	A-7
B.1	Relative Power Distribution of Average Radial Power for Plate "a", Element in Position 12	B-7

LIST OF TABLES

Table	Title	Page
2.1	B-10 Loading of Intercalibrated Tapes Tested in Element Position 22, Fuel Plate "i"	20
2.2	B-10 Loading of 18 Intercalibrated Fuel Plates Tested in Element Position 22, Plate Position "i"	22
2.3	B-10 Loading of 10 Intercalibrated SM-2 Mockup Fuel Elements Tested in Element Position 22	23
2.4	U-235 Reactivity Coefficients	29
2.5	B-10 Reactivity Coefficients	29
2.6	Stainless Steel Reactivity Coefficients (Effect of Water Displacement Not Included)	30
2.7	Void Reactivity Coefficients	31
2.8	Reactivity Measurements Evaluating the Installation of Flow Divider	32
3.1	Relative Power Distribution Along Axial Traverses for Element in Position 12, SM-2 Preliminary Mockup Core	47
3.2	Relative Power Distribution Along Axial Traverses for Element in Position 13, SM-2 Preliminary Mockup Core	48
3.3	Relative Power Distribution Along Axial Traverse for Element in Position 14, SM-2 Preliminary Mockup Core	49
3.4	Relative Power Distribution Along Axial Traverse for Element in Position 21, SM-2 Preliminary Mockup Core	50
3.5	Relative Power Distribution Along Axial Traverses for Element in Position 22, SM-2 Preliminary Mockup Core	51
3.6	Relative Power Distribution Along Axial Traverses for Element in Position 23, SM-2 Preliminary Mockup Core	52
3.7	Relative Power Distribution Along Axial Traverses for Element in Position 31, SM-2 Preliminary Mockup Core	53
3.8	Relative Power Distribution Along Axial Traverses for Element in Position 33, SM-2 Preliminary Mockup Core	54

LIST OF TABLES (CONT'D)

Table	Title	Page
3.9	Relative Power Distribution Along Axial Traverses for Element in Position 34, SM-2 Preliminary Mockup Core	55
3.10	Relative Power Distribution Along Axial Traverses for Element in Position 41, SM-2 Preliminary Mockup Core	55
3.11	Relative Power Distribution Along Axial Traverses for Element in Position 42, SM-2 Preliminary Mockup Core	56
3.12	Relative Power Distribution Along Axial Traverses for Element in Position 43, SM-2 Preliminary Mockup Core	56
3.13	Relative Power Distribution Along Axial Traverses for Element in Position 24 (Control Rod A), SM-2 Preliminary Mockup Core	57
3.14	Relative Power Distribution Along Axial Traverses for Element in Position 44 (Control Rod C), SM-2 Preliminary Mockup Core	58
3.15	Relative Power Distribution Along Axial Traverses for Element in Position 32 (Control Rod F), SM-2 Preliminary Mockup Core	59
3.16	Relative Power Distribution Along Axial Traverses for Element in Position 12, SM-2 Final Mockup Core	70
3.17	Relative Power Distribution Along Axial Traverses for Element in Position 13, SM-2 Final Mockup Core	71
3.18	Relative Power Distribution Along Axial Traverses for Element in Position 14, SM-2 Final Mockup Core	72
3.19	Relative Power Distribution Along Axial Traverses for Element in Position 21, SM-2 Final Mockup Core	73
3.20	Relative Power Distribution Along Axial Traverses for Element in Position 22, SM-2 Final Mockup Core	74
3.21	Relative Power Distribution Along Axial Traverses for Element in Position 23, SM-2 Final Mockup Core	75
3.22	Relative Power Distribution Along Axial Traverses for Element in Position 31, SM-2 Final Mockup Core	76

LIST OF TABLES (CONT'D)

Table	Title	Page
3.23	Relative Power Distribution Along Axial Traverses for Element in Position 33, SM-2 Final Mockup Core	77
3.24	Relative Power Distribution Along Axial Traverses for Element in Position 34, SM-2 Final Mockup Core	78
3.25	Relative Power Distribution Along Axial Traverses for Element in Position 41, SM-2 Final Mockup Core	79
3.26	Relative Power Distribution Along Axial Traverses for Element in Position 42, SM-2 Final Mockup Core	80
3.27	Relative Power Distribution Along Axial Traverses for Element in Position 43, SM-2 Final Mockup Core	81
3.28	Relative Power Distribution Along Axial Traverses for Element in Position 24 (Control Rod A), SM-2 Final Mockup Core	82
3.29	Relative Power Distribution Along Axial Traverses for Element in Position 44 (Control Rod C), SM-2 Final Mockup Core	83
3.30	Relative Power Distribution Along Axial Traverses for Element in Position 32 (Control Rod F), SM-2 Final Mockup Core	84
3.31	Relative Power Distribution Along Axial Traverses for Element in Position 41, SM-2 Preliminary Mockup Core with Suppressor Mockups	97
3.32	Relative Power Distribution Along Axial Traverses for Element in Position 42, SM-2 Preliminary Mockup Core With Suppressor Mockups	98
3.33	Relative Power Distribution Along Axial Traverses for Element in Position 43, SM-2 Preliminary Mockup Core with Suppressor Mockups	99
3.34	Relative Power Distribution Along Axial Traverses for Element in Position 43, SM-2 Preliminary Mockup with Integral Suppressors in Element Position 43	100

LIST OF TABLES (CONT'D)

Table	Title	Page
3.35	Relative Power Distribution Along Axial Traverses for Element in Position 42, Blocked Channel Measurements, SM-2 Mockup Core with Water Reflector, Without Flow Divider	107
3.36	Relative Power Distribution Along Axial Traverses for Element in Position 42, Blocked Channel Measurements, SM-2 Preliminary Mockup Core	108
3.37	Relative Power Distribution Along Axial Traverses for Element in Position 46, Clear Channel Measurements, SM-2 Preliminary Mockup Core	108
3.38	Ratios of Clear Channel to Blocked Channel, Relative Power Measurements for Elements in Positions 46 and 42, SM-2 Preliminary Mockup Core	109
4.1	Gamma Ray Dose Measurements and Film Badge Locations	119
4.2	Gamma Ray Dose Measurements and Film Badge Locations	120
4.3	Calibration of Control Rod Bank Under Simulated Operating Conditions of 2000 psi and 510°F	127
4.4	Critical Rod Configurations	133
B.1	Experimental Foil Activation Data for Element 12	B-1
B.2	Data for Obtaining the Average Power of the SM-2 Preliminary Mockup Core	B-4
C.1	B-10 Analysis	C-1

SUMMARY

A second series of critical experiments were performed on the final SM-2 mockup core to provide additional key data to that reported in APAE No. 54.* Measurements consisted of:

A. REACTIVITY MEASUREMENTS

The SM-2 mockup core contains an estimated 67.9 gm of B-10 distributed uniformly, averaging 1.552 gm per stationary fuel element and 1.282 gm per control rod fuel element.

Core material coefficients were determined at simulated temperature of 510°F attained by inserting strips of aluminum between the fuel plates. The estimated average worths of materials in the core were 0.131 cents/gm for U-235, 3.49 cents/gm for B-10, 0.0276 cents/cc for stainless steel and 0.0509 cents/cc for void.

The use of mockup flux suppressors at the bottom of the stationary fuel elements produced estimated reactivity changes for the entire core of -236 cents and -241 cents for 1/2-in. and 3/4-in. wide suppressors, respectively. The placing of 1/2-in. wide mockup flux suppressors above the active meat of the fuel plates of the seven control rod fuel elements produced a negative reactivity change of 116.1 cents; the placing of these suppressors at the top of the active meat increased the negative reactivity change by 38.9 cents to 155.0 cents.

Reactivity measurements conducted with a flow divider show a core reactivity loss of 165 cents when the flow divider is installed with stainless steel support plates; a loss of 143 cents results when it is attached to the reflector by support pins.

B. ACTIVATION MEASUREMENTS

The relative power distribution for two SM-2 mockup cores was obtained by foil activation. One mockup employed a laminated steel reflector without flow divider; the other employed a laminated steel reflector, flow divider, and flux suppressors at top of the active meat of control rod fuel elements. In each case an extensive number of data points (approximately 1700) were taken and reported for one quadrant of the core permitting the determination of an accurate core average and a detailed description of local effects.

* Noaks, J.W., et al, "SM-2 Critical Experiments - CE-1," APAE No. 54, November 30, 1959.

For both mockups the highest power density was in the region surrounding the center of the core; the lowest along the outer ring of elements. Power peaks occurred in stationary fuel elements at the bottom of the active core and about 5-7 in. above the bottom of the active core, near the critical bank position. In control rod fuel elements without flux suppressors the power exhibited a small gradual increase until near the critical bank position when a very sharp rise occurred, due to the water gap between the absorber and control rod fuel element sections. The addition of flux suppressors to the top of the control rod fuel element sections eliminated this power spike and produced a noticeable reduction in power generation in the region of the interface between the suppressors and the meat. Other power spikes normally occurring at the bottom of the active core and at the radial core-reflector interface were effectively eliminated by placing flux suppressors at the bottom of stationary elements and a thick laminated steel reflector radially around the core. Peak power generation in the final mockup core was 4.6 times the core average and occurred within the central control rod fuel section. The minimum power generation of 0.1 of the core average occurred in element 21 at the edge of the core.

Blocked channel measurements were made to determine the effects on local power generation that result from blocking a fuel element coolant channel with various filler materials for purposes of in-core instrumentation. Results indicate that a coolant channel blocked with stainless steel or aluminum produces a slight flux suppressing effect. The aluminum was used as a mockup substitute for zirconium.

C. MISCELLANEOUS MEASUREMENTS

Gamma ray dose measurements indicate that the center of the core support plate will receive a gamma dose about 0.26 of the maximum of 7.8 R/hr/watt received by the steel reflector; the top and bottom of the fuel elements receive about the same amount of gamma radiation.

Simulation of SM-2 operating conditions (2000 psi and 510°F) resulted in a 4.747 in. increase in the seven rod critical bank position from 8.725 in. to 13.472 in. and a corresponding shift in the calibration curve, with a core reactivity loss of about 7.7 dollars compared to measurements under room conditions.

Stuck rod measurements demonstrated that the reactor will remain subcritical upon full withdrawal of any two rods and certain three and four rod combinations. Criticality positions for other conditions were tabulated and reported.

INTRODUCTION

The experiments described in this report were performed as part of the SM-2 core and vessel development program under AEC Contract No. AT(30-3)-326. These experiments were performed on mockups of the SM-2 core for the purpose of investigating the power distribution and control characteristics of the reactor, and to determine the core reactivity and power distribution effects that result from design modifications and/or additions such as reflectors, flow dividers and flux suppressors.

This report includes the balance of the experimental work performed since publication of APAE No. 54, CE-1[1] and concludes the currently planned program on the SM-2 core. The experiments described include foil activation measurements for determination of relative power distribution in the core. Data is presented on element mapping, effect of flux suppressors, and blocked channel measurements. In addition, reactivity measurements were made to determine the burnable poison loading in the SM-2 fuel elements and to evaluate material coefficients in the core. Survey measurements on relative gamma flux and critical rod configurations are also reported.

Where possible all data is presented in both graphical and tabular form. All measurements were conducted at the Alco Products, Inc. Criticality Facility employing an open control rod array consisting of seven control rod assemblies and 38 stationary fuel elements.

THIS PAGE

WAS INTENTIONALLY

LEFT BLANK

1.0 SYSTEM DESCRIPTION

1.1 INTRODUCTION

A detailed description of the experimental assembly and its relationship to this Facility[2] is presented in the Hazards Summary Report for the SM-2 Critical Experiments[3] and the Hazards Summary Report on the Zero Power Experiments for the Army Package Power Reactor.[4]

The content of this chapter includes a general description of the experimental techniques and core assembly, and a definition of the system nomenclature used, to facilitate interpretation of the balance of the report.

1.2 EXPERIMENTAL ASSEMBLY

1.2.1 Core Support Assembly

The core support assembly consists of a three-tiered stainless steel table located over the center of the reactor tank floor at the Facility. Structural support, alignment and position of the assembly are assured by tie rods and spacers as shown in Fig. 1.1.

The core support has the potential of accommodating reactor cores with a total of 89 fuel elements and control rods, however, a maximum of 38 stationary fuel elements and seven control rod assemblies were utilized in the SM-2 tests. The elements were arranged in a 7 x 7 lattice utilizing an open seven control rod array as shown in Fig. 1.2. Figure 1.3 illustrates the SM-2 core mockup, in place in the reactor tank, with a stainless steel reflector and with associated nuclear instrumentation.

1.2.2 Control Rod Assembly

Reactor control is maintained by the insertion and withdrawal of control rod assemblies which contain both nuclear fuel and box type boron absorbers in a stainless steel basket, Fig. 1.4. The control rod assemblies are driven by overhead drives and drop by gravity on scram. Guide rods and dashpot plungers to act as guides and decelerative devices respectively, are attached to the bottom of the control rod baskets.

1.2.3 Fuel Element Structure

Stationary fuel elements contain up to 18 stainless steel-UO_2 matrix fuel plates, each loaded with 46.3 gm U-235. Control rod fuel elements contain up to 16 similar fuel plates, each loaded with 42.2 gm U-235. The individual fuel

plates are composed of 26.5 w/o uranium oxide held in a 0.030-in. thick matrix of stainless steel and clad with 0.005-in. of stainless steel.

Flexibility of number and distribution of fuel plates in both stationary and control rod fuel elements is provided by extruded polystyrene grooves which hold the fuel plates erect and maintain a center-to-center fuel plate spacing of 0.163-in. Figures 1.5 and 1.6 show a stationary fuel element and control rod fuel element in the partially assembled state. The complete specifications for stationary fuel element, control rod fuel element, and absorber sections are reported in APAE No. 54.[1]

1.2.4 Steel Reflector Assembly

The reflector assembly consists of a number of 1/2-in. stainless steel sheets along the reactor sides and triangular bars along the corners (Fig. 1.1). Laminations of steel and water were obtained with the use of plexiglas spacers.

1.2.5 Flow Divider

The mockup flow divider is a 1/8-in. thick stainless steel plate inserted between the outer two rings of fuel elements, Fig. 1.7.

1.2.6 Neutron Source

A neutron source of encapsulated plutonium-beryllium with an emission rate of 8×10^6 neutrons/sec is used during reactor operation at the Critical Facility. The source is inserted into and withdrawn from the reactor by means of a friction drive acting through an attached 1/4-in. rod.

1.3 EXPERIMENTAL TECHNIQUES

1.3.1 Reactivity Measurements

All reactivity measurements were taken by measuring the difference in control rod position to achieve criticality between some reference condition and the condition under investigation. In order to establish the worth of moving a single rod or bank, it was necessary to obtain a series of rod or bank calibrations by the period method. The time rate of change on the log N trace gives an indication of the reactor period which in turn is related to the change in reactivity through the in-hour formula. A relationship between the angle of the trace taken during a reactor period measurement and the corresponding reactivity change in cents is given in Fig. A.3. The rod worth obtained from a specific period measurement is derived from Fig. A.3 by dividing the reactivity change, in cents, by the difference in rod motion, in inches. Control rod or bank worth measurements were obtained at different rod or bank positions in order to establish a calibration curve such as shown in Fig. A.1; for increased accuracy a least square fitting was obtained using an IBM-650 computer. Thus it is possible

to obtain the total worth of a given reactivity measurement by obtaining the difference in the critical position of a calibrated control rod or bank.

1.3.2 Boron Loading

The SM-2 mockup fuel elements were loaded with boron impregnated tape cut into strips to fit over the uranium matrix of a fuel plate. The tapes are sections of adhesive-backed Mylar film loaded with boron carbide, of approximately 1-3 micron particle size, dispersed in ferrous oxide, thereby providing an ideal method of adding controlled amounts of B-10 to fuel plate surfaces. These boron strips were applied by means of a simple wringer type tape dispenser shown in Fig. 1.8.

1.4 NOMENCLATURE AND EXPLANATIONS

1.4.1 Active Core

That region defined by the upper and lower average limits of the U-235 distributions in the stationary fuel elements and the cell boundaries of the outer row of stationary elements.

1.4.2 Control Rod Withdrawal

Refers to the withdrawal of the absorber section of the control rod from the active core and the consequent simultaneous insertion of fuel.

1.4.3 Control Rod Position

Control rod positions are reported as the distance withdrawn from the position of deepest insertion measured in inches. Deepest insertion represents the nominal alignment of the bottom of the active core with the top limit of the U-235 distribution in the control rod fuel element, or the top limit of the flux suppressor if one is used. Bank positions result from the average position of the individual rods comprising the bank.

1.4.4 Control Rod Array

The open seven rod array referred to in this report is illustrated in Fig. 1.2.

1.4.5 Data Point, Experimental

All experimental data points are plotted as a point (circled, squared or other). Points derived from experimental data by cross plot or integration are represented by crosses.

1.4.6 Temperature

Unless otherwise noted, all measurements were taken at $68^{\circ}F$.

THIS PAGE

WAS INTENTIONALLY

LEFT BLANK

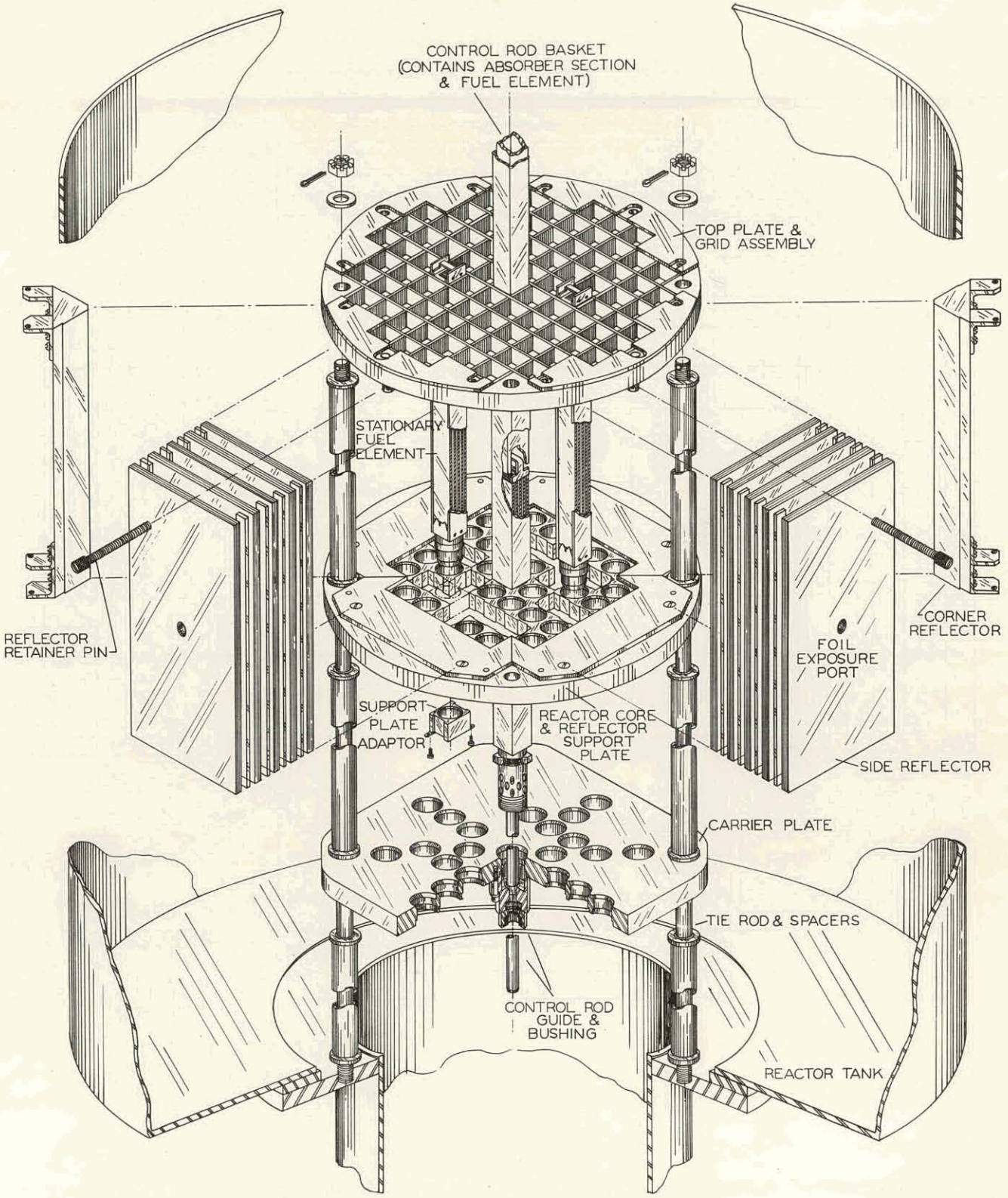

Figure 1.1 Core Support Structure

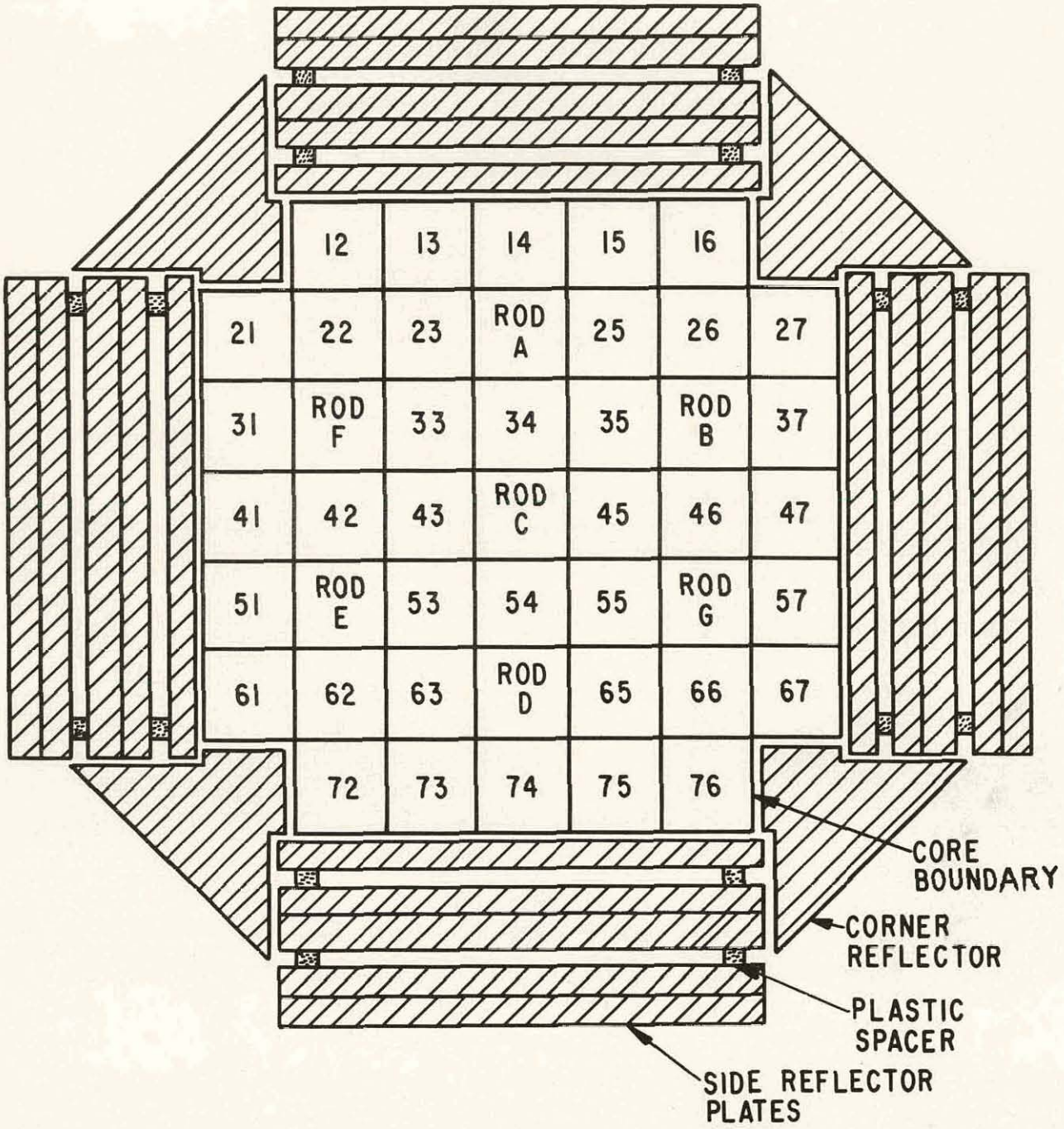

Figure 1.2 Cross Section of SM-2 Core Mockup with Stainless Steel Reflector

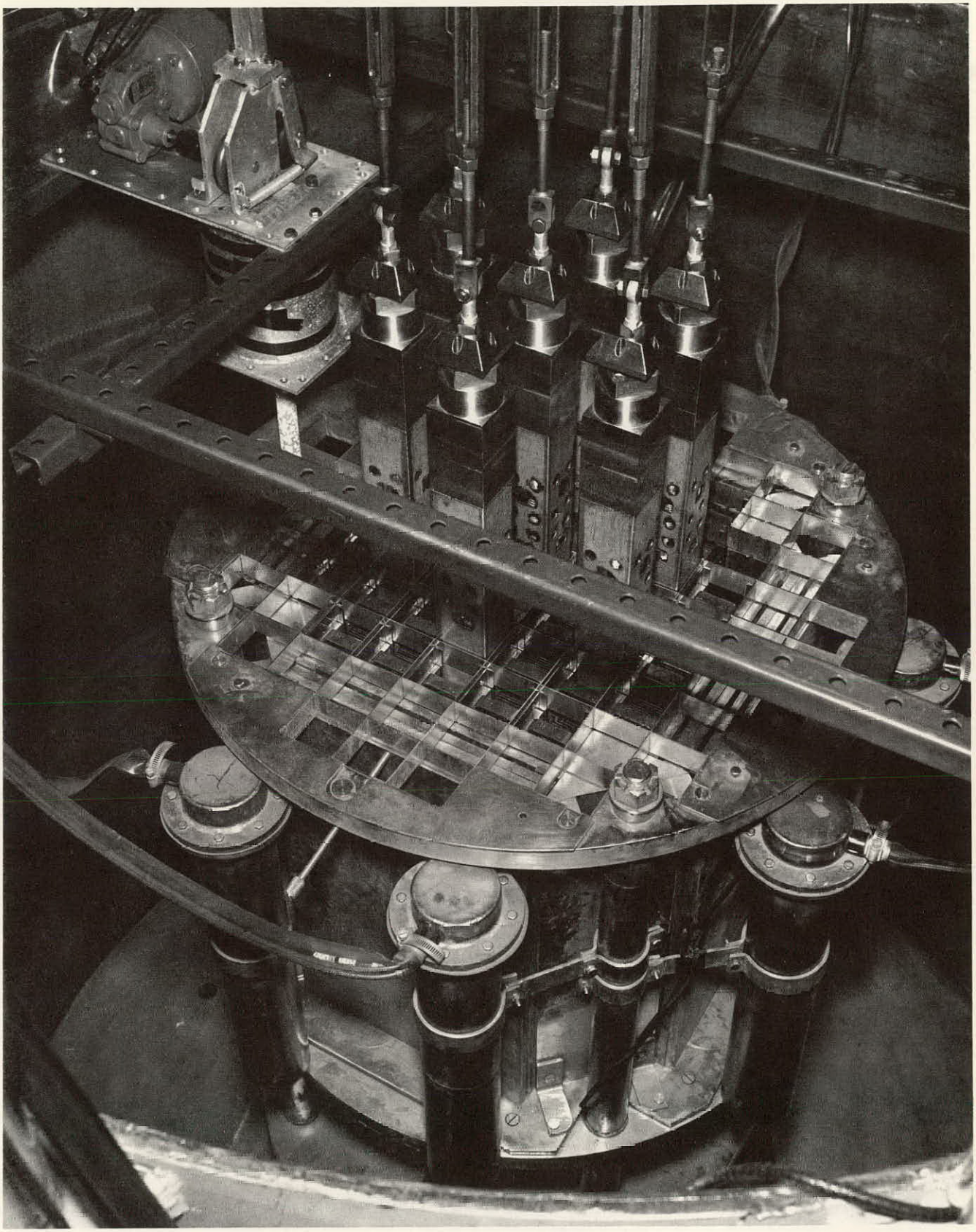

Figure 1.3 SM-2 Core in Reactor Tank

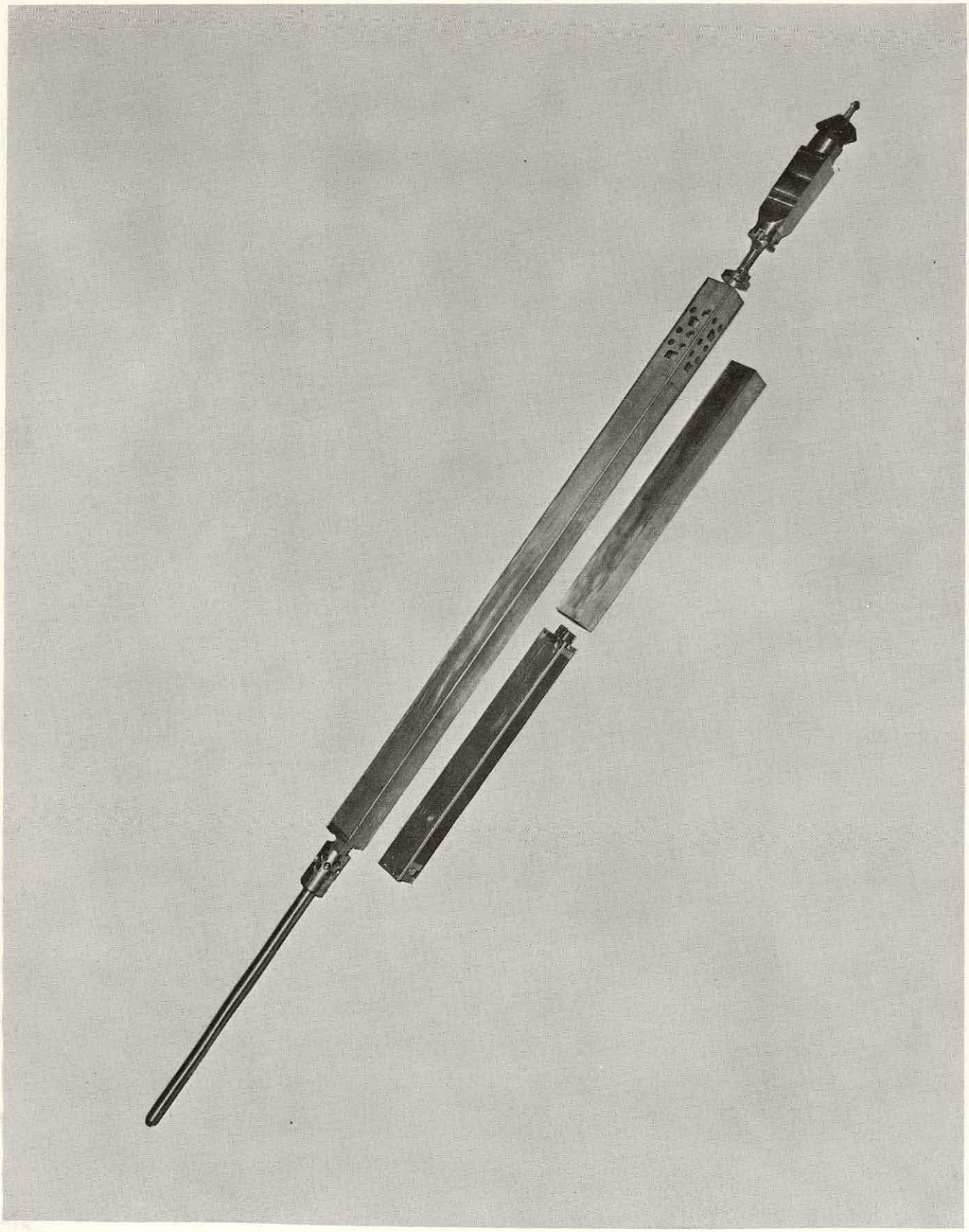

Figure 1.4 Control Rod Assembly

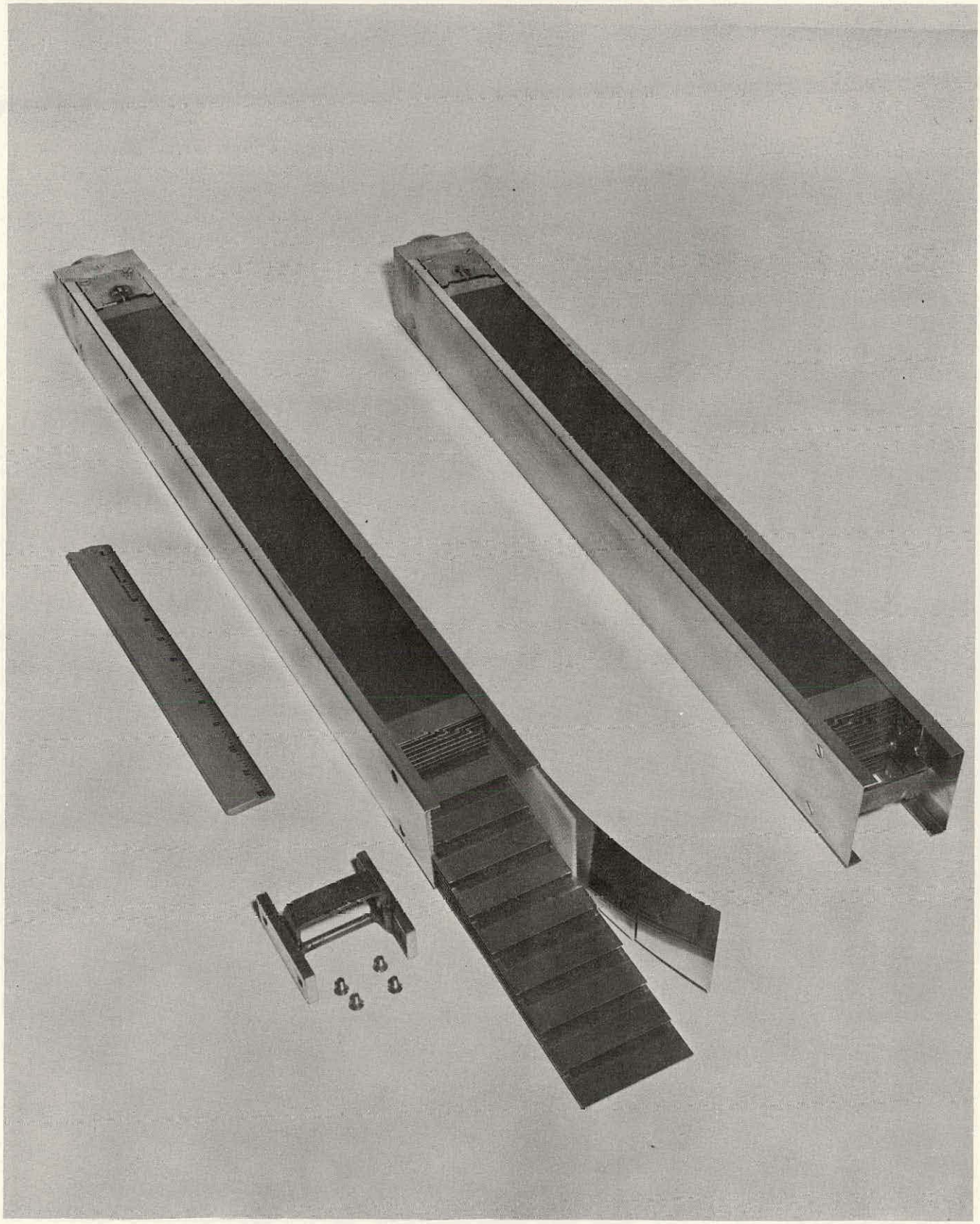

Figure 1.5 Stationary Fuel Element

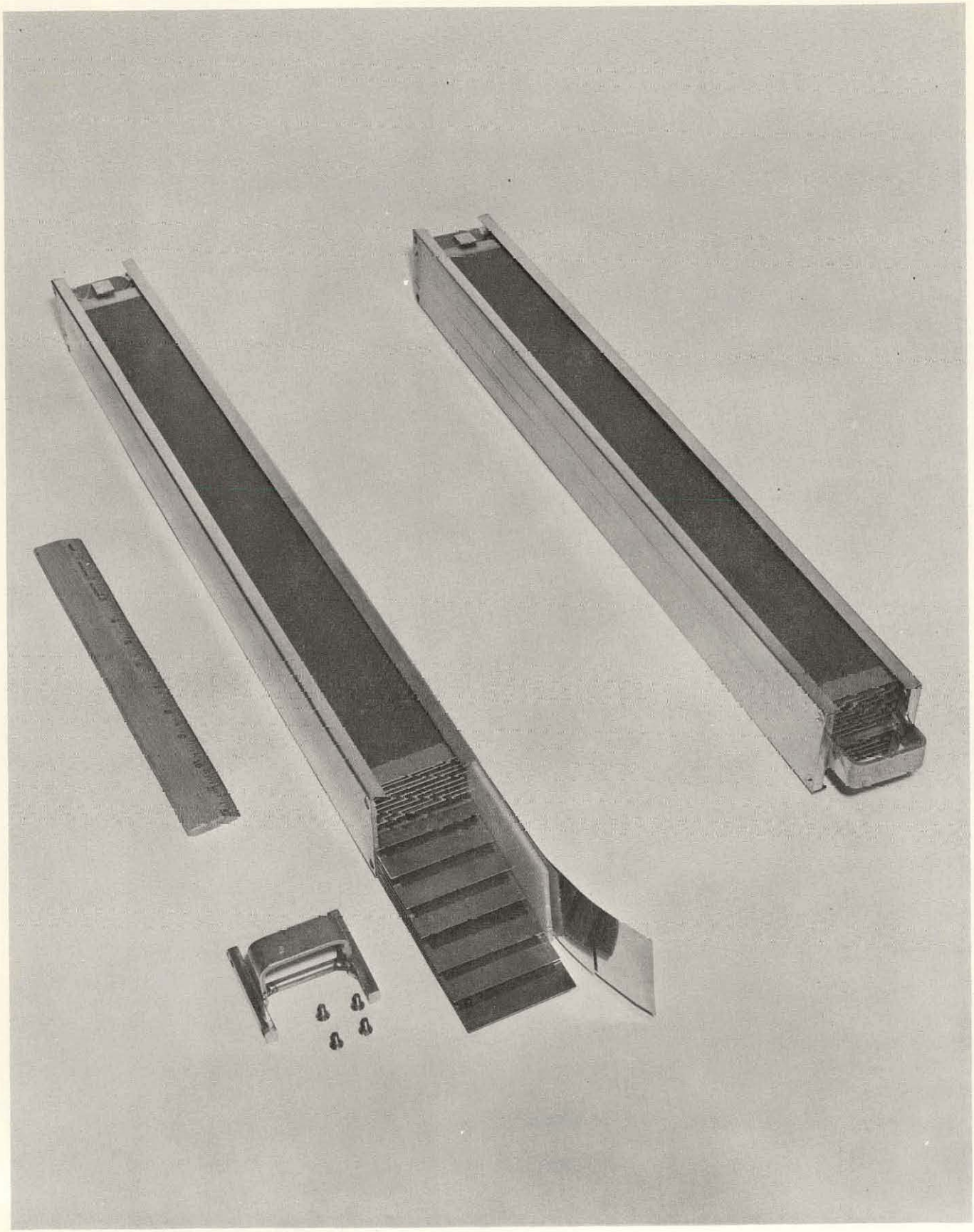

Figure 1.6 Control Rod Fuel Element

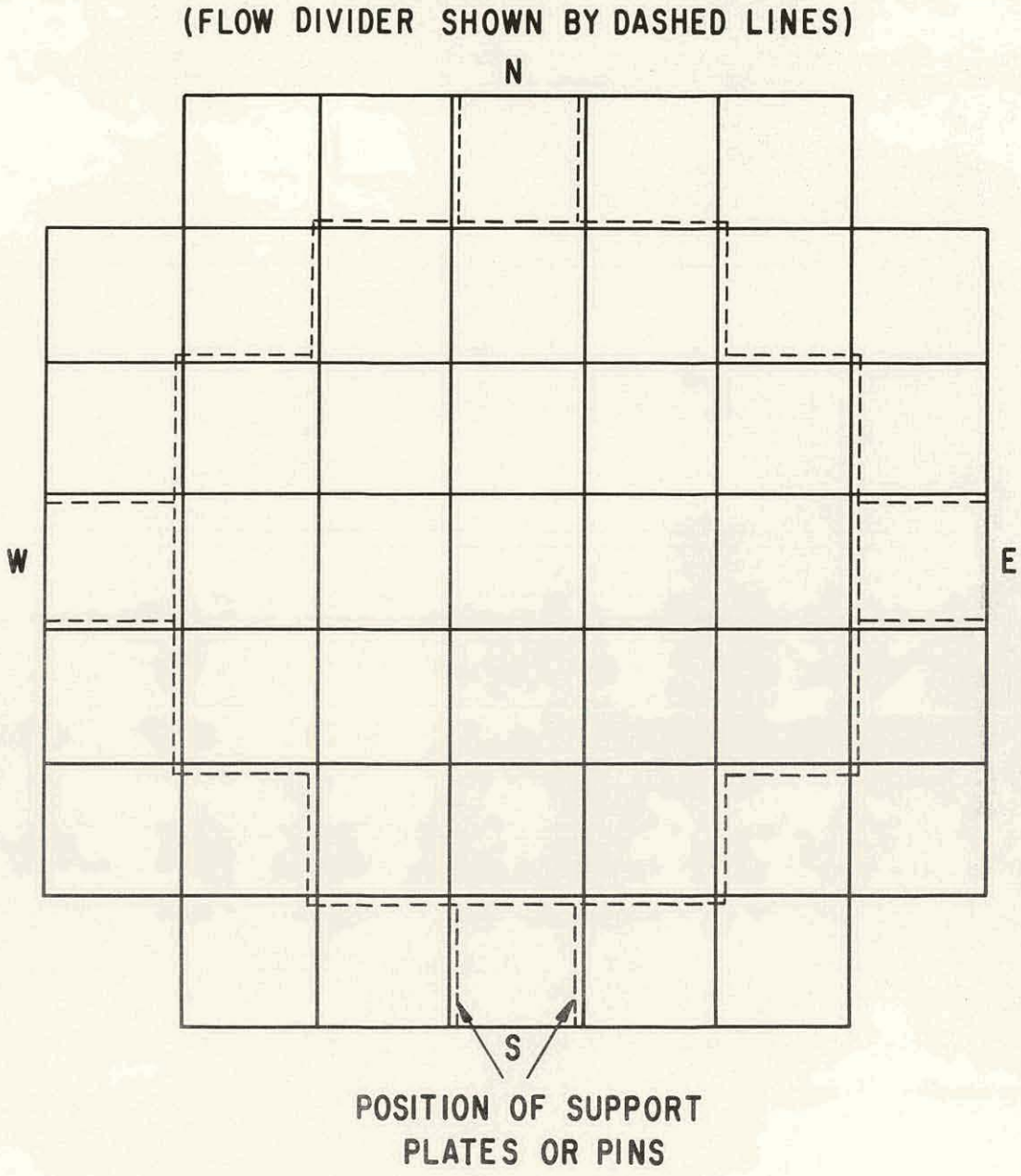

Figure 1.7 Flow Divider Location

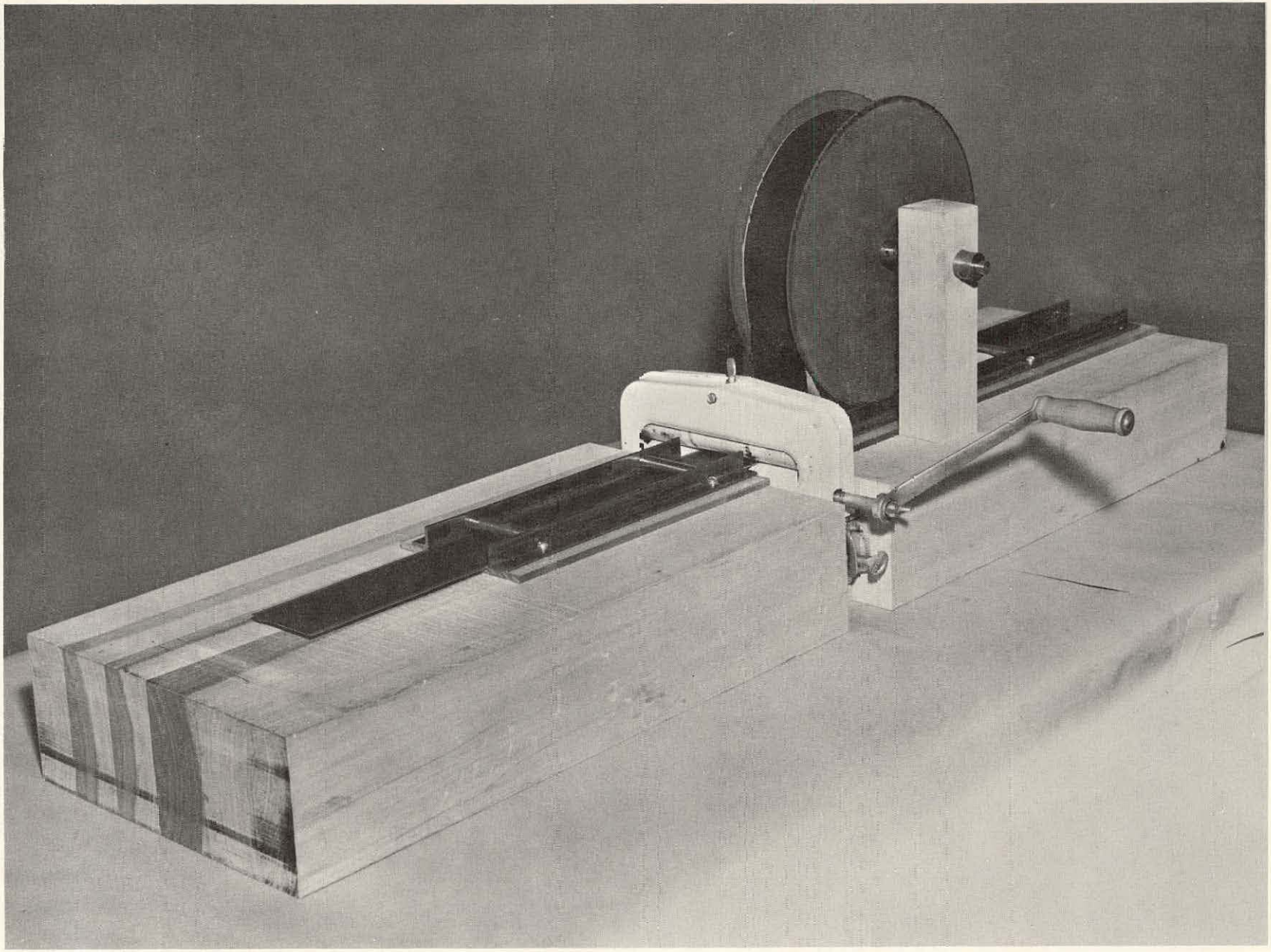

Figure 1.8 Boron Tape Applicator

2.0 REACTIVITY MEASUREMENTS

2.1 INTRODUCTION

In order to properly evaluate the effects on SM-2 core reactivity resulting from subsequent small changes in the core design or specifications, certain reactivity measurements were performed using the SM-2 core mockup. A detailed description of the core and individual fuel element compositions are provided in APAE No. 54,[1] Appendix A, reference loading number 53.

Using the SM-2 core mockup, reactivity measurements were performed under both room temperature and simulated SM-2 operating temperature conditions of 510°F. Reactivity measurements performed under room temperature conditions included: (1) B-10 loading determinations in selected fuel plates and fully assembled SM-2 mockup fuel elements, (2) reactivity comparisons between SM-2 mockup fuel plates and actual first-run SM-2 fuel plates, (3) reactivity worth of flux suppressors, (4) flow divider worth, and (5) worth of fuel element side plates. Reactivity measurements under simulated conditions of operating temperature included worth measurements for B-10, U-235, stainless steel, and voids.

In general these reactivity worth measurements for various materials were obtained for small variations in core materials about the final SM-2 core design point.

2.2 B-10 LOADING IN THE SM-2 CORE MOCKUP FROM CORE REACTIVITY MEASUREMENTS

2.2.1 Introduction

Control of excess core reactivity in the SM-2 is maintained at any time during core life by means of movable control rods. In addition burnable nuclear poison B-10 is added to the fuel matrix of each fuel plate during fuel plate fabrication process for the purpose of extending core life expectancy. The amount of excess reactivity controllable by the movable control rods is fixed by the number, type, and distribution of control rods employed in the basic core design and cannot be easily changed after reactor startup. The burnable poison, on the other hand, is depleted from the core more rapidly than the fuel and results in a maximum control demand upon the movable rods near the core midlife. Considering these plus other control demands resulting from temperature and xenon reactivity effects, it becomes very important to specify to the closest possible tolerance the burnable poison loading in the reactor core, if one is to be assured that adequate system control is to be maintained over the core lifetime.

A series of experiments were conducted at the Alco Critical Facility with the objective of obtaining a more precise determination of the boron-10 loading in the SM-2 core mockup than that previously reported. These measurements were based on physical methods of mass spectroscopy and core reactivity changes; a comparison with the results from chemical analysis is presented.

2.2.2 Experimental Procedures and Results

The experimental procedures employed in these tests were basically that of the standard sample technique in which a series of standard samples containing known and varying amounts of B-10 were prepared and inserted, in succession, into the reactor to generate a curve relating core reactivity change to B-10 loading. A second series of samples containing an unknown amount of B-10 were then intercalibrated with the standards by inserting them into the reactor under test conditions identical with those employed for the standards. The core reactivity change was noted for each of the second series of samples and the B-10 loading obtained for each sample by reference to the curve of reactivity vs. B-10 loading. Having obtained the B-10 loadings, the second series of intercalibrated samples were employed in the various experiments described below.

2.2.2.1 Preparation of the Standard Samples

Boron carbide obtained from the base material used in the manufacture of the Mylar film was utilized in the standard sample preparation. Four samples of B_4C were weighed on an analytical balance and the amount of B-10 in each sample calculated using the total boron weight percent as obtained by chemical analysis from Lucius Pitkin, Inc. and the AEC's New Brunswick laboratory, and the a/o B-10 as obtained from mass spectrograph isotopic analysis by the New Brunswick laboratory. These analyses of the base material have been reported previously[1] and were in good agreement on the composition of the base material.

The four weighed samples of B_4C were combined with a lacquer-thinner binder and applied uniformly over the surface of a polystyrene sheet of essentially the same width, thickness, and length as an SM-2 fuel plate. The ratio of thinner to lacquer was approximately 10 to 1 and complete transfer of material was insured by standard chemical techniques of multiple washing and policing. The surface covered by the B_4C on the polystyrene sheets was held to the nominal fuel matrix length and width specified for the SM-2 flexible critical experiments fuel plates in order to maintain consistency of poison geometry in these and subsequent intercalibrations with Mylar film. One blank sample of lacquer and thinner on polystyrene was prepared as a zero reference piece; however, subsequent tests demonstrated that this blank reference produced no measurable reactivity change between it and the water which it displaced.

2.2.2.2 Calibration of the Standard Samples

Using the four standard samples and the zero reference piece a curve was generated of reactivity change, ΔK_E vs. B-10 loading of the samples (Fig. A.2) in the following manner:

1. The blank was inserted in the center of element position No. 22 (plate position "i"). All the fuel plates were removed from this element position to increase the thermal flux peaking and hence the sensitivity of the method.

2. The reactor was brought critical on calibrated control rod E, five rod bank at 5.75 in. withdrawn, and with control rod F fully withdrawn.

3. The four standard samples mounted in an identical manner were then substituted for the blank, one at a time and critical positions for each obtained on calibrated rod E.

4. Control rod E was calibrated by taking period measurements during the above and subsequent operations.

5. The reactivity differences obtained from measurements (4) and (5) were plotted vs. the known B-10 content of the standards and thus Fig. A.2 was generated.

The results of the above experiments (Fig. A.2) were used as a basis for the following B-10 determinations.

2.2.2.3 Intercalibration of Tapes

A series of similar calibration runs were made with strips of boron impregnated tapes mounted on polystyrene sheets in a manner identical with that of the standard samples. The B-10 content of these tapes was determined from reactivity differences measured on calibrated control rod E, utilizing, ΔK_E vs. B-10 loading curve, Fig. A.2. After calibration these tapes were carefully stripped from the plastic to prevent boron losses. Two tapes, with the approximate B-10 content of an SM-2 reference fuel plate, were placed in layers on one side of a mockup fuel plate of element No. 22 for the purpose of intercalibrating additional fuel plates. Five others were used for B-10 worth determination, and four were sent for chemical analysis.

The B-10 loading of these tapes is given in Table 2.1 together with the four obtained by chemical analysis. To simplify identification of tapes the following nomenclature is used, for example: 1-2 #2 indicates: order 1, batch 2, tape labeled #2.

TABLE 2.1

B-10 LOADING OF INTERCALIBRATED TAPES TESTED IN ELEMENT POSITION 22, FUEL PLATE "i"

	B-10 Loading by Inter-comparison with Standard Tapes		B-10 Loading by Chemical Analysis
Tape No.	mg/cm^2	mg	mg/cm^2
1-2 #2	0.1560	54.4	0.1717+
1-2 #3*	0.1590	55.4	
1-2 #4	0.1585	55.2	0.1408++
2-1 #1	0.0770	26.8	
2-1 #3**	0.0745	25.9	
2-1 #5**	0.0745	25.9	
2-1 #6	0.0717	25.0	0.0551+
2-1 #7**	0.0725	25.3	
2-1 #10**	0.0799	27.8	
2-1 #11	0.0735	25.6	0.0709++
2-1 #12*	0.0755	26.3	
2-1 #13**	0.0781	27.2	

* Tapes applied to mockup fuel plate 139-S-3 to provide reference plate of known B-10 loading.

** Tapes applied to mockup fuel plates in plate positions a, e, j, n, and r of element No. 22 for B-10 worth determination.

\+ Chemical analysis by Lucius Pitkin.

++ Chemical analysis by BMI.

643 033

2.2.2.4 Intercalibration of Mockup Fuel Plates

Calibrated tapes 1-2 #3 and 2-1 #12 were placed on plate 139S-3 in position "i" of element No. 22 for the purpose of establishing a reference fuel plate. These two tapes were chosen because they have about the same B-10 loading as the SM-2 mockup fuel plates. The calibrated tapes were placed one at a time on the fuel plate and the net reactivity change produced by each was measured in order to obtain B-10 worth as a function of B-10 loading. The addition of calibrated tape 1-2 #3 with 55.4 mg B-10 produced a reactivity change equal to 197.9 cents per gm B-10. The further addition of calibrated tape 2-1 #12 brought the total B-10 content to 81.7 mg and lowered the B-10 worth to 178.1 cents per gm B-10 for the two tapes and to 136.4 cents per gm B-10 for the second added tape 2-1 #12. This change in boron worth is attributed mainly to boron self-shielding, flux depression effects, and a slight hardening of the local neutron energy spectrum.

The remaining 17 fuel plates were loaded successively in position "i" of element No. 22 and their B-10 loadings were determined from individual reactivity changes between them and the reference fuel plate and utilizing the established B-10 loading and worth in the reference.

B-10 loading for each of the fuel plates is given in Table 2.2. The average B-10 content amounted to 0.0828 gm per fuel plate for a total of 1.4905 gm for 18 plates comprising stationary fuel element No. 22.

B-10 worth for element 22 was determined by applying tapes 2-1 #3, 2-1 #5, 2-1 #7, 2-1 #10 and 2-1 #13 to plates a, e, j, n, and r respectively. The measured reactivity difference rendered a B-10 worth of 56.62 cents per gm for element No. 22 in position 22.

2.2.2.5 Intercalibration of Mockup Fuel Elements

The B-10 loading of nine fuel elements was determined by intercalibrating them with the element in position 22. Each element was placed in turn in lattice position 22; the difference in reactivity between the element under test and the zero position established by element No. 22 was assumed to be a measure of the difference in B-10 loading. Any variations in fuel contents were assumed to be negligible; the B-10 loadings are given in Table 2.3.

The B-10 loadings of control rod fuel elements were calculated by ratioing the average stationary fuel element B-10 loading by the differences in the number of fuel plates and cross-sectional areas of the tapes applied. The average B-10 loading thus obtained was 1.278 gm per control rod fuel element and the estimated total B-10 content of the SM-2 mockup core was 67.9 gm.

TABLE 2.2
B-10 LOADING OF 18 INTERCALIBRATED FUEL PLATES
TESTED IN ELEMENT POSITION 22, PLATE POSITION "i"

Plate Position In Element 22**	Plate No.	B-10 Loading, gm
a	57-S-6	0.0867
b	138-S-1	0.0801
c	105-S-1	0.0851
d	139-S-3*	0.0817
e	137-S-1	0.0842
f	138-S-4	0.0803
g	156-S-6	0.0828
h	139-S-6	0.0840
i	137-S-3	0.0819
j	139-S-1	0.0812
k	137-S-6	0.0849
l	139-S-4	0.0778
m	138-S-6	0.0790
n	111-S-1	0.0833
o	137-S-5	0.0849
p	160-S-2	0.0856
q	162-S-4	0.0828
r	156-S-2	0.0842
Total		1.4905
Average		0.0828

* Reference fuel plate, containing intercalibrated tape Nos. 1-2 #3 and 2-1 #12 used to intercalibrate the other 17 fuel plates.

** After intercalibration, fuel plates were placed in positions indicated for the purpose of obtaining a standard mockup fuel element.

TABLE 2.3
B-10 LOADING OF 10 INTERCALIBRATED SM-2 MOCKUP FUEL ELEMENTS TESTED IN ELEMENT POSITION 22

Fuel Element No.	B-10 Loading, gm
12	1.498
22*	1.491
27	1.583
37	1.522
47	1.548
57	1.520
67	1.590
74	1.659
75	1.549
76	1.551
Average	1.551

* Average reference fuel element used to intercalibrate the other nine fuel elements.

2.2.2.6 Comparison Between BMI Reference Element and Mockup Element

Fuel element No. 22 was assembled with the 18 intercalibrated mockup fuel plates and the critical position of calibrated control rod E determined. The mockup plates were then removed and 18 SM-2, BMI manufactured reference fuel plates substituted, and the new critical position determined. The change in reactivity was calculated from the difference in the critical positions. This change represented the additional amount of B-10 required on the mockup fuel elements to match the worth of the integral B-10 of the reference fuel element; if the reactivity change due to slight fuel loading difference was assumed to be negligible. This required additional B-10 was calculated to be 0.262 gm based on an experimentally determined B-10 worth of 56.62 cents/gm for mockup element No. 22. Since the 18 mockup fuel plates contained a total of 1.491 gm B-10, therefore total B-10 required on mockup plates to have the same reactivity effect as BMI reference plates is 1.753 gm for an average B-10 loading of 0.0974 gm per mockup fuel plate. This compares with the value of 0.0911 gm/plate reported by BMI for the reference plates.

Further interpretation of these data are complicated due to the larger fuel matrix dimensions of the BMI reference fuel plates compared to those of the SM-2 mockup plates.[1][6]

2.2.2.7 Conclusions

In carrying out the preceding experiments, reactivity differences were measured, then converted to equivalent grams of B-10. However, reactivity differences are not all caused by differences in B-10 loadings. Other sources contribute in varying degrees as follows:

1. Contribution of fuel loading difference to reactivity differences was assumed to be negligible since U-235 loadings can be accurately assayed and the difference in U-235 loadings were less than 0.2%.

2. Method of applying burnable poison; in BMI reference plates it was incorporated in the fuel matrix as spherical particles of zirconium diboride, while in the mockup it was applied to the surface of the fuel plates as boron carbide coated Mylar tape.

3. Effect due to difference in particle size; the boron carbide in the Mylar tapes has a diameter of one to three microns, whereas zirconium diboride particles average about 100 microns. Also during manufacture, mockup fuel plates were reduced about 12 to 1, thus containing uranium oxide particles with an average diameter of 66 microns; the BMI reference plates were reduced only about 6 to 1 with an average uranium oxide diameter of 112 microns.

4. Self-shielding of B-10 particles; in applying burnable poison in layers, the B-10 particles tend to shield each other and hence they become less effective as neutron absorbers. This is demonstrated by the change in B-10 worth from 197.9 cents when one tape is applied to a fuel plate to 136.4 cents when two are applied. The self-shielding effect on the worth of B-10 when it is integrated into the fuel matrix was not determined.

5. Difference in B-10 worth due to external and internal loading.

6. Difference in fuel matrix size between the reference and the mockup fuel plates.

After the above experiments were completed, additional chemical analyses were made on tapes taken from the same orders and batches. The results show the boron loading on the tapes to be very uniform; however, the results obtained from the two independent laboratories differed by about 12% for the order 1 batch 2 tape and by about 2% for the order 2 batch 1 tape. The results of the chemical analyses are given in Appendix C.

643 037

2.3 MATERIAL COEFFICIENTS

2.3.1 Introduction

Reactivity worth measurements were made at a simulated operating temperature of 510°F. The operating temperature was simulated by inserting aluminum strips in the stationary and control rod fuel elements. A detailed discussion of the temperature mockup is given in Section 4.2.3. The worth in cents per gm or cents per cc was determined for B-10, U-235, stainless steel, and void throughout one quadrant of the core, excepting the control rod fuel elements where only B-10 worths were measured. To obtain an estimate of the average worth of U-235, stainless steel and void in the whole core, the average for stationary elements was multiplied by the ratio of the average B-10 worth in the core to that in stationary elements only. This is justified since they were all measured in the same core under exactly the same conditions.

Prior to the worth measurements, a short heterogeneity experiment was performed to establish the adequacy of the experimental method, since usually it is not feasible to add a given material to a fuel element without introducing some heterogeneity.

2.3.2 Procedure

Reactivity differences were measured using calibrated control rods D and G as a two rod bank. The five rod bank (A, B, C, E, F) was placed at 12.600 in. withdrawn. This choice allows for measurements to be made in a quadrant of the core that is least perturbed by rod motion. Also preliminary measurements have indicated that the calibration curve for control rods D & G is smooth and essentially linear. A two rod calibrated bank was chosen instead of a single calibrated rod because the reactivity differences are large for B-10 measurements. All measurements were made relative to a zero position defined as the critical position with SM-1 standard element in position No. 76 and SM-2 mockup element 76 in position No. 22. This procedure leaves element No. 22 free for substitution measurements into the other positions of the quadrant. The zero position was taken at the beginning and end of each day to nullify effect of temperature change.

2.3.3 Heterogeneity Measurements

Since it is not usually feasible to add a given material to a fuel element without introducing some heterogeneity, a short experiment was made to determine the size of this heterogeneity factor. The experiment was performed by replacing six fuel plates (each 40 mils thick) by six 40-mil thick plates (4-10 mil pieces) of stainless steel clad of essentially the same width and length. The size of the heterogeneity factor was determined by arranging the stainless steel plates in 6, 3, 2 and 1 discrete bundles and measuring the reactivity difference for each arrangement in element position No. 33. Reactivity differences obtained in this manner were converted into cents per gram of U-235 since the difference

between the fuel plates and the stainless steel plates was U-235 (neglecting the U-238 and difference in particle size). This was done so that these results could be directly compared with the U-235 material coefficient later obtained using heavily loaded fuel plates. Figure 2.1 presents the data. The curve was linearly extrapolated to 18 bundles (the number of fuel plates in an element). The heterogeneity effect is seen to be small after about 5 bundles. The uranium worth obtained using 18 heavily loaded fuel plates is in good agreement with the value predicted from the extrapolated data.

2.3.4 U-235 Worth

Uranium worth measurements were made using 18 heavily loaded fuel plates to avoid the possibility of heterogeneity effects. First, element No. 22 was substituted into each element position of one quadrant of the core and the critical position determined on calibrated rods D and G with the five rod bank (A, B, C, E, F) at 12.600 in. Then, element No. 22 was loaded with 18 heavily loaded fuel plates and the same boron tapes and substituted through the same quadrant of the core in the same manner. The resulting reactivity differences determined the uranium worth for the quadrant.

Table 2.4 lists the worths thus obtained together with those previously obtained at room temperature.

It is noted that the average U-235 worth at simulated temperature (510°F) is approximately 24% less than the average U-235 worth at room temperature.

2.3.5 B-10 Worth

The boron impregnated Mylar tape was stripped off fuel plates a, e, j, n, and r of element No. 22. Then element No. 22 was substituted into the other stationary fuel element positions of the quadrant. For the control rods the boron tape was stripped off fuel plates a, d, i, m and p. The critical position for each measurement was determined on the calibrated two rod bank D & G with the five rod bank (A, B, C, E, F) at 12.600 in. The B-10 worth was calculated from reactivity differences using B-10 loadings determined in the previous section and APAE 54.(1)

Table 2.5 presents the B-10 worth data obtained at simulated temperature and that previously obtained at room temperature.

The average B-10 worth at simulated temperature (510°F) is about 24% less than the average B-10 worth at room temperature which is the same amount the U-235 worth was decreased. This is the expected result since both U-235 and B-10 are essentially 1/v absorbers.

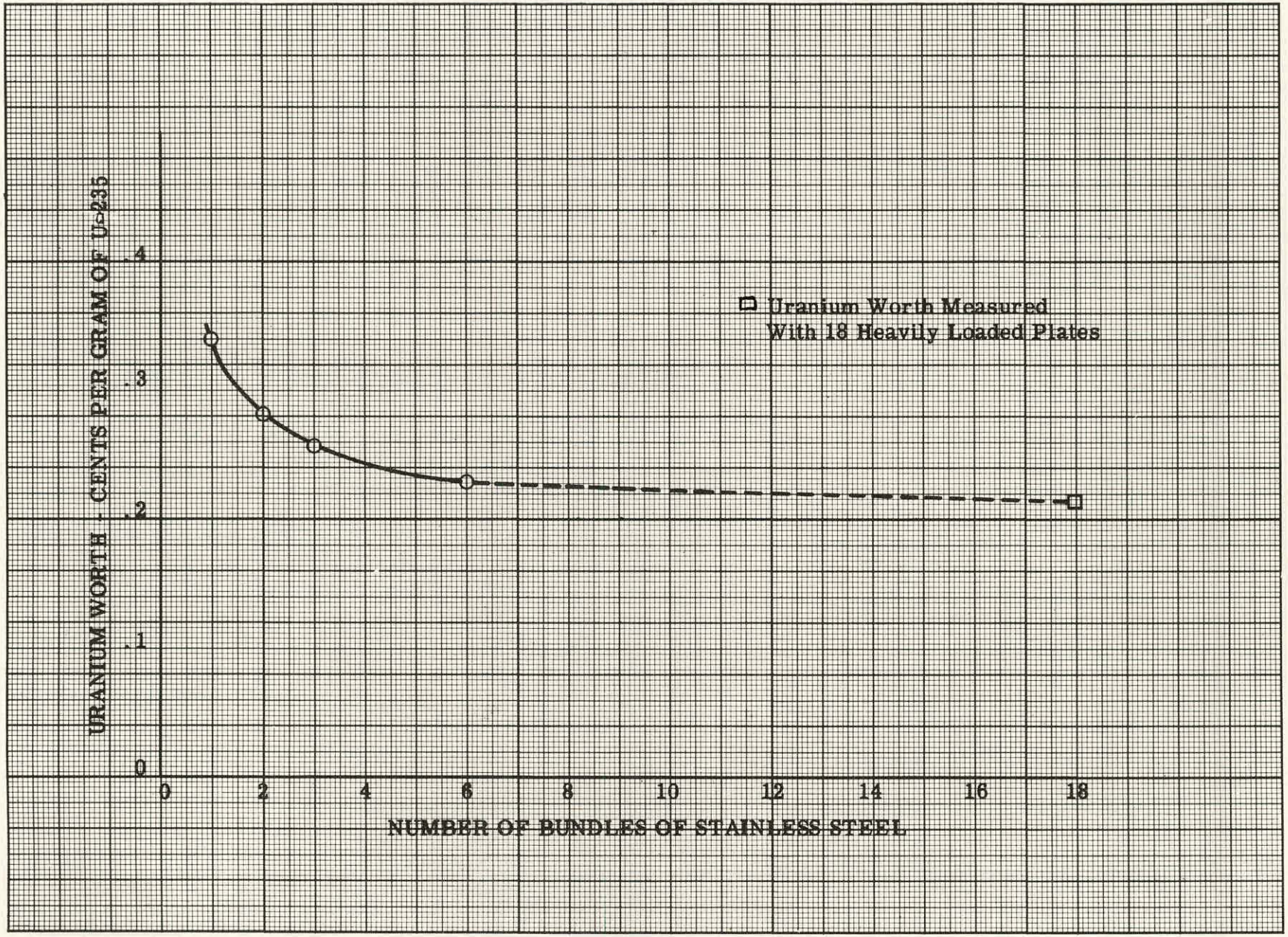

Figure 2.1 Heterogeneity Factor, Uranium Worth Vs. No. of Stainless Steel Bundles, Element in Position 33

THIS PAGE

WAS INTENTIONALLY

LEFT BLANK

TABLE 2.4
U-235 REACTIVITY COEFFICIENTS

Element Position	U-235 Worth ¢/gm At Simulated Temp. 510°F	U-235 ¢/gm At Room Temp. 68°F(1)
12	0.052	0.067
13	0.065	0.098
14	0.091	0.110
21	0.048	0.057
22	0.115	0.146
23	0.189	0.211
31	0.057	0.084
33	0.213	0.295
34	0.264	0.321
41	0.063	0.098
42	0.143	0.220
43	0.242	0.312
Average for stationary fuel elements	0.120	0.157
Estimated Core Average	0.131	

TABLE 2.5
B-10 REACTIVITY COEFFICIENTS

Element Position	B-10 Worth in ¢/gm At Simulated Temp. 510°F	B-10 Worth in ¢/gm At Room Temp. 68°F(1)
12	8.4	17.0
13	21.7	25.6
14	22.5	28.0
21	7.2	14.6
22	29.1	38.6
23	45.5	57.0
31	16.3	22.6
33	59.8	79.5
34	74.6	87.7
41	20.4	25.5
42	42.4	58.9
43	71.8	87.5
Control Rod A	50.0	-
Control Rod F	41.2	-
Control Rod C	88.4	-
Average for stationary fuel elements	32.0	42.0
Estimated Core Average	34.9	-

643 041

2.3.6 Stainless Steel Worth

Stainless steel worth or coefficient was determined by replacing the aluminum strips in element No. 22 by an equivalent volume of stainless steel clad. Reactivity differences were measured in the same manner as for other worth measurements. Since the stainless steel replaced an equal volume of the aluminum the reactivity differences measured were due to the differences in nuclear cross sections of aluminum and stainless steel only and did not include the effect of water displacement. The effect of water displacement or void worth is discussed in the next section. Table 2.6 lists the stainless worth at simulated temperature (510°F).

TABLE 2.6
STAINLESS STEEL REACTIVITY COEFFICIENTS -
EFFECT OF WATER DISPLACEMENT NOT INCLUDED

Element No.	Stainless Steel Worth ¢/cc at Simulated Temp. 510°F.
12	0.0064
13	0.0083
14	0.0121
21	0.0068
22	0.0157
23	0.0312
31	0.0102
33	0.0593
34	0.0683
41	0.0128
42	0.0422
43	0.0686
Average for stationary fuel elements	0.0253
Estimated Core Average	0.0276

2.3.7 Void Worth

The void coefficient or worth was obtained by removing the aluminum strips from element No. 22 and substituting it in the element positions of the quadrant of the core being measured. The reactivity differences were measured on calibrated rods D and G with the five rod bank (A, B, C, E, F) at 12.600 in. In calculating the void coefficient the cross section of aluminum was assumed negligible. Table 2.7 lists the coefficients obtained at simulated temperature, 510°F.

TABLE 2.7
VOID REACTIVITY COEFFICIENTS

Element No.	Void Worth ¢/cc
12	0.0149
13	0.0259
14	0.0250
21	0.0116
22	0.0365
23	0.0767
31	0.0236
33	0.0910
34	0.1022
41	0.0298
42	0.0631
43	0.1071
Average for stationary fuel elements	0.0467
Estimated Core Average	0.0509

The average void coefficient for the stationary fuel elements is 0.0467 cents per cc. This value obtained by a series of individual measurements compares very well with the average value of about 0.04 cents/cc obtained when the water was displaced from all of the fuel elements by inserting aluminum strips to simulate the operating conditions (510°F at 2000 psi).* The fact that the average value (0.0467 cents/cc) obtained by individual measurements is higher than the value obtained from one single perturbation is to be expected since the sum of a series of small perturbations is usually larger than if the perturbation was made in a single step, due to changes in the neutron flux spectrum.

It should be noted that the void coefficients given in Table 2.7 can be added to the stainless steel coefficients in Table 2.6 if the total stainless steel worth or coefficient is desired, including water displacement.

2.4 REACTIVITY MEASUREMENTS USING FLOW DIVIDER

The basic SM-2 flow divider design has been reported previously.[6] This test provides data from which the reactivity effects resulting from the use of a flow divider and flow divider support structures may be evaluated. Flow divider reactivity evaluation was made by inserting 1/8-in. stainless steel sheets

* Refer to Section 4.2 and APAE No. 54[1].

between the outer ring of elements as shown in Fig. 1.7. The core was supported on a 1-in. thick plastic sheet placed on top of the existing stainless steel core support plate. The plastic insert was machined to accommodate the end boxes of the stationary fuel elements so that the proper spacing was achieved for the SM-2 core design with flow divider. Reactivity measurements were taken to evaluate:

1. The effect of raising the core upwards to accommodate the new plastic support plate.

2. The effect of spreading the outer ring of elements by the installation of the plastic support plate.

3. The effect of installing the flow divider between the outer ring of elements.

4. The effect of attaching flow divider to steel reflector by stainless steel support pins.

5. The effect of attaching flow divider to steel reflectors by stainless steel plates.

The results of these measurements are given in the following table.

TABLE 2.8
REACTIVITY MEASUREMENTS EVALUATING THE INSTALLATION OF FLOW DIVIDER

	Reactivity Change (cents)
1. Effect of raising core 1-in. by means of plastic strips placed under fuel elements.	-12
2. Effect of spreading spacing of elements	-28
3. Effect of flow divider	-110
4. Effect of using 32 pin supports for flow divider	-5
5. Effect of using 8 plate supports for flow divider	-27

The first of these reactivity effects results from replacing the steel core support plate with an equivalent volume of water, and hence establishes the reactivity change resulting from the use of the lucite support plate. Since this

reactivity change results from equipping the experiment it should not be attributed to effects introduced by the flow divider. However, the test data has potential application in the event significant changes are incorporated into the final SM-2 core support plate design which result in a significant change in the volume of steel in that region. The remainder of these measurements indicate the effects on SM-2 core reactivity resulting from the use of a 1/8-in. flow divider inserted as shown in Fig. 1.7. The individual reactivity effects result from increased effective core diameter by increasing the fuel element spacing in certain regions to accommodate the flow divider, insertion of the 1/8-in. thick flow divider and the consequent displacement of some core moderator in that region, and the use of pin or plate type flow divider supports.

Table 2.8 shows that the effect of placing the flow divider in the core supported by pins results in a loss of 143 cents reactivity; the substitution of support plates for pins increases reactivity loss to 165 cents. The linear extrapolation of previous measurements[1] renders a comparative estimated core reactivity change of 172 cents for a flow divider mockup, which did not provide for a mockup of the flow divider supports or increased fuel element spacing. The above measurements were carried out using the entire seven rod bank to measure reactivity changes; the worth of the bank at various positions is given in Fig. 2.2.

2.5 SUPPRESSOR REACTIVITY

The core reactivity change resulting from the use of mockup flux suppressors was determined by comparing the relative control rod bank positions at criticality to that obtained when testing "blank" suppressors which contained no neutron absorbing material. Elements Nos. 12, 13, 14, 21, 22, 23, 33, 34 and 41 were mocked up with Mylar tape as described later in Section 3.2; the reactivity calculated from these nine elements was ratioed to the total number of elements in the core. This produced estimated reactivity changes at room temperature for the entire core of -$2.36 and -$2.41 for the 1/2-in. and 3/4-in. wide mockup suppressors, respectively.

2.6 ADDITIONAL REACTIVITY MEASUREMENTS

The additional reactivity measurements discussed in this section were performed on the final SM-2 mockup with flow divider at room temperature.

2.6.1 Effect of Mockup Control Rod Flux Suppressors

The control rod flux suppressors were mocked up by applying 26 layers of boron impregnated Mylar tape to each side of the control rod fuel plates exactly as the stationary fuel element suppressors (refer to Section 3.2). Two separate measurements were made: (1) the 1/2-in. wide suppressors were placed directly

above the top of the active meat of the fuel plates of the seven control rods; (2) the 1/2-in. wide suppressors were placed on the upper 1/2-in. portion of the active meat of the fuel plates of the seven control rods.

The placing of the 1/2-in. wide mockup flux suppressors above the active meat of the fuel plates of the seven control rods produced a negative reactivity change of 116.1 cents which changed the seven rod bank critical position from 7.845 in. to 8.352 in. The placing of the 1/2-in. wide suppressors on the upper 1/2-in. portion of the active meat of the fuel plates of the seven control rods produced a negative reactivity change of 155.0 cents which corresponded to a final seven rod bank critical position of 8.531 in. The suppressors were left in this latter position when the final foil measurements were made. It is thought that this mockup is better than the first one as the spacing between the upper edge of the mockup suppressors and the bottom edge of the absorber sections is more nearly correct.

2.6.2 Worth of Side Plates

The SM-2 mockup has an equivalent side plate thickness of 0.0327 in. while the design side plate thickness is 0.040 in. Fifteen mils of stainless steel clad was added to each of 38 stationary fuel elements (10 mils on east side and 5 mils on west side) to bring the equivalent mockup side plate thickness to the 0.040 in. design thickness. The net reactivity change due to the additional clad in 38 elements was -23.5 cents.

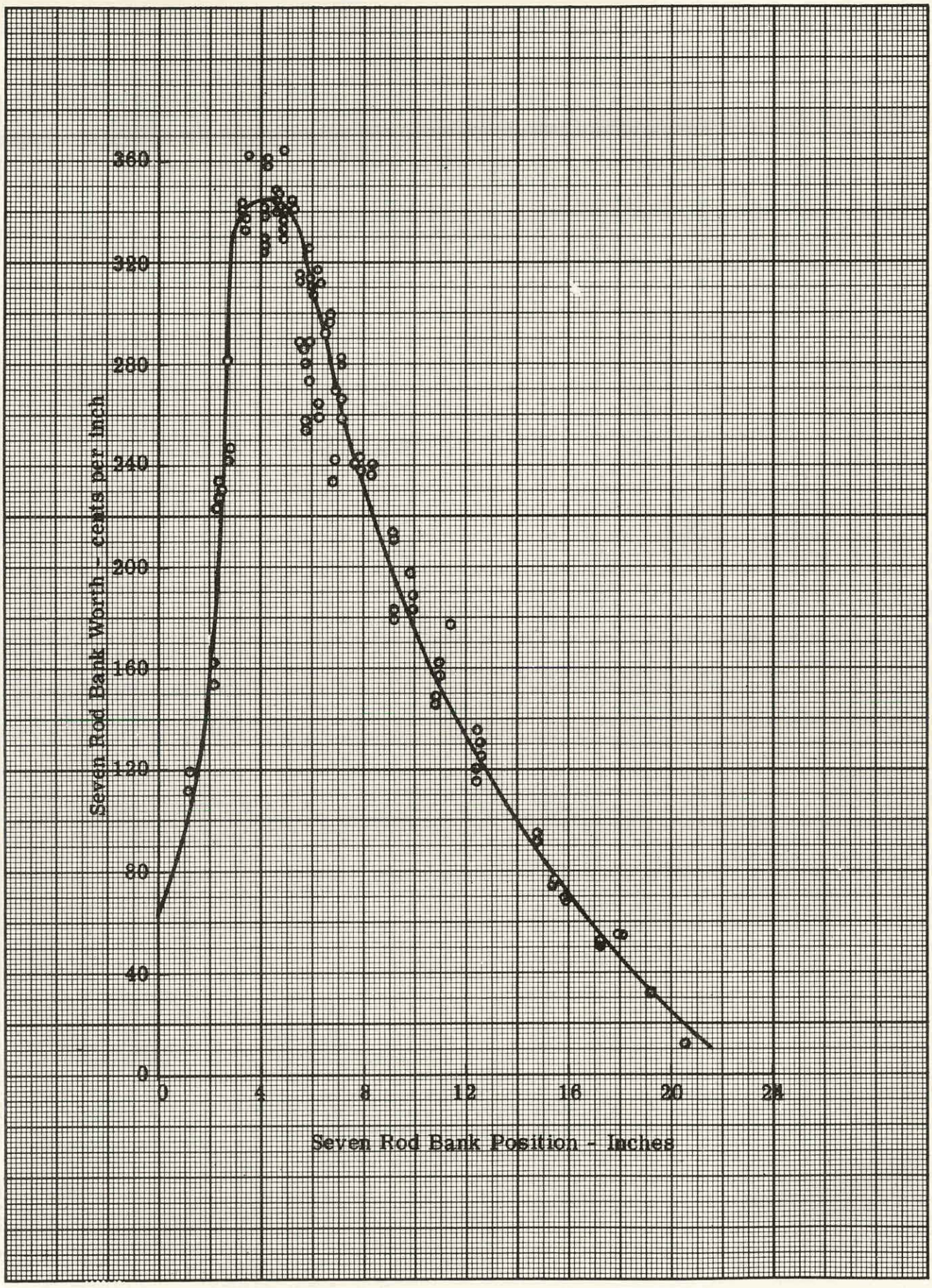

Figure 2.2 Composite Seven Rod Bank Calibration

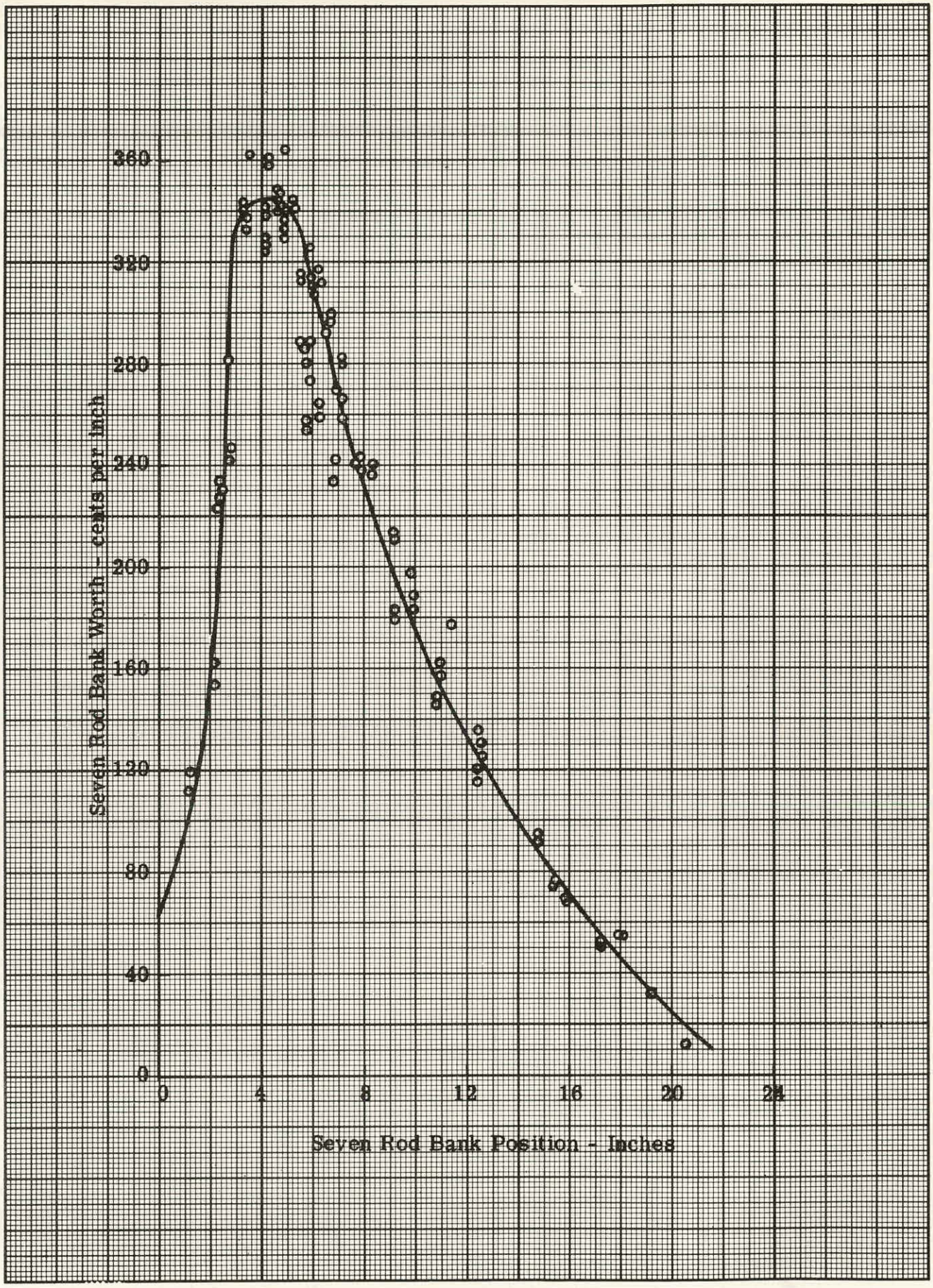

Figure 2.2 Composite Seven Rod Bank Calibration

THIS PAGE

WAS INTENTIONALLY

LEFT BLANK

3.0 ACTIVATION MEASUREMENTS

3.1 INTRODUCTION

The relative power distribution in the SM-2 core was obtained by uranium foil activation measurements throughout one quadrant of the core for two separate SM-2 core mockups:

1. Preliminary mockup with laminated steel reflected core without flow divider.

2. Final mockup with laminated steel reflected core with 0.125-in. flow divider and 0.5-in. mockup flux suppressors at the top of the active meat of the control rod fuel elements.

The resulting data yielded the core average for each mockup and enabled a more definitive fine structure study to be made of the intercell power distribution and/or fission flux, than those previously reported.(1)

The effectiveness of both mockup and integral suppressors located at the lower boundary of the stationary fuel elements in reducing the high power spikes occurring near the bottom of the active meat was determined during a separate series of measurements. Blocked channel measurements were also performed to determine the effects on local power generation that result from blocking a fuel element coolant channel.

3.2 CORE MAPPING

3.2.1 Introduction

Activation measurements were performed using bare uranium foils taped directly to the fuel plates for the purpose of obtaining a ratio of measured activity to that of a reference. The reference foil for all activation measurements in this series was located at the centerline of the south side of fuel plate "i" of element No. 34 at an axial elevation of 6 in. above the bottom of the active core.

Approximately 1700 data points were taken in one quadrant of the core to obtain an accurate core average based upon core symmetry and a detailed description of local effects. Each data point was then normalized to the average activation; thus, the core average becomes unity by definition.

3.2.2 Procedure

The fuel element to be mapped was instrumented with 19 w/o fully enriched uranium-aluminum alloy foils of approximately 12-14 mg in weight and 0.25 in. diameter. The foils were taped to five fuel plates each of 12 stationary fuel ele-

ments and three control rod fuel elements, representing a complete quadrant of the full core. The five fuel plates chosen included the two outside plates and the center plate which were mapped extensively, and two other intermediate fuel plates which were mapped as required and in varying degrees. This choice represents complete axial and radial traverses of the core. Since the core is symmetrical, mapping of only one quadrant was necessary to determine the core average. Typical foil locations for a stationary fuel element are shown in Fig. 3.1. The foils were activated in the SM-2 mockup core for 30 minutes at 30-40 watt power levels. The foils were then removed and counted with the aid of two scintillation counters.

3.2.3 Nomenclature

The following nomenclature is used in this chapter to define foil locations.

1. Position: Location of foil measured from the bottom of the active core in inches.

2. Axial plane: Plane perpendicular to the core axis and measured from the bottom of the active core in inches.

3. Central radial plane: Plane parallel to the north-south plane of the core and passing through the core centerline.

4. Radial plane: Plane parallel to the north-south plane of the core, distance measured from the central radial plane in inches.

5. Using the Tables: In the following tables all data points have been normalized to a core average power generation of unity (ref. par. 3.2.5). Data plots of relative power vs. location may be obtained in the following manner.

   Axial power distributions are obtained by reading the vertical columns in the appropriate tables. As an example, take the relative power distribution along the centerline of core position 42. Reference to Fig. 3.2, 3.3 and 3.4 indicates that these data points are located on fuel plate "j" and on the 5.88-in. west radial plane of core position 42. Thus, by referring to Table 3.11 for fuel element position 42, fuel plate "j" at the 5.88 WRP and plotting down the vertical columns, the curve for Fig. 3.8 was generated where the foil position and relative power generation fall along the abscissa and ordinate respectively.

   Radial power distribution may be obtained by reading the appropriate table entries in the horizontal direction. As an example, take the radial power distribution through fuel element positions 41, 42, 43 and 44 (control rod C), and on an axial plane which is 5 in. above the bottom of the active core. Again by reference to Fig. 3.2, 3.3 and 3.4 it is established that these data points are located on fuel plate "j" for positions

41, 42 and 43 and on fuel plate "i" for position 44, which is a control rod and consequently has fewer fuel plates per element and a slightly different plate identification. Reference to fuel plate "j" in Tables 3.10, 3.11, 3.12 and fuel plate "i" in Table 3.14 all at an axial position of 5 in. above the bottom of the active core renders the curve in Fig. 3.10 where the relative power generation has been plotted as a function of radial distance from the core centerline.

If a radial power distribution is desired in a direction which is normal to the plane of the fuel plates and at a specific axial elevation, then the following procedure applies. By reference to Fig. 3.3 and 3.4 the core position and fuel plates of interest are established. Then by reference to the appropriate tables the relative power generation in the selected plates at the selected axial elevation is obtained. As an example, if the radial power distribution through core positions 14, 24 (control rod A), 34, and 44 (control rod C) is desired at an axial elevation of 5 in., the following procedure applies. By reference to Fig. 3.2, 3.3 and 3.4 it is established that all data points are located along the central radial plane in core positions 14, 24, 34 and 44 at an axial position of 5 in., and all data points falling between plates "i" through "p" for core position 44, "a" through "r" for core position 34, "a" through "p" for core position 24 and "a" through "r" for core position 14 are desired. Then these data points may be obtained from Tables 3.3, 3.9, 3.13 and 3.14, and a radial power distribution normal to the plane of the fuel plates constructed.

As indicated, Fig. 3.3 shows the locations of various radial planes in the west side of the core, these planes being perpendicular to the plane of the figure. In the following tables, C.R.P. stands for central radial plane; W.R.P. stands for west radial plane; E.R.P. stands for east radial plane.

3.2.4 Data Processing

The data were processed in a manner identical to that described in AP Note 246.[5] This method yields the relative activity of the different foils to that of the reference, allowing corrections for weight, counter background, and radioactive decay. All of the data reported in this chapter were normalized to the core average thus permitting rapid inspection of high power areas.

3.2.5 Core Average

A useful relationship for purposes of core design is the local power generation related to that of the core average. Since all power measurements were related to an arbitrary reference in the core, the procedure described below was utilized in obtaining a core average that is unity by definition.

First, the relative power averages for each plate, then for each fuel element, and finally for the power generating core volume were obtained. Fuel

plate averages relative to that of the reference point were obtained from measurements across the face of the fuel plates at several axial positions. These measurements were integrated by applying the 3-point or the 5-point Simpson's rule to obtain an average single set of values for the 3- and 5-point radial traverses measured along the fuel plate at various positions above the bottom of the active core. This procedure was followed for each of the five fuel plates selected to be mapped in each fuel element; the distances between radial traverse planes represented strips of equal width required for this integration.

Each set of average values obtained was plotted as a function of axial position for each fuel plate. The curves were integrated by determining the areas under them using a planimeter. These integrated values represented the average power along each fuel plate and within a fuel cell. The average activity of a complete fuel cell was obtained by plotting the average plate values obtained against the distances between the fuel plates selected. The curves were integrated by again employing Simpson's rule giving the average power for each fuel cell.

The core average power value was obtained by summing all the fuel cell power averages and dividing by the power generating volume of the core. This value was equated to 1.00, and the experimental data points were normalized to this core average of unity. In determining the core average the cell averages for the control rod fuel elements have been weighted to include only the portion of the fuel plates actually inserted in the active core. A typical calculation for obtaining the core average is outlined in Appendix B.

3.2.6 Experimental Results Employing Laminated Steel Reflector Without Flow Divider (SM-2 Preliminary Mockup Core)

Figure 3.4 gives the complete normalized power averages for each fuel element in the core. Of the 45 core positions, 14 stationary fuel elements clustered about the center of the core exceed the core average. The cell average for the control rod fuel elements are reported as less than the core average even though they have a higher than average power density over the region, since they were weighted to include only the portion of the fuel plates actually in the active core (ref. Table B-2), the seven rod critical bank position being 6.94 in.

Tables 3.1 through 3.15 present the normalized activity distribution along axial traverses of stationary fuel elements in positions 12, 13, 14, 21, 22, 23, 31, 33, 34, 41, 42, 43 and for control rod fuel elements A, C, and F in positions 24, 44, and 32 respectively. Plates a, e, j, n, and r were selected for these measurements for the stationary fuel elements; plates a, d, i, m and p for the control rod fuel elements. The data range from a normalized low of 0.06 of the core average for plate "r" of stationary fuel element position 21 on the edge of the core to a high of 7.88 of the core average for plate "i" of control rod C in position 44 in the middle of the core.

The power traverses shown in Fig. 3.5 through 3.8 are typical of the power distribution axially along a fuel plate. Figures 3.5 and 3.6 show the power of the centerline traverses of plate "j" normalized to the core average for stationary fuel elements positions 12, 13, 14, and 21, 22, 23, respectively. Figures 3.7 and 3.8 show similar traverses for fuel element positions 31, 33, 34,and 41, 42, 43, respectively. It may be concluded from the above that all stationary fuel elements exhibit a large power peak at the bottom of the active core when flux suppressors are not employed, and a smaller axial peak about 4-6 in. above the bottom of the active core. The power gradually diminishes as it approaches the top of the active meat. For example in element position 43, along centerline of fuel plate "j", this power peaking is about 4.5 times the core average at the bottom of the active meat and 2.24 times the core average at an axial position 5 in. above it, while it is only 0.18 of the core average at the top of the active meat of the core.

Figure 3.9 shows the normalized power of the centerline traverses of fuel plate "j" of control rods A, C, and F for the portion of the fuel plates actually in the active core. There is a very small uniform increase in the normalized activity from the bottom of the active core to near the critical bank position of 6.94 in. at which point the power exhibits a very sharp increase shown by the almost vertical lines in Fig. 3.9.

Figure 3.10 shows a typical radial power traverse 5 in. above the bottom of the active core along the center of stationary fuel elements in positions 41, 42, 43, and control rod C in position 44, indicating the overall rise in power upon approaching the center of the core and the power minima along the centerline of a fuel element in relation to its outer edges.

The measurements of this configuration show an overall maximum-to-average power generation of 7.88 to 1 where the maximum is in the central control rod. The maximum-to-average considering the spike at the bottom of the core is 5.50 to 1. Ignoring both of these spikes the internal maximum-to-average is 4.39 to 1 occurring within the central control rod fuel element. These measurements indicate the need for flux suppressors.

3.2.7 Experimental Results Employing Laminated Steel Reflector, Flow Divider and Flux Suppressors at the Top of the Active Meat of the Control Rod Fuel Elements(SM-2 Final Mockup Core)

To the preliminary SM-2 mockup core was added a 0.125-in. stainless steel flow divider inserted between the two outer rings of elements which were slightly displaced, as shown in Fig. 1.7 and described in Section 2.4. In addition, 0.5-in. mockup flux suppressors were placed at the top of the active meat of all control rod fuel elements. The relative power distribution for the final SM-2 core mockup was obtained in the same manner as that described in the preliminary tests. The critical bank position for these tests was 8.54 in. withdrawn.

THIS PAGE

WAS INTENTIONALLY

LEFT BLANK

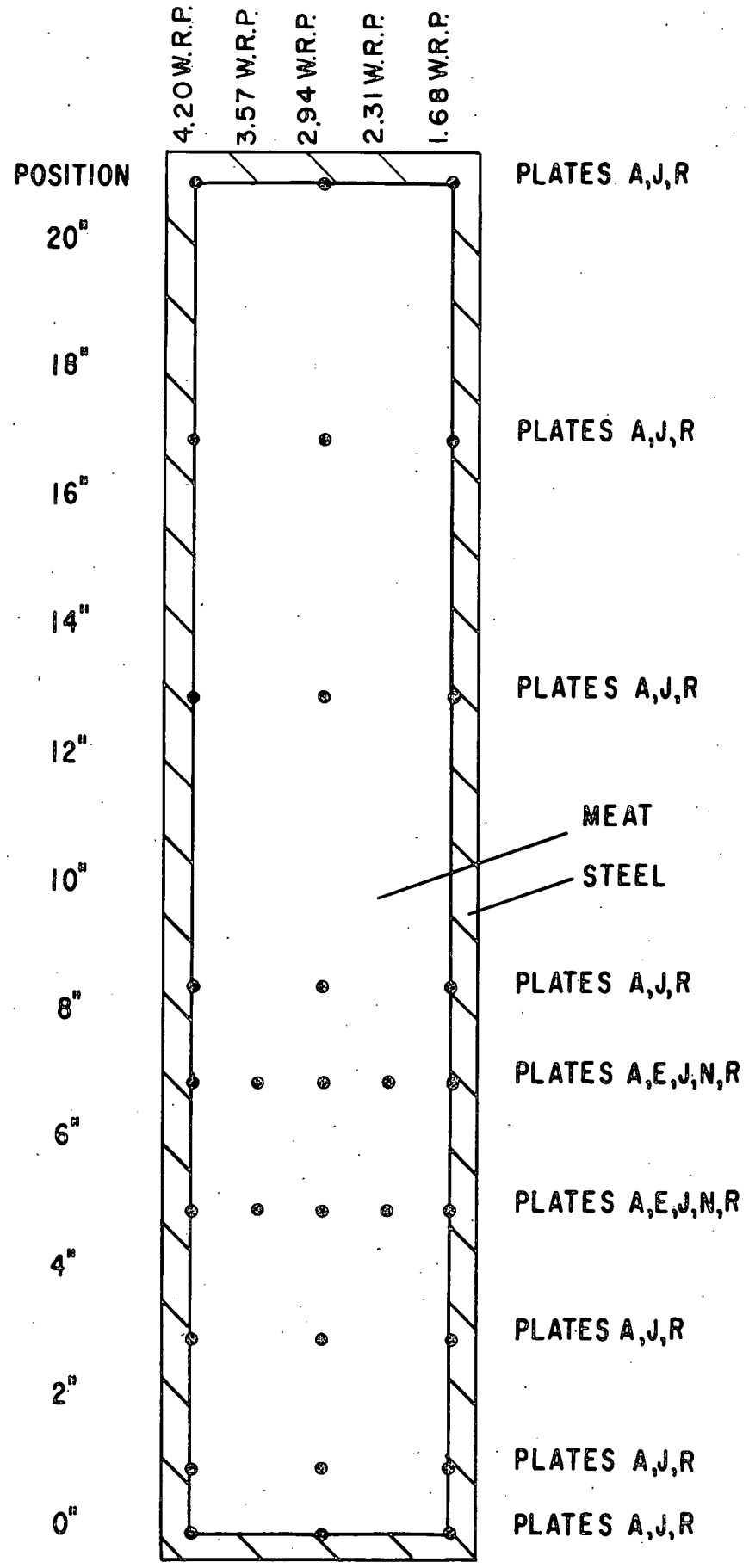

Figure 3.1 Uranium Foil Locations on Element in Position 13

Stationary Element Fuel Plate Arrangement

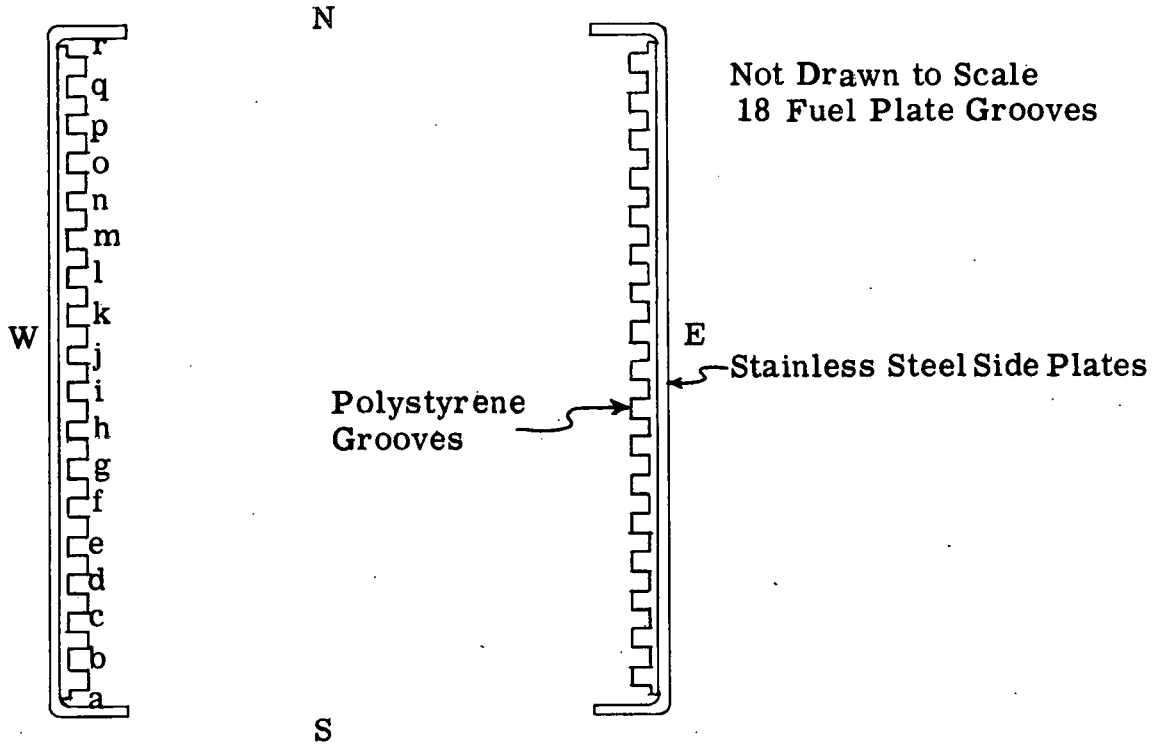

Control Rod Element Fuel Plate Arrangement

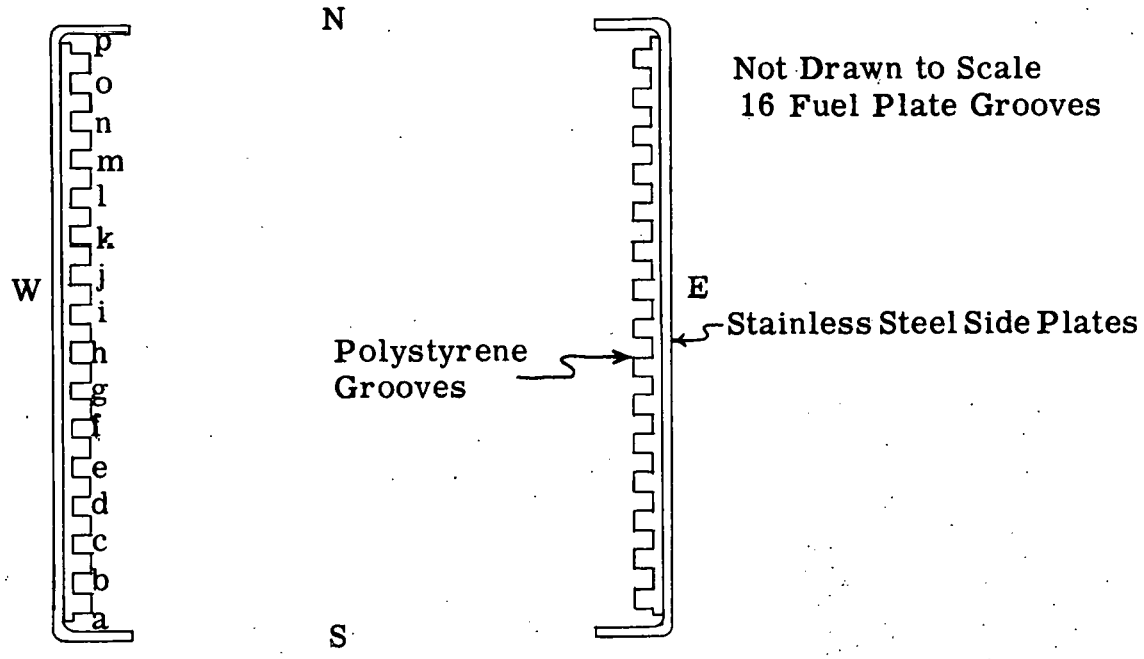

Figure 3.2 Fuel Plate Arrangement

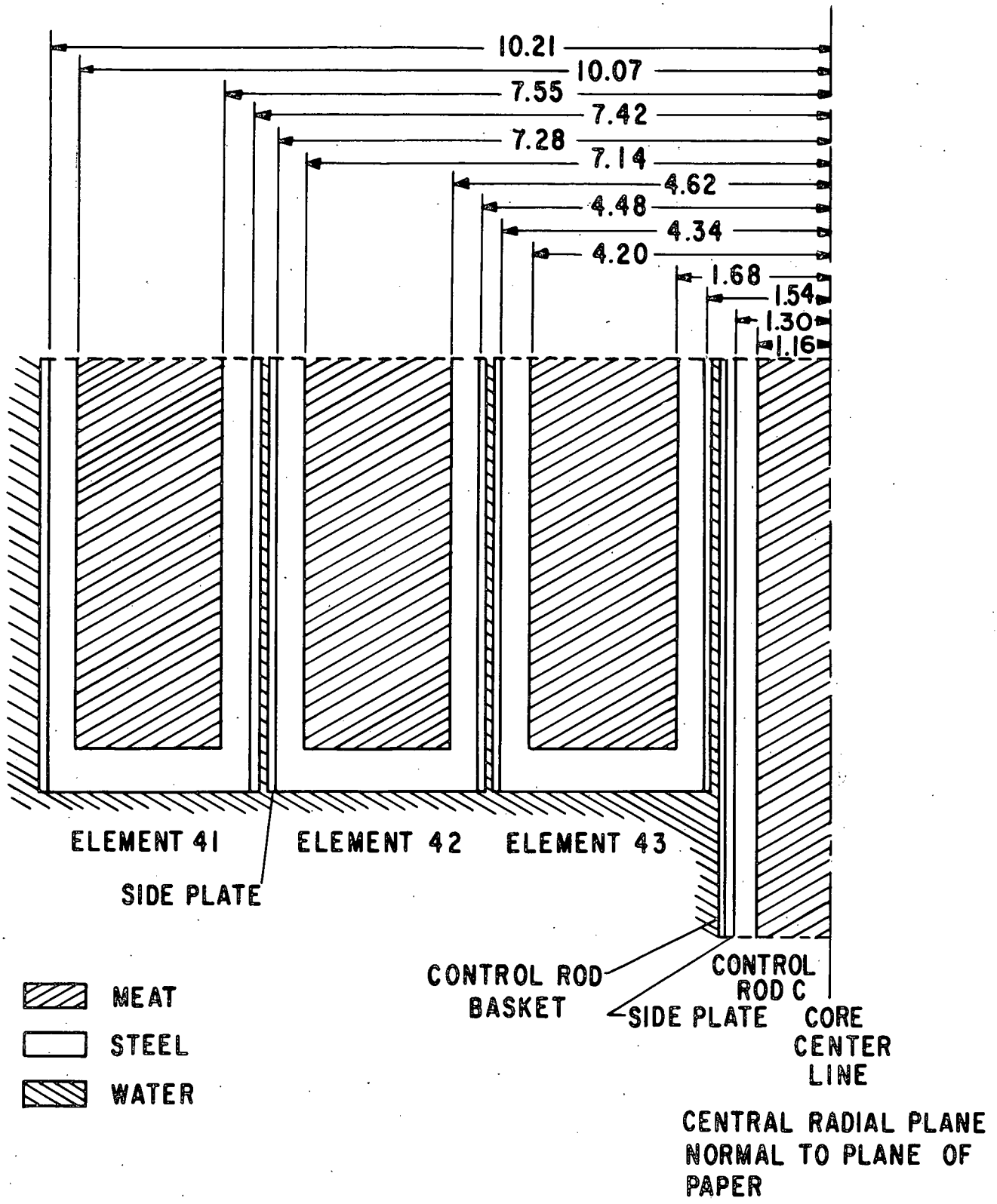

Figure 3.3 Location of Radial Planes Without Flow Divider, Section of Core Through Center of Elements in Positions 41, 42, 43 and 44

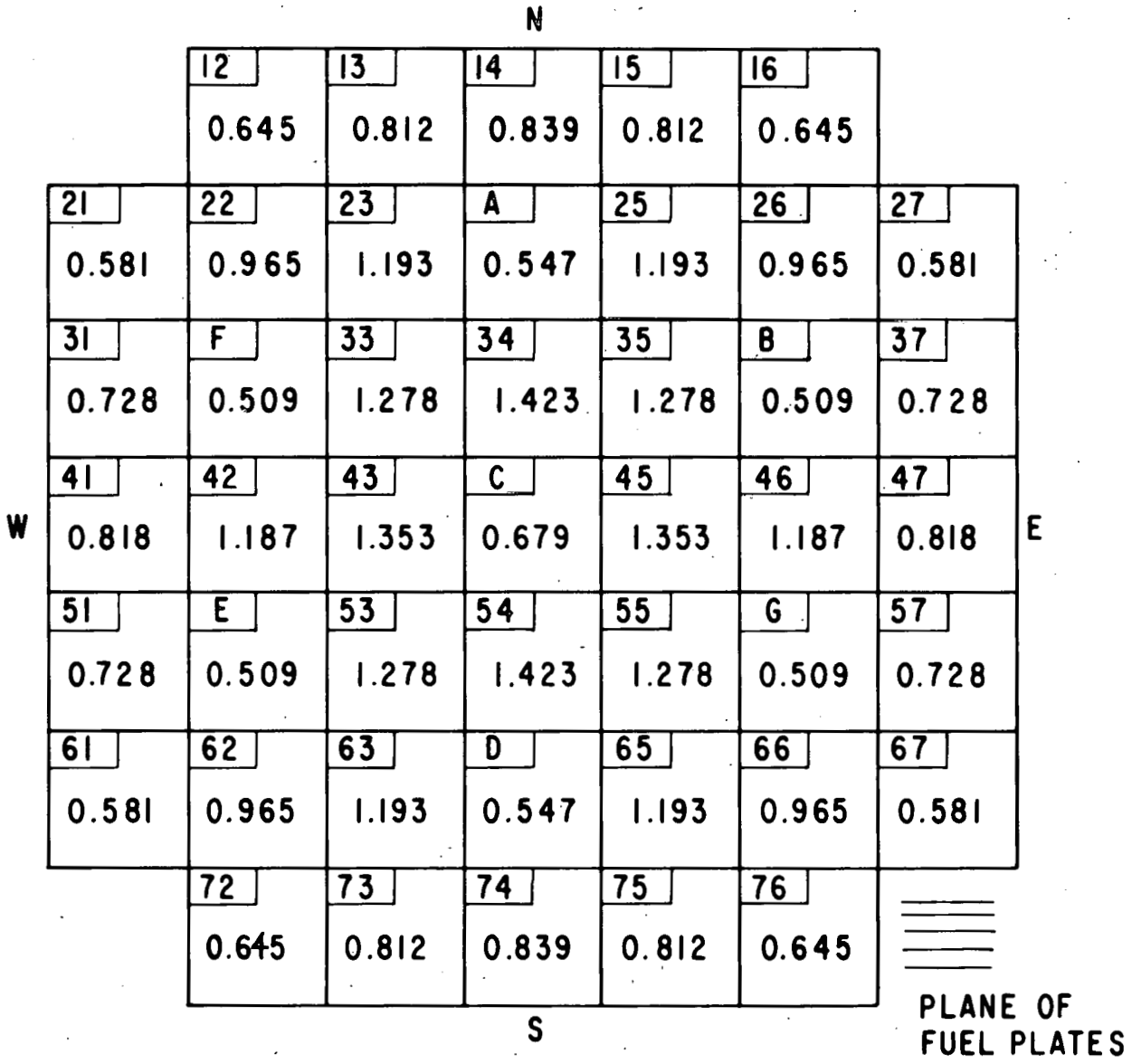

Figure 3.4 Relative Power Distribution in SM-2 Preliminary Mockup Core, Normalized to Core Average

Table 3.1
Relative Power Distribution Along Axial Traverses For Element in Position 12
SM-2 Preliminary Mockup Core

	Plate "a"					Plate "e"					Plate "j"				
Position	7.14 WRP	6.51 WRP	5.88 WRP	5.25 WRP	4.62 WRP	7.14 WRP	6.51 WRP	5.88 WRP	5.25 WRP	4.62 WRP	7.14 WRP	6.51 WRP	5.88 WRP	5.25 WRP	4.62 WRP
0	1.43		2.06		2.39						0.87		1.41		2.04
1	0.95		0.93		1.67						0.60		0.60		1.30
3	1.22		1.27		2.11						0.78		0.83		1.69
5	1.34	1.24	1.39	1.48	2.36	1.13	1.11	1.06	1.50	2.11	0.85	0.83	0.90	1.11	1.69
6															
6.94	1.30	1.22	1.30	1.46	2.20	1.06	0.95	1.13	1.22	2.03	0.85	0.81	0.87	1.00	1.76
7.64															
8.5	1.18		1.13		2.02						0.78		0.78		1.58
13	0.72		0.65		1.11						0.48		0.55		0.85
17			0.44										0.26		
21	0.19		0.16		.27						0.13		0.15		0.25

	Plate "n"					Plate "r"				
Position	7.14 WRP	6.51 WRP	5.88 WRP	5.25 WRP	4.62 WRP	7.14 WRP	6.51 WRP	5.88 WRP	5.25 WRP	4.62 WRP
0						0.56		0.74		1.04
1						0.53		0.46		0.83
3						0.56		0.63		1.02
5	0.81	0.74	0.85	0.91	1.48	0.63	0.58	0.69	0.81	1.13
6										
6.94	0.76	0.67	0.72	0.87	1.34	0.60	0.63	0.69	0.76	1.06
7.64										
8.5						0.56		0.58		1.06
13						0.37		0.39		0.67
17								0.21		
21						0.09		0.10		0.17

Table 3.2
Relative Power Distribution Along Axial Traverses For Element in Position 13
SM-2 Preliminary Mockup Core

	Plate "a"					Plate "e"					Plate "j"				
Position	4.20 WRP	3.57 WRP	2.94 WRP	2.31 WRP	1.68 WRP	4.20 WRP	3.57 WRP	2.94 WRP	2.31 WRP	1.68 WRP	4.20 WRP	3.57 WRP	2.94 WRP	2.31 WRP	1.68 WRP
0	2.56		2.31		2.93						2.06		2.08		2.41
1	1.67		1.20		2.08						1.27		0.76		1.61
3	2.24		1.55		2.68						1.57		1.02		1.94
5	2.23	1.64	1.76	1.74	2.87	2.20	1.32	1.32	1.43	2.54	1.69	1.13	1.15	1.28	2.08
6															
6.94	2.13	1.28	1.52	1.65	2.73	2.02	1.30	1.22	1.37	2.22	1.65	1.18	1.06	1.22	2.02
7.64															
8.5	1.98		1.32		1.99						1.52		0.97		1.71
13	1.13		0.76		1.02						0.95		0.56		0.97
17			0.41										0.30		
21	0.28		0.19		0.25						0.24		0.16		0.25

	Plate "n"					Plate "r"				
Position	4.20 WRP	3.57 WRP	2.94 WRP	2.31 WRP	1.68 WRP	4.20 WRP	3.57 WRP	2.94 WRP	2.31 WRP	1.68 WRP
0						1.20		1.06		1.30
1						0.87		0.63		1.02
3						1.09		0.83		1.28
5	1.65	1.00	0.95	1.13	1.65	1.30	0.85	0.90	0.95	1.32
6										
6.94	1.65	0.95	1.02	1.09	1.65	1.11	0.87	0.81	0.91	1.30
7.64										
8.5						0.97		0.83		1.15
13						0.58		0.48		0.67
17										
21						0.15		0.11		0.19

Table 3.3
Relative Power Distribution Along Axial Traverses For Element in Position 14
SM-2 Preliminary Mockup Core

	Plate "a"			Plate "e"			Plate "j"			Plate "n"			Plate "r"		
Position	1.26 WRP	0.63 WRP	CRP	1.26 WRP	0.63 WRP	CRP	1.26 WRP	0.63 WRP	CRP	1.26 WRP	0.63 WRP	CRP	1.26 WRP	0.65 WRP	CRP
0	2.89		2.35				2.62	2.17	2.28				1.32		1.29
1	2.12		1.43				1.50	0.94	0.94				.96		0.68
3	2.68		1.92				1.87	1.21	1.21				1.19		0.86
5		2.11	1.97	2.35	1.08	1.42	2.02	1.36	1.28	1.72	1.14	1.10	1.28	0.93	0.94
6	2.86		1.93				1.94		1.20				1.29		0.94
6.94	2.92	2.37	2.86	2.23	1.38	1.28	1.86	1.21	1.13	1.68	1.05	1.04	1.32	0.90	0.90
7.64	2.69		2.59				1.72		1.06				1.29		0.85
8.5	1.84		1.18				1.60	1.05	0.95				1.14		0.81
13	0.81		0.40				0.94	0.57	0.53				0.65		0.46
17	0.43		0.20				0.52	0.27	0.29				0.40		0.27
21	0.18		0.09				0.25	0.15	0.13				0.17		0.11

Table 3.4
Relative Power Distribution Along Axial Traverses For Element in Position 21
SM-2 Preliminary Mockup Core

	Plate "a"					Plate "e"					Plate "j"				
Position	10.07 WRP	9.44 WRP	8.81 WRP	8.18 WRP	7.55 WRP	10.07 WRP	9.44 WRP	8.81 WRP	8.18 WRP	7.55 WRP	10.07 WRP	9.44 WRP	8.81 WRP	8.18 WRP	7.55 WRP
0	1.04		1.61		2.41						0.97		1.52		2.41
1	0.72		0.87								0.67		0.67		1.57
3	0.95		1.11		2.20						0.85		0.83		1.85
5	1.10	1.00	1.18	1.41	2.20	1.04	0.85	0.97	1.18	2.24	0.95	0.81	0.95	1.11	1.99
6															
6.94	1.00	1.04	1.10	1.24	2.11	0.97	0.87	0.91	1.09	2.11	0.97	0.69	0.85	1.04	1.83
7.64															
8.5	0.90		0.91		1.67						0.81		0.74		1.61
13	0.53		0.50		G.72						0.50		0.39		0.90
17	0.26	0.30	0.28	0.32	G.41						0.26	0.24	0.24	0.26	
21	0.13	0.12	0.10	0.10	0.18						0.10	0.08	0.10	0.12	0.21

	Plate "n"					Plate "r"				
Position	10.07 WRP	9.44 WRP	8.81 WRP	8.18 WRP	7.55 WRP	10.07 WRP	9.44 WRP	8.81 WRP	8.18 WRP	7.55 WRP
0						0.48		0.74		1.24
1						0.44		0.44		0.93
3						0.46		0.58		1.27
5	0.81	0.65	0.83	0.87	1.85	0.56	0.55	0.69	0.78	1.37
6										
6.94	0.74	0.69	0.76	0.90	1.65	0.55	0.50	0.60	0.74	1.37
7.64										
8.5						0.53		0.53		1.18
13						0.30		0.35		0.67
17						0.18	0.18	0.19	0.24	0.39
21						0.06	0.11	0.08	0.12	0.18

Table 3.5
Relative Power Distribution Along Axial Traverses For Element in Position 22
SM-2 Preliminary Mockup Core

	Plate "a"					Plate "e"					Plate "j"				
Position	7.14 WRP	6.51 WRP	5.88 WRP	5.25 WRP	4.62 WRP	7.14 WRP	6.51 WRP	5.88 WRP	5.25 WRP	4.62 WRP	7.14 WRP	6.51 WRP	5.88 WRP	5.25 WRP	4.62 WRP
0	2.26		2.20		3.37						2.39		2.28		3.70
1	1.65		1.55		2.56						1.43		1.09		2.26
3	2.20		2.04		3.45						1.80		1.32		2.72
5	2.43	1.64	2.20	2.45	3.45	2.26	1.57	1.57	1.74	2.93	1.96	1.34	1.43	1.69	2.82
6	2.36		2.15		3.49						2.13		1.41		2.84
6.94	2.35	2.26	2.36	2.54	3.39	2.04	1.48	1.39	1.52	2.80	1.89	1.30	1.27	1.52	2.56
7.64	2.48		2.45		3.39						1.80		1.20		2.54
8.5	2.91		1.20		2.39						1.59		1.20		2.26
13	0.58		0.48		1.00						0.97		0.63		1.22
17											0.50		0.35		0.65
21	0.13		0.12		2.48						0.25		0.17		0.27

	Plate "n"					Plate "r"				
Position	7.14 WRP	6.51 WRP	5.88 WRP	5.25 WRP	4.62 WRP	7.14 WRP	6.51 WRP	5.88 WRP	5.25 WRP	4.62 WRP
0						1.67		1.78		2.77
1						1.18		1.00		1.76
3						1.39		1.27		2.28
5	1.98	1.22	1.32	1.48	2.72	1.52	1.22	1.30	1.34	2.48
6						1.52		1.27		2.61
6.94	1.69	1.27	1.34	1.43	2.39	1.30	1.18	1.28	1.39	2.33
7.64						1.39		1.28		2.15
8.5						1.34		1.09		2.26
13						0.78		0.65		1.22
17										
21						0.24		0.15		3.07

Table 3.6
Relative Power Distribution Along Axial Traverses For Element in Position 23
SM-2 Preliminary Mockup Core

	Plate "a"					Plate "e"					Plate "j"				
Position	4.20 WRP	3.57 WRP	2.94 WRP	2.31 WRP	1.68 WRP	4.20 WRP	3.57 WRP	2.94 WRP	2.31 WRP	1.68 WRP	4.20 WRP	3.57 WRP	2.94 WRP	2.31 WRP	1.68 WRP
0	3.82		3.56		4.00						3.67		3.65		3.42
1	2.48		1.65		2.78								1.34		2.62
3	3.08		2.04		3.52						2.63		1.64		3.05
5	3.32	2.20	2.15	2.45	3.76	3.24	1.83		1.98	3.58	2.96	1.71	1.78	1.94	3.27
6	3.21		2.20		3.74						2.84		1.83		
6.94	3.02	1.92	1.96	2.04	3.56	2.72	1.69	1.87	1.85	3.49	2.59	1.57	1.65	1.64	3.19
7.64	2.80		1.87		3.19						2.52		1.61		3.02
8.5	2.24				2.48						2.31		1.50		1.98
13	1.02		0.78		1.06						1.34		0.76		0.85
17											0.72		0.48		0.41
21	0.27		0.18		0.25						0.39		0.20		0.24

	Plate "n"					Plate "r"				
Position	4.20 WRP	3.57 WRP	2.94 WRP	2.31 WRP	1.68 WRP	4.20 WRP	3.57 WRP	2.94 WRP	2.31 WRP	1.68 WRP
0						2.96		2.80		3.26
1						1.74		1.22		2.24
3						2.28		1.50		2.73
5	2.70	1.69	1.74	1.71	2.96	2.36	1.65	1.69	1.71	2.73
6						2.43		1.59		2.93
6.94	2.45	1.55			3.21	2.36	1.59	1.50	1.64	2.82
7.64						2.26		1.48		2.68
8.5						1.99		1.32		2.02
13						1.24		0.72		0.90
17										
21						0.32		0.18		0.20

Table 3.7
Relative Power Distribution Along Axial Traverses For Element in Position 31
SM-2 Preliminary Mockup Core

	Plate "a"					Plate "e"					Plate "j"				
Position	10.07 WRP	9.44 WRP	8.81 WRP	8.18 WRP	7.55 WRP	10.07 WRP	9.44 WRP	8.81 WRP	8.18 WRP	7.55 WRP	10.07 WRP	9.44 WRP	8.81 WRP	8.18 WRP	7.55 WRP
0	1.32		1.99		2.65						1.46		2.22		2.59
1	0.93		0.95		1.83						.90		0.87		1.80
3	1.15		1.27		2.33						1.06		1.11		2.28
5	1.24	1.18	1.27	1.52	2.65	1.30	1.09	1.24	1.41	2.59	1.22	0.97	1.18	1.39	2.36
6	1.22		1.22		2.65						1.24		1.09		2.36
6.94	1.11	1.04	1.18	1.34	2.41	1.11	.91	1.04	1.28	2.52	1.11	0.93	1.00	1.24	2.56
7.64	1.02		1.09		2.48						1.18		0.95		2.61
8.5	0.95		0.97		1.85						1.15		0.85		1.46
13	0.53		0.53								0.60		0.50		0.69
17											0.32		0.21		0.48
21	0.15		0.13		0.17						0.15		0.12		0.24

	Plate "n"					Plate "r"				
Position	10.07 WRP	9.44 WRP	8.81 WRP	8.18 WRP	7.55 WRP	10.07 WRP	9.44 WRP	8.81 WRP	8.18 WRP	7.55 WRP
0						1.28		1.98		2.54
1						.81		0.87		1.78
3						1.04		1.09		2.08
5	1.48	0.93	1.20	1.34	2.33	1.15	0.97	1.18	1.34	2.17
6						1.13		1.13		2.28
6.94	1.13	0.95	1.04	1.30	2.45	1.13	1.02	1.04	1.24	2.45
7.64						1.04		0.93		2.20
8.5						1.00		1.00		1.67
13						0.55		0.53		0.65
17										
21						0.13		0.11		0.17

Table 3.8
Relative Power Distribution Along Axial Traverses for Element in Position 33
SM-2 Preliminary Mockup Core

	Plate "a"					Plate "e"					Plate "j"				
Position	4.20 WRP	3.57 WRP	2.94 WRP	2.31 WRP	1.68 WRP	4.20 WRP	3.57 WRP	2.94 WRP	2.31 WRP	1.68 WRP	4.20 WRP	3.57 WRP	2.94 WRP	2.31 WRP	1.68 WRP
0	3.76		3.81		4.32						3.67		4.19		5.00
1	2.87		1.85		2.91						2.72		1.57		2.82
3	3.24		2.36		3.76						2.89		1.98		3.44
5	3.42	2.63	2.48	2.69	4.04	3.61	2.15	2.08	2.08	3.49	4.04	2.08	2.11	2.28	3.58
6	3.49		2.27		3.93						3.28		1.96		3.52
6.94	3.37	2.15	2.24	2.41	3.45	3.81	1.94	1.92	2.04	3.15	3.33	1.89	1.96	1.94	3.30
7.64	3.12		1.87		3.58						3.17		1.71		3.00
8.5	2.36		1.74		2.91						2.48		1.52		2.36
13	0.95		0.85		1.41						1.02		0.74		1.30
17													0.35		
21	0.24		0.17		0.27						0.25		0.19		

	Plate "n"					Plate "r"				
Position	4.20 WRP	3.57 WRP	2.94 WRP	2.31 WRP	1.68 WRP	4.20 WRP	3.57 WRP	2.94 WRP	2.31 WRP	1.68 WRP
0						3.70		3.81		3.91
1						2.54		1.57		2.56
3						2.82		2.02		3.19
5	3.58	1.94	1.83	2.02	3.49	3.19	2.08	2.11	2.22	3.52
6						3.21		2.02		3.26
6.94	3.63	2.06	1.96	2.22	3.54	3.00	1.98	1.89	1.98	3.26
7.64						3.00		1.71		2.84
8.5						2.31		1.52		2.48
13						0.91		0.76		1.02
17										
21						0.26		0.17		0.25

Table 3.9
Relative Power Distribution Along Axial Traverses For Element in Position 34
SM-2 Preliminary Mockup Core

	Plate "a"			Plate "e"			Plate "j"			Plate "n"			Plate "r"		
Position	1.26 WRP	0.63 WRP	CRP	1.26 WRP	0.63 WRP	CRP	1.26 WRP	0.63 WRP	CRP	1.26 WRP	0.63 WRP	CRP	1.26 WRP	0.63 WRP	CRP
0	4.46		3.21	5.22		4.39	5.50		4.54	5.00		4.14	4.14		3.44
1	3.63		2.24	3.10		1.67	2.78		1.67	2.96		1.76	3.08		2.06
3	4.32		2.70	3.70		2.13	3.33		2.15	3.63		2.13	2.15		2.41
5	4.32	3.15	3.02	3.89	2.33	2.36	3.63	2.20	2.20	3.67	2.28	2.26	3.70	2.70	2.56
6	4.23		2.84	3.63		2.13	3.58		2.15	3.70		2.11	3.84		2.54
6.94	4.30	3.47	3.37	3.24	2.20	2.04	3.47	2.36	1.96	3.21	2.20	2.11	3.26	2.61	2.70
7.64	3.93		3.63	3.24		1.94	3.02		1.89	3.10		1.87	3.58		2.89
8.5	2.73		1.78	2.82		1.61	2.63		1.50	2.28		1.69	2.39		1.59
13	1.09		0.63	1.22		0.76	1.39		0.85	1.30		0.87	1.24		0.74
17									0.44						0.39
21	0.28		0.17	0.35		0.21	0.34		0.35	0.45		0.26	0.34		0.26

Table 3.10
Relative Power Distribution Along Axial Traverses For Element in Position 41
SM-2 Preliminary Mockup Core

	Plate "a"	Plate "j"					Plate "n"					Plate "r"				
Position	8.81 WPR	10.07 WRP	9.44 WRP	8.81 WRP	8.18 WRP	7.55 WRP	10.07 WRP	9.44 WRP	8.81 WRP	8.18 WRP	7.55 WRP	10.07 WRP	9.44 WRP	8.81 WRP	8.18 WRP	7.55 WRP
0	2.24	1.48		2.31		3.54	1.37		2.36		3.49	1.55		2.35		3.00
1	0.91	0.93		0.93		2.13	0.97		.93		2.17	0.91		0.97		2.06
3	1.22	1.15		1.20		2.36	1.18		1.28		2.59	1.22		1.27		2.50
5	1.28	1.20	1.18		1.46	2.54	1.22	1.15	1.27	1.60	2.63	1.30	1.18	1.28	1.47	2.31
6	1.30	1.24		1.27		2.56	1.27		1.30		2.63	1.34		1.37		2.48
6.94	1.24	1.13	1.02	1.13	1.30	2.41	1.11	1.02	1.15	1.37	2.43	1.20	1.09	1.22	1.43	2.43
7.64	1.22	1.13		1.13		2.15	1.15		1.15		2.22	1.11		1.22		2.28
8.5	1.00	0.95		0.97		1.96	1.09		0.95		1.96	1.00		1.00		1.61
13	0.53	0.58		0.58		1.09	0.56		0.55		0.95	0.63		0.63		0.78
21	0.16	0.19		0.18		0.30	0.16		0.13		0.25	0.16		0.16		0.21

Table 3.11
Relative Power Distribution Along Axial Traverses For Element in Position 42
SM-2 Preliminary Mockup Core

	Plate "j"					Plate "n"					Plate "r"				
Position	7.14 WRP	6.51 WRP	5.88 WRP	5.25 WRP	4.62 WRP	7.14 WRP	6.51 WRP	5.88 WRP	5.25 WRP	4.62 WRP	7.14 WRP	6.51 WRP	5.88 WRP	5.25 WRP	4.62 WRP
0	3.86		3.49		4.21	3.72		3.93		4.56	3.37		3.30		4.50
1	2.31		1.41		2.52	2.31		1.39		2.61	2.73		1.69		3.00
3	2.82		1.80		3.15	2.87		1.98		3.33	2.73		2.24		3.72
5	2.82	1.83	1.83	2.13	3.39	2.84	1.96	1.92	2.36		3.00	2.17	2.35	2.54	3.44
6	2.68		1.80		3.39	2.87		1.89		3.58	2.82		2.06		3.70
6.94	2.52	1.59	1.69	1.87	3.00	2.61	1.67	1.87	2.43	3.82	2.96	2.24	2.45	2.70	3.52
7.64	2.33		1.52		2.84	2.50		1.80		3.00	2.84		2.76		3.56
8.5	1.99		1.34		2.91	2.02		1.61		3.00	2.17		1.48		2.59
13	1.00		0.67		1.27	0.90		0.63		1.20	0.72		0.44		1.06
17															
21	0.25		0.16		0.27	0.25		0.18		0.26	0.18		0.12		0.26

Table 3.12
Relative Power Distribution Along Axial Traverses For Element in Position 43
SM-2 Preliminary Mockup Core

	Plate "j"					Plate "n"					Plate "r"				
Position	4.20 WRP	3.57 WRP	2.94 WRP	2.31 WRP	1.68 WRP	4.20 WRP	3.57 WRP	2.94 WRP	2.31 WRP	1.68 WRP	4.20 WRP	3.57 WRP	2.94 WRP	2.31 WRP	1.68 WRP
0	4.83		4.54		4.46	4.74		4.28		4.76	4.21		4.44		4.46
1	2.70		1.64		3.28	2.59		1.71		3.39	2.65		1.65		3.24
3	3.26		2.13		4.02	3.24		2.17		4.02	3.28		2.70		3.63
5	3.39	2.26	2.24	2.43	4.09	3.65	2.35	2.28	2.36	4.21	3.19	2.33	2.39	1.80	3.98
6	3.44		2.17		4.04	3.58		2.26		4.13	3.42		2.22		3.91
6.94	3.07	1.94	1.92	2.20	4.54	3.37	2.02	1.98	2.17	4.28	3.35	2.13	2.15	2.33	3.89
7.64	3.00		1.76		4.13	2.91		1.80		3.91	3.19		1.96		3.67
8.5	2.63		1.67		2.48	2.56		1.64		2.54	2.39		1.69		2.68
13	1.27		0.72		0.90	1.22		0.78		0.85	1.02		0.85		1.06
17															
21	0.27		0.18		0.21	0.26		0.18		0.18	0.26		0.18		0.22

Table 3.13
Relative Power Distribution Along Axial Traverses For Element in Position 24 (Control Rod A)
SM-2 Preliminary Mockup Core

	Plate "a"			Plate "d"			Plate "i"			Plate "m"			Plate "p"		
Position	1.16 WRP	0.58 WRP	CRP	1.16 WRP	0.58 WRP	CRP	1.16 WRP	0.58 WRP	CRP	1.16 WRP	0.58 WRP	CRP	1.16 WRP	0.58 WRP	CRP
0	2.89	1.99	1.92	2.41	1.37	1.39	2.31	1.24	1.18	1.99	1.27	1.18	2.36	1.39	1.39
1	2.59	1.99	3.72	2.54	1.61	1.59	2.39	1.59	1.39	2.28	1.48	1.46	2.17	1.64	1.55
3	3.45	2.48	2.43	2.72	2.10	2.02	3.08	1.92	1.89	2.95	1.78	1.83	2.91	1.89	1.89
5	3.39	2.59	2.52	3.12	2.04	2.08	3.28	2.02	1.98	2.91	1.94	1.85	2.84	2.04	2.04
6	3.39	2.59	2.41	3.21	2.13	2.08	3.43	1.99	2.04	2.95	2.13	1.89	3.08	2.13	1.99
6.94	4.87	5.24	5.00	5.41	5.85	6.21	5.62	6.08	6.43	5.17	5.89	6.19	4.52	4.54	4.76

Table 3.14
Relative Power Distribution Along Axial Traverses For Element in Position 44 (Control Rod C)
SM-2 Preliminary Mockup Core

	Plate "a"	Plate "d"	Plate "i"					Plate "m"				
Position	CRP	CRP	1.16 WRP	0.58 WRP	CRP	0.58 ERP	1.16 ERP	1.16 WRP	0.58 WRP	CRP	0.58 ERP	1.16 ERP
0	1.98	1.50	2.82	1.59	1.50	1.59		2.96	1.59	1.48	1.52	2.91
1	2.15	1.92	3.24	1.94	1.89	1.98	3.21	3.07	1.96	1.78	1.94	3.10
3	2.59	2.22	3.82	2.45	2.31	2.36	3.80	3.74	2.35	2.31	2.31	
5	2.76	2.41	4.13	2.61	2.43	2.45	4.02	3.86	2.48	2.48	2.52	
6	2.59	2.41	3.91	2.54	2.48	2.52	4.00	3.82	2.33	2.33	2.43	4.04
6.94	5.52	6.80	6.33	6.98	7.88	7.49		6.34	7.02	7.74	7.19	6.28

	Plate "p"				
Position	1.16 WRP	0.58 WRP	CRP	0.58 ERP	1.16 ERP
0	3.21	2.22	2.15	1.98	3.17
1	3.35	2.36	2.15	2.13	3.19
3	3.89	2.20	2.68	2.68	4.00
5	4.17	3.08	3.00	2.84	4.39
6	4.32	3.00	2.82	2.89	4.16
6.94	5.99	6.33	6.82	6.78	5.96

Table 3.15
Relative Power Distribution Along Axial Traverses For Element in Position 32 (Control Rod F)
SM-2 Preliminary Mockup Core

	Plate "a"					Plate "d"					Plate "i"				
Position	7.03 WRP	6.46 WRP	5.88 WRP	5.30 WRP	4.73 WRP	7.03 WRP	6.46 WRP	5.88 WRP	5.30 WRP	4.73 WRP	7.03 WRP	6.46 WRP	5.88 WRP	5.30 WRP	4.73 WRP
0	1.96		1.61		2.78	1.69		1.13		2.59	1.69		1.04		2.41
1	1.99		1.69		2.73	1.80		1.39		2.61	1.85		1.34		2.63
3	2.39				3.28	2.26		1.71		3.28	2.28		1.83		3.14
5	2.45	1.99	2.35	2.36	3.37	2.45	1.64	1.65	1.92	3.47	2.45	1.74	1.83	2.02	3.21
6	2.54		2.08		3.45	2.43		1.83		3.44	2.45		1.80		3.26
6.94	3.60		4.69	4.91	4.65	4.13	4.93	5.80	5.85	5.61	4.21	5.36	5.96	5.80	5.32

	Plate "m"					Plate "p"				
Position	7.03 WRP	6.46 WRP	5.88 WRP	5.30 WRP	4.73 WRP	7.03 WRP	6.46 WRP	5.88 WRP	5.30 WRP	4.73 WRP
0	1.61		1.00		2.31	1.83		1.27		2.24
1	1.76		1.27		2.45	1.69		1.43		2.36
3	2.11		1.55		3.21	2.13		1.78		2.91
5	2.17	1.57	1.69	1.80	3.02		1.78	1.87	1.87	3.00
6	2.28		1.65		3.21	2.28		1.78		3.08
6.94	4.21	5.06	5.39	5.39	5.13	3.58	3.95	4.44	4.16	4.35

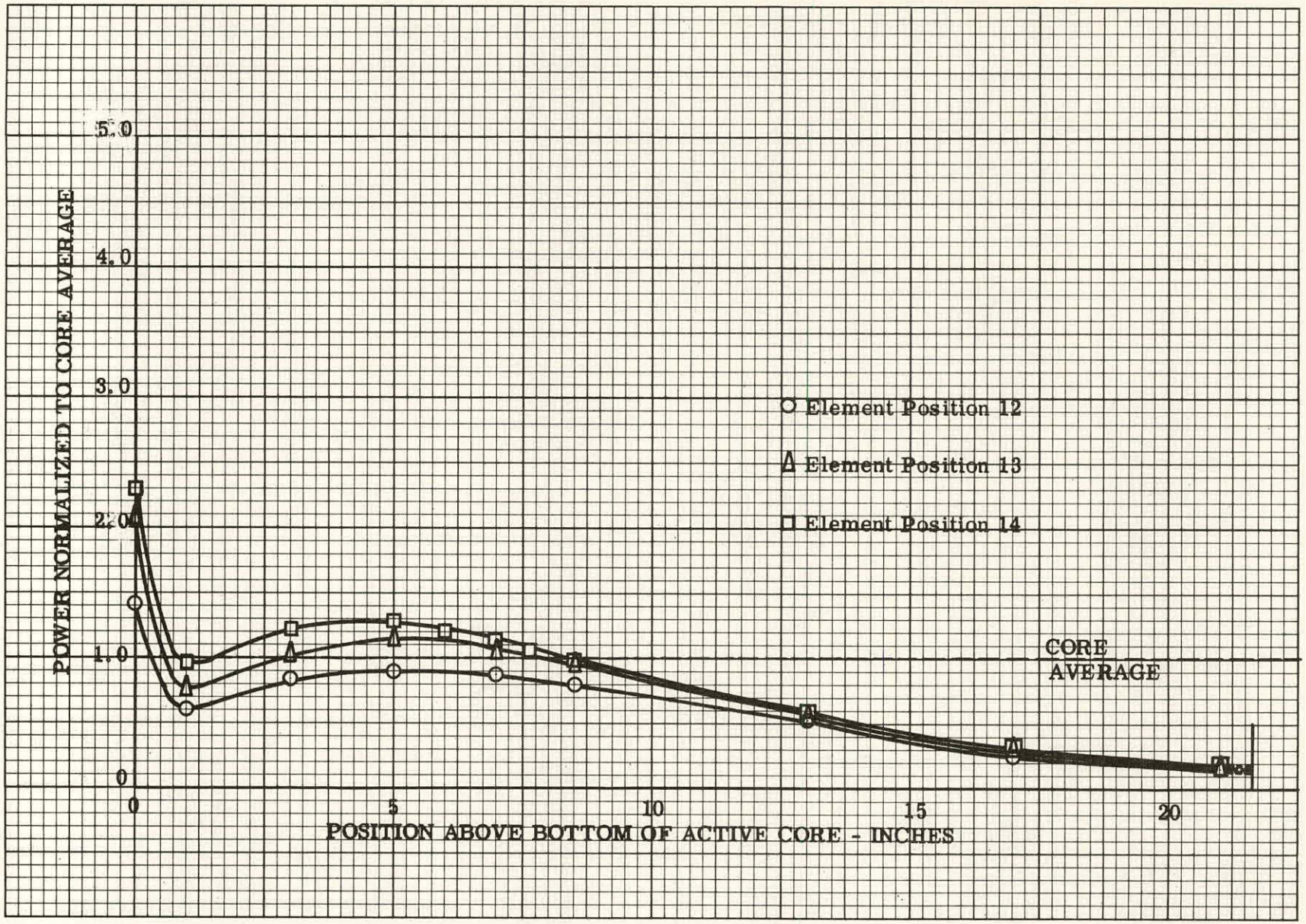

Figure 3.5 Relative Power Distribution Along Axial Traverse on Centerline of Fuel Plate "j", Elements in Positions 12, 13 and 14, SM-2 Preliminary Mockup Core

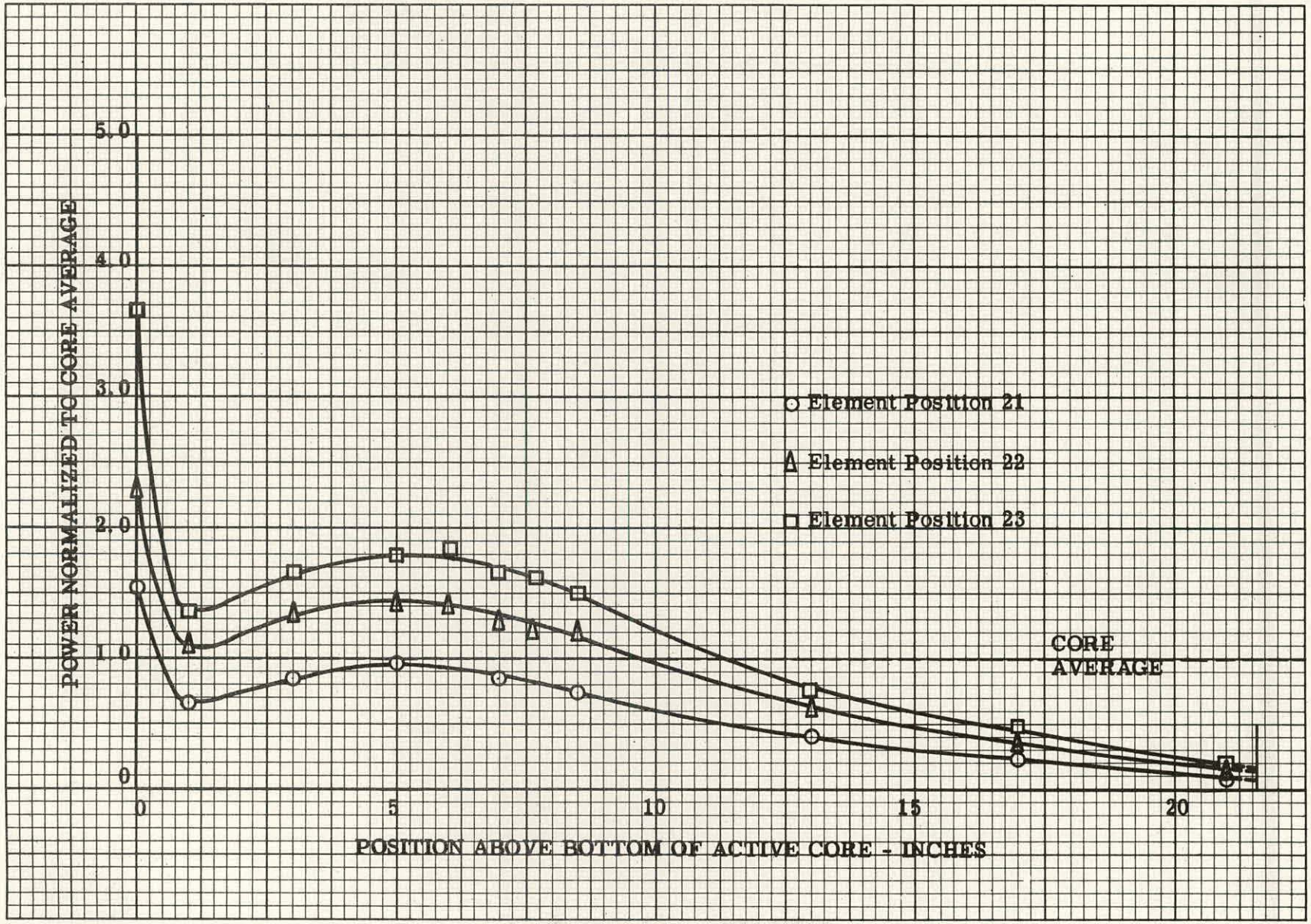

Figure 3.6 Relative Power Distribution Along Axial Traverse on Centerline of Fuel Plate "j", Elements in Positions 21, 22 and 23, SM-2 Preliminary Mockup Core

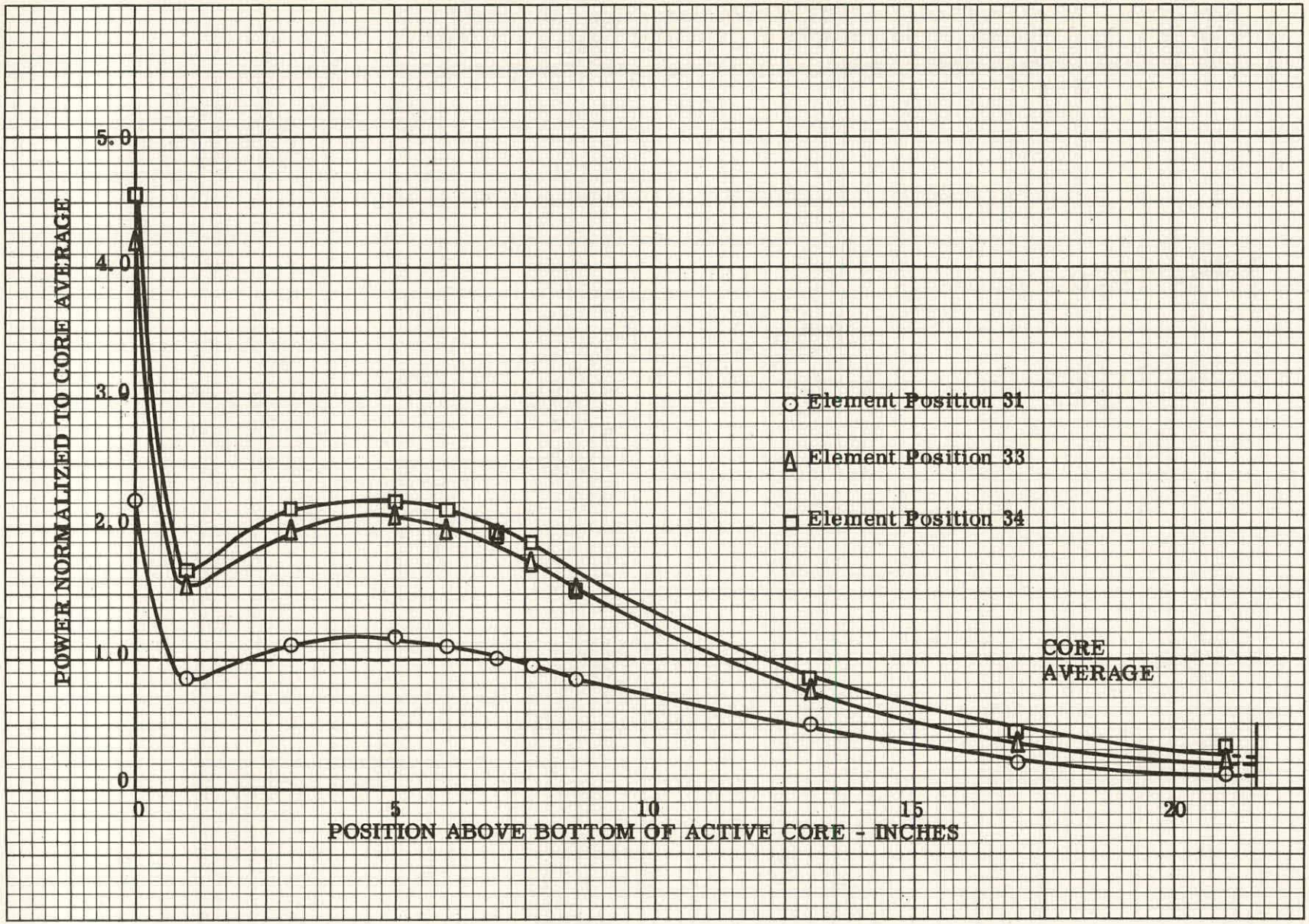

Figure 3.7 Relative Power Distribution Along Axial Traverse on Centerline of Fuel Plate "j", Elements in Positions 31, 33 and 34, SM-2 Preliminary Mockup Core

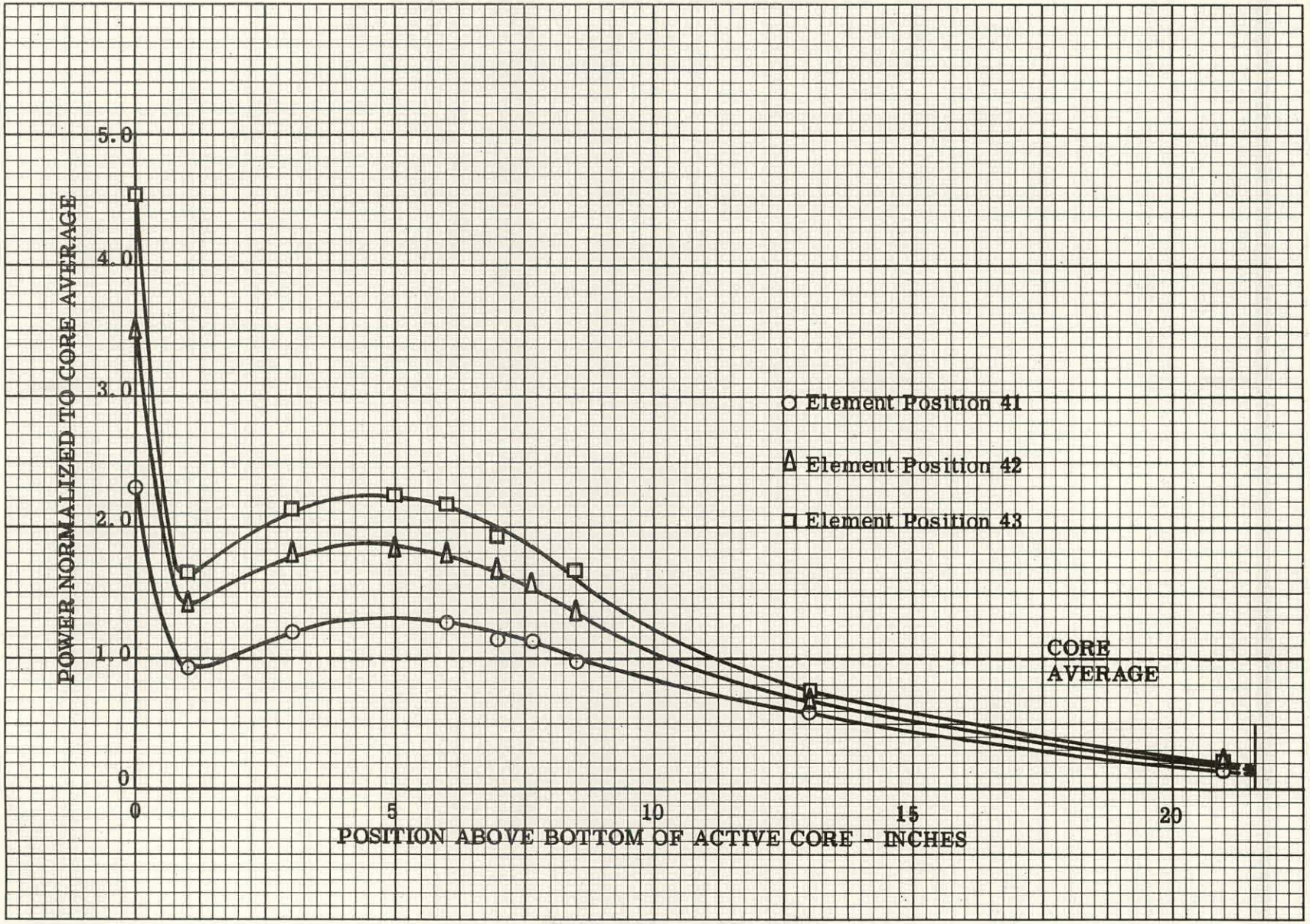

Figure 3.8 Relative Power Distribution Along Axial Traverse on Centerline of Fuel Plate "j", Elements in Positions 41, 42 and 43, SM-2 Preliminary Mockup Core

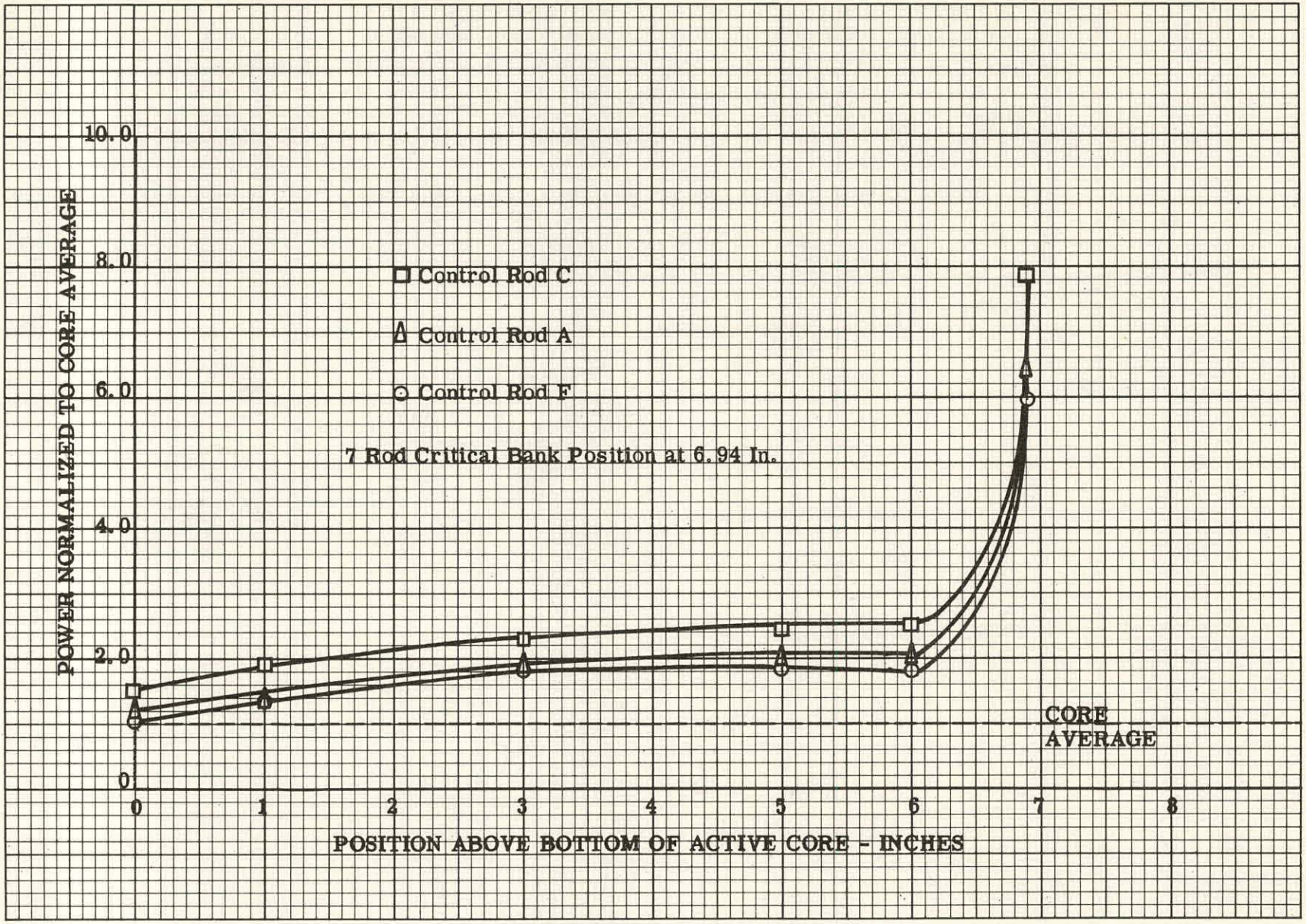

Figure 3.9 Relative Power Distribution Along Axial Traverse on Centerline of Fuel Plate "i" of Control Rods A, C and F, SM-2 Preliminary Mockup Core

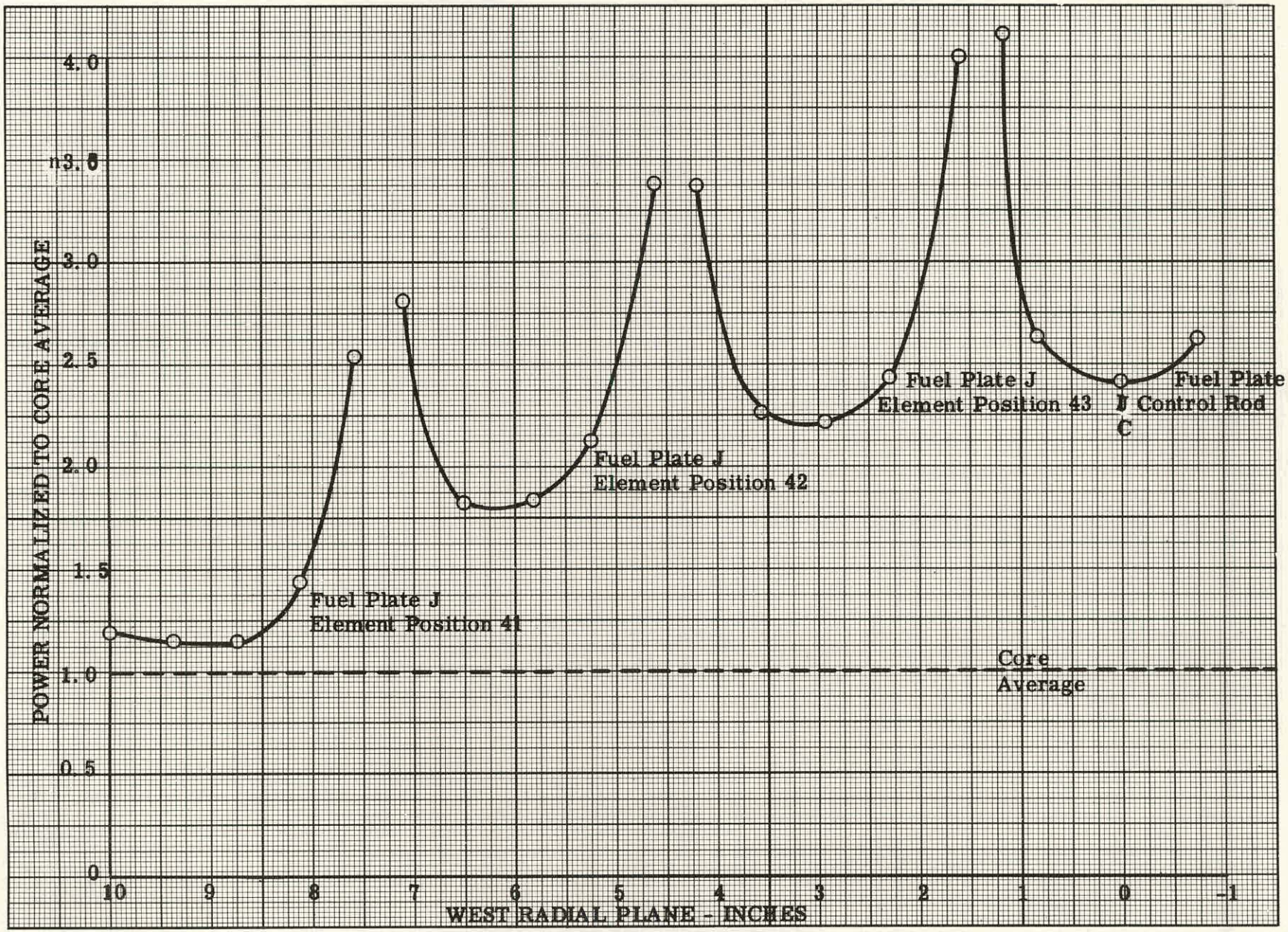

Figure 3.10 Relative Power Distribution Along Radial Traverse 5 In. Above Bottom of Active Core, SM-2 Preliminary Mockup Core

THIS PAGE

WAS INTENTIONALLY

LEFT BLANK

Figure 3.11 gives the complete normalized power averages in the core. Fourteen stationary fuel elements surrounding the center of the core exceed the core average, while all elements at the core boundary are less than the core average. The control rod fuel elements which have higher than average power density have been corrected to include only the portion of the fuel plates actually in the active core.

Tables 3.16 through 3.30 present the activity distributions normalized to a core average of unity along axial traverses of stationary fuel elements in positions 12, 13, 14, 21, 22, 23, 31, 33, 34, 41, 42, 43 and for fuel elements of control rods A, C, and F in positions 24, 44, and 32, respectively. Again plates a, e, j, n and r were selected for mapping for stationary fuel elements and plates a, d, i, m, and p for the control rod fuel elements.

The use of the data tables is identical to that described previously (ref. par. 3.2.3); however due to the relocation of the outer fuel elements in order to accommodate the flow divider mockup, the data points in these fuel elements are slightly displaced relative to those recorded in the preliminary SM-2 core mockup.

The data ranged from normalized lows of 0.09 and 0.10 of the core average for plate "r" of elements 21 and 12 at the outer edge of the core to highs of 4.74 for plate "r" of element position 43, 4.62 for plate "p" of control rod C, and 4.57 for plate "a" of element position 34, all in the center of the core. As expected the flux suppressors placed at the top of the active meat of fuel elements of control rods considerably reduced the power spikes (ref. Fig. 3.9) usually occurring in that region.

Figures 3.12 and 3.13 respectively show the activity of the centerline traverses of plate "j" for stationary fuel elements in positions 12, 13, 14 and 21, 22, 23 normalized to the core average. Figures 3.14 and 3.15 show similar traverses for fuel elements in positions 31, 33, 34 and 41, 42, 43 respectively. Figure 3.16 shows the same traverses for plate "i" of control rods A, C, and F.

For the stationary fuel elements again there is a large power peak at the bottom of the active core and a smaller axial peak about 5-7 in. above it. The power diminishes gradually until a low is reached at the top of the active core. As an example, along the centerline traverse of plate "j" of element position 43 the power peaking is about 4.3 times the core average at the bottom of the active core and 2.3 times at an axial position 5 in. above it. It is only 0.2 of the core average at the top of the active core. For the portion of the control rod fuel elements actually in the core, only one power peak is apparent at an axial position 5-6 in. above the bottom of the active core with a large dip at the bottom of the flux suppressors. Taking the centerline traverse along plate "i" of control rod C, the highest normalized relative power of 2.47 occurs 6 in. above the bottom of the active core while it is only 0.95 at the bottom of the flux suppressor.

Figure 3.17 illustrates a radial power traverse 5 in. above the bottom of the active core along the center of stationary fuel elements in positions 41, 42, 43 and control rod C in position 44. The rise in power operation is evident as the

THIS PAGE

WAS INTENTIONALLY

LEFT BLANK

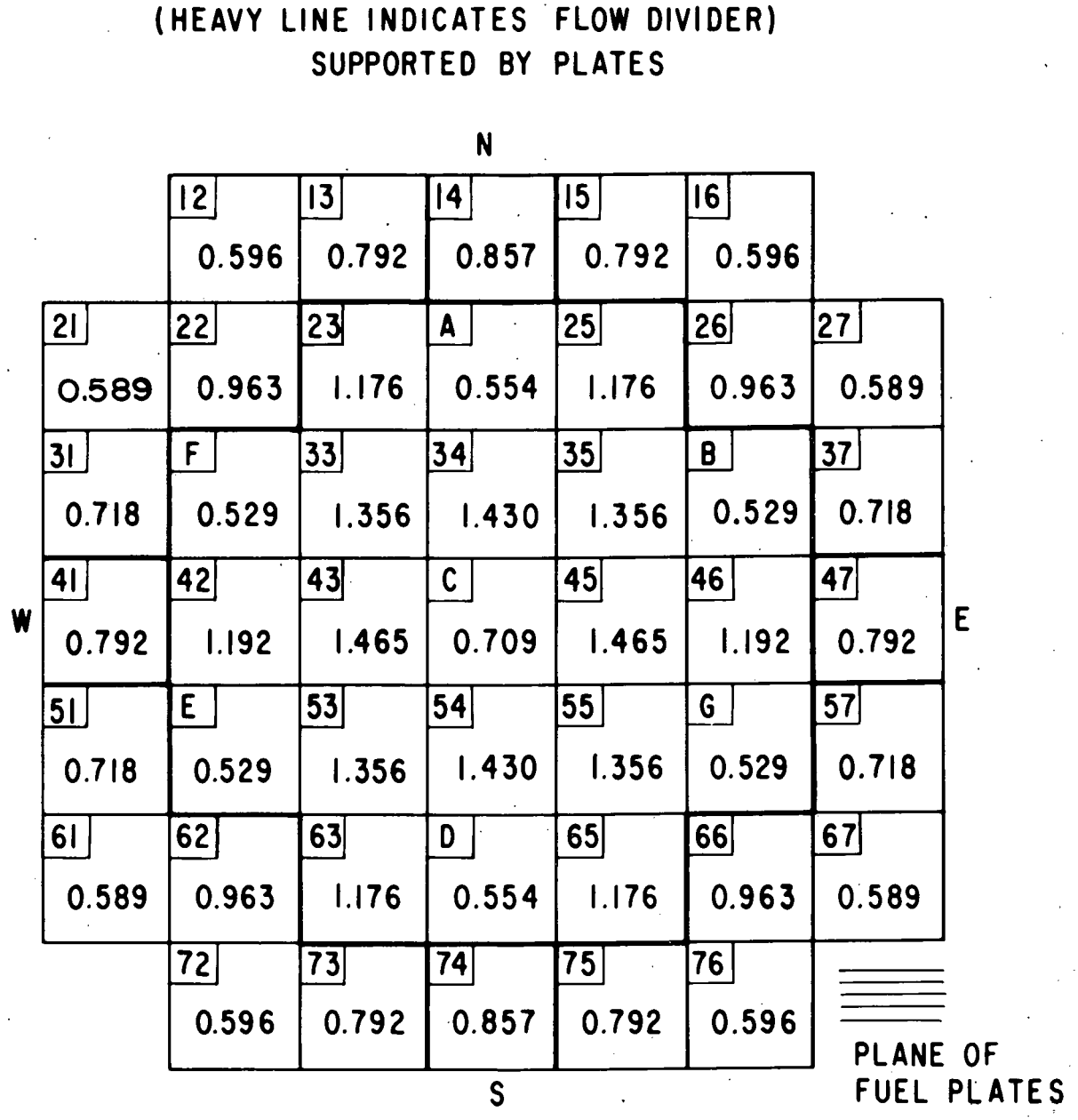

Figure 3.11 Relative Power Distribution in the SM-2 Final Mockup Core, Normalized to Core Average

Table 3.16
Relative Power Distribution Along Axial Traverses for Element in Position 12
"SM-2 Final Mockup Core"

	Plate "a"					Plate "e"					Plate "j"				
Position	7.27"WRP	6.64"WRP	6.01"WRP	5.38"WRP	4.75"WRP	7.27"WRP	6.64"WRP	6.01"WRP	5.38"WRP	4.75"WRP	7.27"WRP	6.64"WRP	6.01"WRP	5.38"WRP	4.75"WRP
0	1.32		1.80		2.14						0.69		0.92		1.66
1	0.85		0.83		1.44						0.49		0.55		1.20
3			1.12		1.95						0.67		0.76		1.41
5	1.22	1.17	1.29	1.44	2.22	0.99	0.88	0.97	1.06	1.87	0.74	0.76	0.88	0.92	1.71
6	1.34		1.32		2.02						0.79		0.85		1.69
6.94	1.29	1.12	1.22	1.41	2.05		0.92	0.95	1.13	1.85	0.81	0.81	0.85	0.92	1.59
8.5	1.19		1.10		1.85						0.72		0.69		1.48
13	0.76		0.71		1.12						0.46		0.46		0.95
17	0.39		0.37		0.58						0.28		0.28		0.53
21	0.19		0.17		0.27						0.12		0.12		0.23

	Plate "n"					Plate "r"				
Position	7.27"WRP	6.64"WRP	6.01"WRP	5.38"WRP	4.75"WRP	7.27"WRP	6.64"WRP	6.01"WRP	5.38"WRP	4.75"WRP
0						0.50		0.76		0.95
1						0.36		0.43		0.76
3						0.52		0.52		0.90
5	0.67	0.65	0.67	0.85	1.34	0.64	0.57	0.64	0.74	0.98
6						0.62		0.64		1.02
6.94	0.67	0.67	0.69	0.88	1.32	0.62	0.60	0.62	0.69	1.02
8.5						0.62		0.60		0.90
13						0.36		0.36		0.62
17						0.24		0.21		0.36
21						0.14		0.10		0.17

Table 3.17
Relative Power Distribution Along Axial Traverses for Element in Position 13
"SM-2 Final Mockup Core"

	Plate "a"					Plate "e"					Plate "j"				
Position	4.33"WRP	3.70"WRP	3.07"WRP	2.44"WRP	1.81"WRP	4.33"WRP	3.70"WRP	3.07"WRP	2.44"WRP	1.81"WRP	4.33"WRP	3.70"WRP	3.07"WRP	2.44"WRP	1.81"WRP
0	2.10		2.33		2.75						1.76		1.55		1.99
1	1.50		1.20		1.92						1.06		0.76		1.46
3	1.85		1.62		2.77						1.36		0.99		1.66
5	2.03	1.76	1.62	1.80	2.73	1.87	1.39	1.34	1.46	2.59	1.66	1.06	1.13	1.34	2.15
6	2.26		1.80		2.86						1.18		1.06		2.01
6.94	2.29	1.64	1.64	1.87	2.59	1.71	1.22	1.25	1.36	2.45	1.52	1.02	1.11	1.52	2.10
8.5	2.36		1.48		2.26						1.39		0.95		1.99
13	1.16		2.61		1.04						0.90		0.65		1.11
17	0.62		0.44		0.55						0.51		0.30		0.51
21	0.30		0.18		0.23						0.25		0.16		0.28

	Plate "n"					Plate "r"				
Position	4.33"WRP	3.70"WRP	3.07"WRP	2.44"WRP	1.81"WRP	4.33"WRP	3.70"WRP	3.07"WRP	2.44"WRP	1.81"WRP
0						0.92		0.90		1.39
1						0.79		0.62		1.02
3						0.95		0.79		1.27
5	1.27	0.97	1.04	1.11	1.87	1.06	0.88	0.90	0.95	1.43
6						1.18		0.92		1.46
6.94	1.27	0.95	0.95	1.06	1.87	1.04	0.83	0.83	0.88	1.41
8.5						0.99		0.83		1.18
13						0.60		0.55		0.67
17						0.39		0.25		0.39
21						0.14		0.12		0.14

Table 3.18
Relative Power Distribution Along Axial Traverses for Element in Position 14
"SM-2 Final Mockup Core"

	Plate "a"			Plate "e"			Plate "j"			Plate "n"			Plate "r"		
Position	1.26"WRP	0.63"WRP	CRP	1.26"WRP	0.63"WRP	CRP	1.26"WRP	0.63"WRP	CRP	1.26"WRP	0.63"WRP	CRP	1.26"WRP	0.63"WRP	CRP
0	2.86		1.86				2.08		1.71				1.07		0.95
1	2.17		1.45				1.46		0.83				0.71		0.55
3	2.77		1.95				1.92		1.04				0.90		0.86
5	2.97	2.38	2.10	2.38	1.41	1.32	1.92	1.18	1.18	1.94	1.06	1.04	1.37	0.90	0.86
6	2.90		2.21				2.06		1.18				1.39		0.88
6.94	2.80	1.99	1.99	1.84	1.24	1.34	1.80	1.18	1.13	-	1.06	0.92	1.18	0.88	0.80
8.5	2.45		1.71				1.69		1.11				0.95		0.84
13	1.08		0.59				0.85		0.60				0.61		0.40
17	0.54		0.37				0.51		0.30				0.27		0.23
21	0.24		0.15				0.23		0.14				0.13		0.15

Table 3.19
Relative Power Distribution Along Axial Traverses for Element in Position 21
"SM-2 Final Mockup Core"

	Plate "a"					Plate "e"					Plate "j"				
Position	10.20"WRP	9.57"WRP	8.94"WRP	8.31"WRP	7.68"WRP	10.20"WRP	9.57"WRP	8.94"WRP	8.31"WRP	7.68"WRP	10.20"WRP	9.57"WRP	8.94"WRP	8.31"WRP	7.68"WRP
0	1.18		1.78		2.13						0.87		1.00		1.85
1	0.81		0.74		1.46						0.60		0.62		1.29
3	1.02		0.97		1.94						0.87		0.78		1.54
5	1.11	0.95	1.11	1.25	2.06	1.13	0.81	0.92	1.09	1.94	0.89	0.71	0.87	0.96	1.90
6	1.18		1.06		2.01						0.96		0.83		1.90
6.94	1.13	0.92	0.99	1.16	1.82	1.13	0.83	0.90	1.09	1.80	1.00	0.76	0.78	0.98	1.69
8.5	1.09		0.88		1.71						0.87		0.76		1.56
13	0.67		0.55		0.79						0.62		0.47		0.94
17	0.37		0.28		0.44						0.38		0.25		0.49
21	0.18		0.12		0.21						0.16		0.13		0.22

	Plate "n"					Plate "r"				
Position	10.20"WRP	9.57"WRP	8.94"WRP	8.31"WRP	7.68"WRP	10.20"WRP	9.57"WRP	8.94"WRP	8.31"WRP	7.68"WRP
0						0.53		0.69		1.18
1						0.39		0.37		0.83
3						0.53		0.51		0.99
5	0.83	0.67	0.74	0.90	1.55	0.42	0.51	0.58	0.69	1.18
6						0.62		0.60		1.13
6.94	0.85	0.65	0.76	0.95	1.52	0.55	0.51	0.53	0.67	1.16
8.5						0.58		0.53		1.06
13						0.37		0.32		0.58
17						0.25		0.16		0.42
21						0.12		0.09		0.18

Table 3.20
Relative Power Distribution Along Axial Traverses for Element in Position 22
"SM-2 Final Mockup Core"

	Plate "a"					Plate "e"					Plate "j"				
Position	7.27"WRP	6.64"WRP	6.01"WRP	5.38"WRP	4.75"WRP	7.27"WRP	6.64"WRP	6.01"WRP	5.38"WRP	4.75"WRP	7.27"WRP	6.64"WRP	6.01"WRP	5.38"WRP	4.75"WRP
0	2.22		2.06		2.75						2.17		1.80		2.47
1	1.69		1.57		2.31						1.32		1.02		1.82
3	2.10		1.96		2.73						1.52		1.22		2.31
5	2.33	2.01	2.17	2.33	3.14	2.03	1.41	1.57	1.71	2.86	2.01	1.25	1.34	1.48	2.54
6	2.33		2.08		3.16						1.87		1.32		2.49
6.94	2.22	1.82	2.10	2.22	3.00	1.92	1.39	1.43	1.57	2.70	1.87	1.20	1.18	1.43	2.38
8.5	1.78		1.66		2.52						1.66		1.18		2.10
13	0.76		0.53		0.97						1.02		0.62		1.20
17	0.42		0.30		0.51						0.44		0.37		0.62
21	0.18		0.14		0.21						0.23		0.18		0.25

	Plate "n"					Plate "r"				
Position	7.27"WRP	6.64"WRP	6.01"WRP	5.38"WRP	4.75"WRP	7.27"WRP	6.64"WRP	6.01"WRP	5.38"WRP	4.75"WRP
0						1.32		1.39		1.96
1						0.97		0.88		1.48
3						1.27		1.13		1.99
5	1.69	1.20	1.25	1.36	2.54	1.48	1.25	1.25	1.29	2.13
6						1.43		1.25		2.15
6.94	1.64	1.11	1.22	1.43	2.40	1.39	1.20	1.22	1.25	2.24
8.5						1.32		1.06		1.89
13						0.74		0.62		1.06
17						0.49		0.37		0.53
21						0.18		0.14		0.23

Table 3.21
Relative Power Distribution Along Axial Traverses for Element in Position 23
"SM-2 Final Mockup Core"

	Plate "a"					Plate "e"					Plate "j"				
Position	4.20"WRP	3.57"WRP	2.94"WRP	2.31"WRP	1.68"WRP	4.20"WRP	3.57"WRP	2.94"WRP	2.31"WRP	1.68"WRP	4.20"WRP	3.57"WRP	2.94"WRP	2.31"WRP	1.68"WRP
0	3.63		3.95		3.79						2.86		2.54		3.07
1	2.56		1.57		2.80						1.92		1.20		2.36
3	3.23		2.06		3.40						2.36		1.52		2.89
5	3.81	2.45	2.43	2.96	3.88	3.19	1.96	1.94	2.06	3.53	2.70	1.71	1.69	1.85	3.21
6	3.49		2.26		3.12						2.56		1.69		3.00
6.94	3.33	2.26	2.17	2.59	3.63	3.05	1.92	1.76	1.94	3.49	2.52	1.69	1.59	1.76	2.96
8.5	2.91		1.85		2.86						2.29		1.39		2.47
13	1.27		0.97		1.13						1.25		0.69		0.79
17	0.62		0.46		0.60						0.62		0.35		0.42
21	0.28		0.23		0.28						0.28		0.16		0.16

	Plate "n"					Plate "r"				
Position	4.20"WRP	3.57"WRP	2.94"WRP	2.31"WRP	1.68"WRP	4.20"WRP	3.57"WRP	2.94"WRP	2.31"WRP	1.68"WRP
0						2.45		2.31		2.86
1						1.78		1.32		2.03
3						2.10		1.43		2.56
5	2.70	1.59	1.64	1.82	3.16	2.40	1.66	1.69	1.64	2.80
6						2.26		1.64		2.52
6.94	2.56	1.62	1.57	1.73	3.03	2.36	1.69	1.64	1.85	2.59
8.5						1.92		1.36		2.08
13						1.11		0.79		0.95
17						0.60		0.42		0.44
21						0.28		0.16		0.23

Table 3.22
Relative Power Distribution Along Axial Traverses for Element in Position 31
"SM-2 Final Mockup Core"

	Plate "a"					Plate "e"					Plate "j"				
Position	10.20"WRP	9.57"WRP	8.94"WRP	8.31"WRP	7.68"WRP	10.20"WRP	9.57"WRP	8.94"WRP	8.31"WRP	7.68"WRP	10.20"WRP	9.57"WRP	8.94"WRP	8.31"WRP	7.68"WRP
0	1.29		1.62		2.15						2.77		1.92		2.19
1	1.02		0.95								0.90		0.74		1.73
3	1.36		1.34		2.56						1.52		0.97		2.15
5	1.50	1.39	1.59	1.96	2.96	1.27	0.95	1.06	1.43	2.10	1.36	1.16	1.11	1.27	2.36
6	1.39		1.52		2.84						1.71		1.06		2.29
6.94	1.39	1.25	1.48	1.76	2.66	1.20	0.95	1.06	1.25	2.36	1.27	0.88	1.02	1.20	2.10
8.5	1.32		1.27		2.24						1.29		0.83		1.85
13	0.81		0.72		0.85						0.65		0.49		0.62
17	0.42		0.35		0.37						0.58		0.30		0.35
21	0.21		0.14		0.16						0.21		0.14		0.18

	Plate "n"					Plate "r"				
Position	10.20"WRP	9.57"WRP	8.94"WRP	8.31"WRP	7.68' WRP	10.20"WRP	9.57"WRP	8.94"WRP	8.31"WRP	7.68"WRP
0						0.90		1.41		1.99
1						0.79		0.72		1.66
3						-		0.90		2.15
5	1.25	0.90	0.97	1.16	2.36	1.27	1.11	1.02	1.16	2.22
6						-		1.04		2.24
6.94	1.32	0.95	0.95	1.13	2.29	1.18	0.90	1.02	1.25	2.29
8.5						0.88		0.95		-
13						-		0.49		0.74
17						0.35		0.25		0.39
21						0.21		0.14		0.18

Table 3.23
Relative Power Distribution Along Axial Traverses for Element in Position 33
"SM-2 Final Mockup Core"

	Plate "a"					Plate "e"					Plate "j"				
Position	4.20"WRP	3.57"WRP	2.94"WRP	2.31"WRP	1.68"WRP	4.20"WRP	3.57"WRP	2.94"WRP	2.31"WRP	1.68"WRP	4.20"WRP	3.57"WRP	2.94"WRP	2.31"WRP	1.68"WRP
0	3.97		3.79		4.00						3.86		3.83		-
1	2.68		1.71		2.77						2.73		1.57		2.82
3	3.56		2.24		3.74						3.67		2.08		3.67
5	3.79	2.47	2.47	2.70	4.09	3.77	2.17	2.19	2.29	3.97	3.56	2.26	2.22	2.45	3.60
6	3.60		2.47		3.72								2.13		3.28
6.94	3.53	2.33	2.17	2.38	3.44	3.49	2.08	2.01	1.92	3.58	3.58	1.78	2.03	2.19	3.16
8.5	2.86		1.94		3.12						3.14		1.69		3.14
13	1.13		0.92		1.20						0.81		0.72		1.32
17	0.49		0.39		0.60						0.42		0.37		0.58
21	0.23		0.16		0.30						0.18		0.16		0.30

	Plate "n"					Plate "r"				
Position	4.20"WRP	3.57"WRP	2.94"WRP	2.31"WRP	1.68"WRP	4.20"WRP	3.57"WRP	2.94"WRP	2.31"WRP	1.68"WRP
0						3.42		3.35		4.04
1						2.49		1.52		2.73
3						3.19		2.01		3.40
5	3.30	2.19	2.22	2.40	3.67	-	2.29	2.15	2.38	3.42
6						3.51		2.19		3.40
6.94	2.84	2.10	1.92	1.94	3.49	3.60	2.17	2.10	2.29	3.23
8.5						2.89		1.85		2.10
13						1.04		0.88		1.20
17						0.55		0.44		0.60
21						0.23		0.23		0.28

Table 3.24
Relative Power Distribution Along Axial Traverses for Element in Position 34
"SM-2 Final Mockup Core"

	Plate "a"			Plate "e"			Plate "j"			Plate "n"			Plate "r"		
Position	1.26"WRP	0.63"WRP	CRP	1.26"WRP	0.63"WRP	CRP	1.26"WRP	0.63"WRP	CRP	1.26"WRP	0.63"WRP	CRP	1.26"WRP	0.63"WRP	CRP
0	4.50		3.44				-		3.65				3.42		2.49
1	3.47		2.40				-		1.64				2.59		1.69
3	4.41		2.91				-		2.08				3.47		2.26
5	4.57	3.53	3.33	3.97	2.45	-	-	2.33	2.29	3.44	2.31	2.24	3.86	2.73	2.45
6	4.50		3.26				3.65		2.22				3.86		2.40
6.94	4.23	3.12	3.10	3.47	2.33	-	3.49	2.31	2.10	3.53	2.22	2.01	3.40	2.49	2.29
8.5	3.40		2.29				2.91		1.82				2.82		1.69
13	1.25		0.65				1.36		0.83				1.13		0.51
17	0.60		0.32				0.76		0.42				0.60		0.25
21	0.25		0.14				0.30		0.14				0.28		0.16

Table 3.25
Relative Power Distribution Along Axial Traverses for Element in Position 41
"SM-2 Final Mockup Core"

	Plate "j"					Plate "n"					Plate "r"				
Position	10.20"WRP	9.57"WRP	8.94"WRP	8.31"WRP	7.68"WRP	10.20"WRP	9.57"WRP	8.94"WRP	8.31"WRP	7.68"WRP	10.20"WRP	9.57"WRP	8.94"WRP	8.31"WRP	7.68"WRP
0	1.36		2.22		2.84						1.34		2.19		2.52
1	0.95		0.83		1.99						0.97		0.99		2.01
3	1.18		1.04		2.29						1.13		1.18		2.38
5	1.18	1.04	1.18	1.39	2.59	1.29	1.09	1.18	1.48	2.70	1.29	1.25	1.32	1.64	2.54
6	1.43		1.20		2.66						1.29		1.39		2.43
6.94	1.34	1.04	1.13	1.41	2.38	1.29	1.04	1.18	1.34	2.54	1.13	1.22	1.29	1.57	2.40
8.5	1.22		0.95		2.10						1.16		1.11		1.96
13	0.76		0.49		1.04						0.67		0.65		0.92
17	0.37		0.28		0.58						0.42		0.32		0.49
21	0.18		0.12		0.25						0.16		0.14		0.21

Table 3.26
Relative Power Distribution Along Axial Traverses for Element in Position 42
"SM-2 Final Mockup Core"

	Plate "j"					Plate "n"					Plate "r"				
Position	7.14"WRP	6.51"WRP	5.88"WRP	5.25"WRP	4.62"WRP	7.14"WRP	6.51"WRP	5.88"WRP	5.25"WRP	4.62"WRP	7.14"WRP	6.51"WRP	5.88"WRP	5.25"WRP	4.62"WRP
0	3.05		2.68		3.88						2.22		1.96		3.72
1	2.01		1.41		2.59						2.01		1.55		2.89
3	2.45		1.78		3.16						2.56		1.99		3.60
5	2.75	1.94	1.94	2.24	3.51	2.73	1.87	1.94	2.19	3.86	2.91	2.10	2.19	2.33	4.04
6	2.61		1.92		3.65						2.86		2.15		4.13
6.94	2.61	1.78	1.89	2.06	3.40	2.49	1.78	1.82	2.08	3.44	2.66	1.82	2.01	2.10	3.74
8.5	2.03		1.46		3.00						2.10		1.59		2.98
13	1.06		0.72		1.41						0.76		0.42		1.04
17	0.53		0.35		0.74						0.46		0.25		0.55
21	0.23		0.14		0.30						0.21		0.12		0.21

Table 3.27
Relative Power Distribution Along Axial Traverses for Element in Position 43
"SM-2 Final Mockup Core"

	Plate "j"					Plate "n"					Plate "r"				
Position	4.20"WRP	3.57"WRP	2.94"WRP	2.31"WRP	1.68"WRP	4.20"WRP	3.57"WRP	2.94"WRP	2.31"WRP	1.68"WRP	4.20"WRP	3.57"WRP	2.94"WRP	2.31"WRP	1.68"WRP
0	3.58		4.32		4.16						4.16		3.79		4.74
1	2.80		1.71		3.12						2.63		1.78		3.00
3	3.40		2.19		3.90						3.40		2.24		4.04
5	3.47	2.40	2.29	2.49	4.39	3.70	2.33	2.33	2.61	4.20	3.63	2.61	2.45	2.59	4.07
6	3.58		2.19		4.11						3.81		2.38		3.95
6.94	3.40	2.19	2.13	2.33	3.79	3.40	2.19	2.13	2.36	3.86	3.35	2.29	2.29	2.38	3.86
8.5	2.66		1.87		3.10						2.80		1.99		3.21
13	1.29		0.81		0.88						1.13		0.85		1.16
17	0.65		0.42		0.44						0.53		0.46		0.58
21	0.23		0.21		0.18						0.25		0.16		0.23

Table 3.28
Relative Power Distribution Along Axial Traverses for Element in Position 24 (Control Rod A)
"SM-2 Final Mockup Core"

	Plate "a"			Plate "d"			Plate "i"			Plate "m"			Plate "p"		
Position	1.16"WRP	0.58"WRP	CRP	1.16"WRP	0.58"WRP	CRP	1.16"WRP	0.58"WRP	CRP	1.16"WRP	0.58"WRP	CRP	1.16"WRP	0.58"WRP	CRP
-3	1.20		0.92				0.88		0.42				0.83		0.55
-1	3.14		2.24				2.10		0.85				2.19		1.25
0	2.84		1.96				2.03		1.06				1.99		1.22
1	2.96		1.96				2.24		1.32				2.08		1.69
3	3.40		2.43				2.91		1.69				2.66		1.82
5	3.83	2.84	2.77	3.47	2.03	2.06	3.30	1.99	1.89	2.89	1.76	1.69	2.89	2.10	2.13
6	3.53		2.52				3.23		1.85				2.98		2.03
6.94	3.40	2.47	2.33	3.42	1.85	1.78	3.42	1.69	1.71	2.63	1.62	1.62	2.66	1.87	1.85
8.04	1.85		1.69				1.87		0.74				1.89		0.81
8.54	3.33		1.94				2.89		1.94				2.47		1.57

Table 3.29
Relative Power Distribution Along Axial Traverses for Element in Position 44 (Control Rod C)
"SM-2 Final Mockup Core"

	Plate "i"			Plate "m"			Plate "p"		
Position	1.16" WRP	0.58" WRP	CRP	1.16" WRP	0.58" WRP	CRP	1.16" WRP	0.58" WRP	CRP
-3	1.20		0.58				1.43		0.99
-1	2.47		1.18				3.47		2.08
0	2.52		1.43				3.33		2.15
1	2.52		1.87				3.51		2.31
3	3.23		2.38				4.13		2.77
5	4.02	2.61	2.40	4.02	2.49	2.33	4.62	3.37	3.05
6	4.02		2.47				4.09		3.07
6.94	3.70	2.36	2.29	2.82	2.29	2.03	3.60	2.80	2.56
8.04	2.33		0.95				2.13		1.11
8.54	3.00		2.08				3.07		1.69

Table 3.30
Relative Power Distribution Along Axial Traverses for Element in Position 32 (Control Rod F)
"SM-2 Final Mockup Core"

	Plate "a"					Plate "d"					Plate "j"				
Position	7.04"WRP	6.46"WRP	5.88"WRP	5.30"WRP	4.72"WRP	7.04"WRP	6.46"WRP	5.88"WRP	5.30"WRP	4.72"WRP	7.04"WRP	6.46"WRP	5.88"WRP	5.30"WRP	4.72"WRP
-3	0.85		0.83		1.16						0.65		0.42		0.99
-1	2.22		1.71		3.19						1.43				2.43
0	2.03		1.59		2.80						1.64		0.92		2.45
1	2.08		1.52		2.56						1.87		1.22		2.63
3	2.61		2.01		3.30						2.54		1.69		2.89
5	2.86	2.29	2.26	2.66	3.70	2.59	1.71	1.89	1.94	3.30	2.68	1.78	1.79	2.01	3.33
6	2.77		2.22		3.28						2.47		1.79		3.28
6.94	2.56	2.10	2.13	2.31	3.26	2.22	1.55	1.62	1.76	2.96	1.80	1.59	1.66	1.78	2.98
8.04	1.69		1.22		2.29						1.06		0.65		1.69
8.54	1.92		1.64		2.43						1.66		1.20		2.03

	Plate "m"					Plate "p"				
Position	7.04"WRP	6.46"WRP	5.88"WRP	5.30"WRP	4.72"WRP	7.04"WRP	6.46"WRP	5.88"WRP	5.30"WRP	4.72"WRP
-3						0.76		0.53		1.06
-1						1.85		1.18		2.73
0						1.76		1.48		2.40
1						1.89		1.48		2.52
3						3.05		1.96		3.23
5	2.77	1.69	1.69	1.92	3.40	2.56	1.99	2.17	2.31	3.79
6						2.56		1.92		3.42
6.94	2.33	1.43	1.52	1.71	3.03	2.31	1.82	1.82	2.19	3.74
8.04						1.32		0.90		2.10
8.54						1.85		1.78		3.00

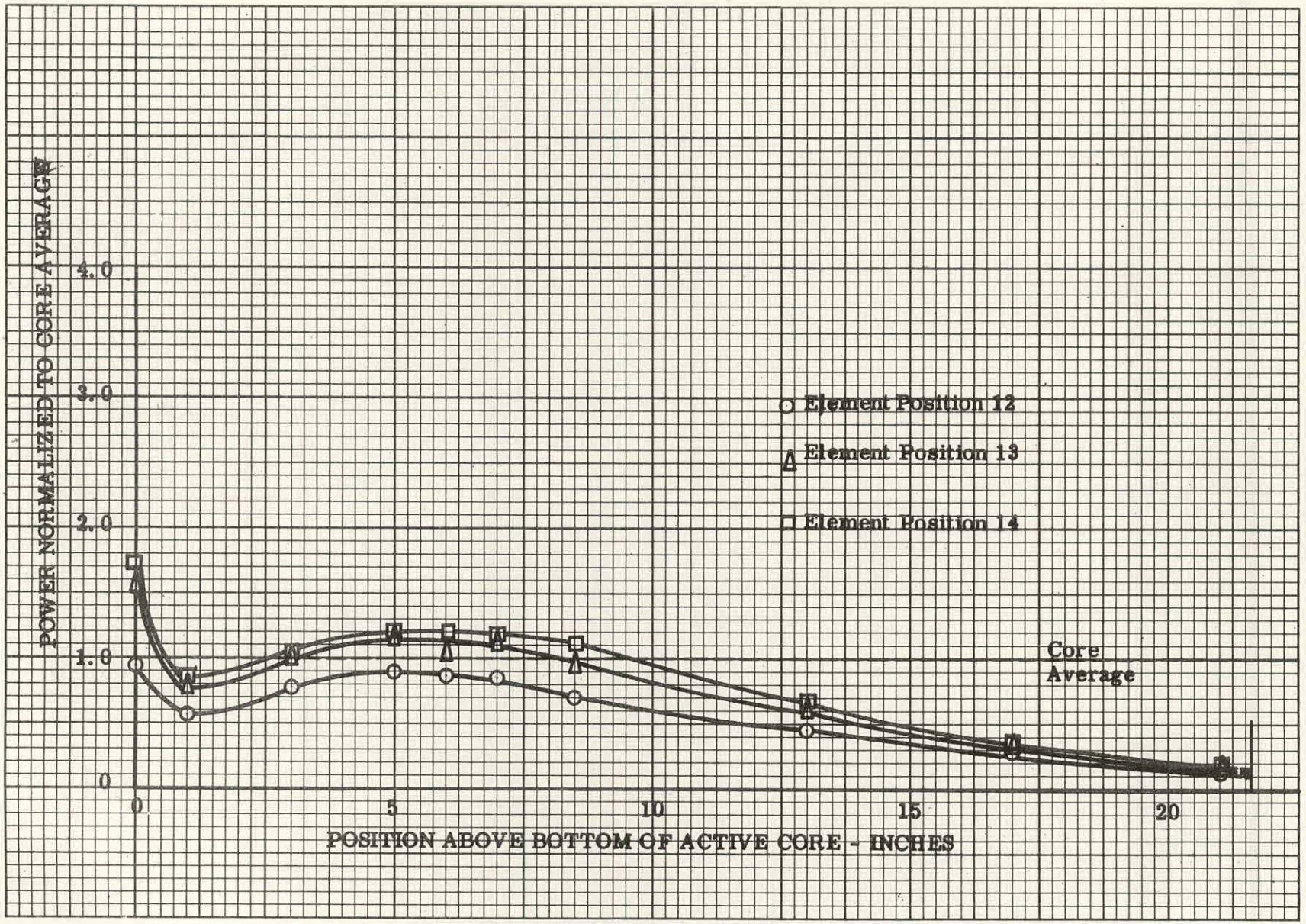

Figure 3.12 Relative Power Distribution Along Axial Traverse on Centerline of Fuel Plate "j", Elements in Positions 12, 13 and 14, SM-2 Final Mockup Core

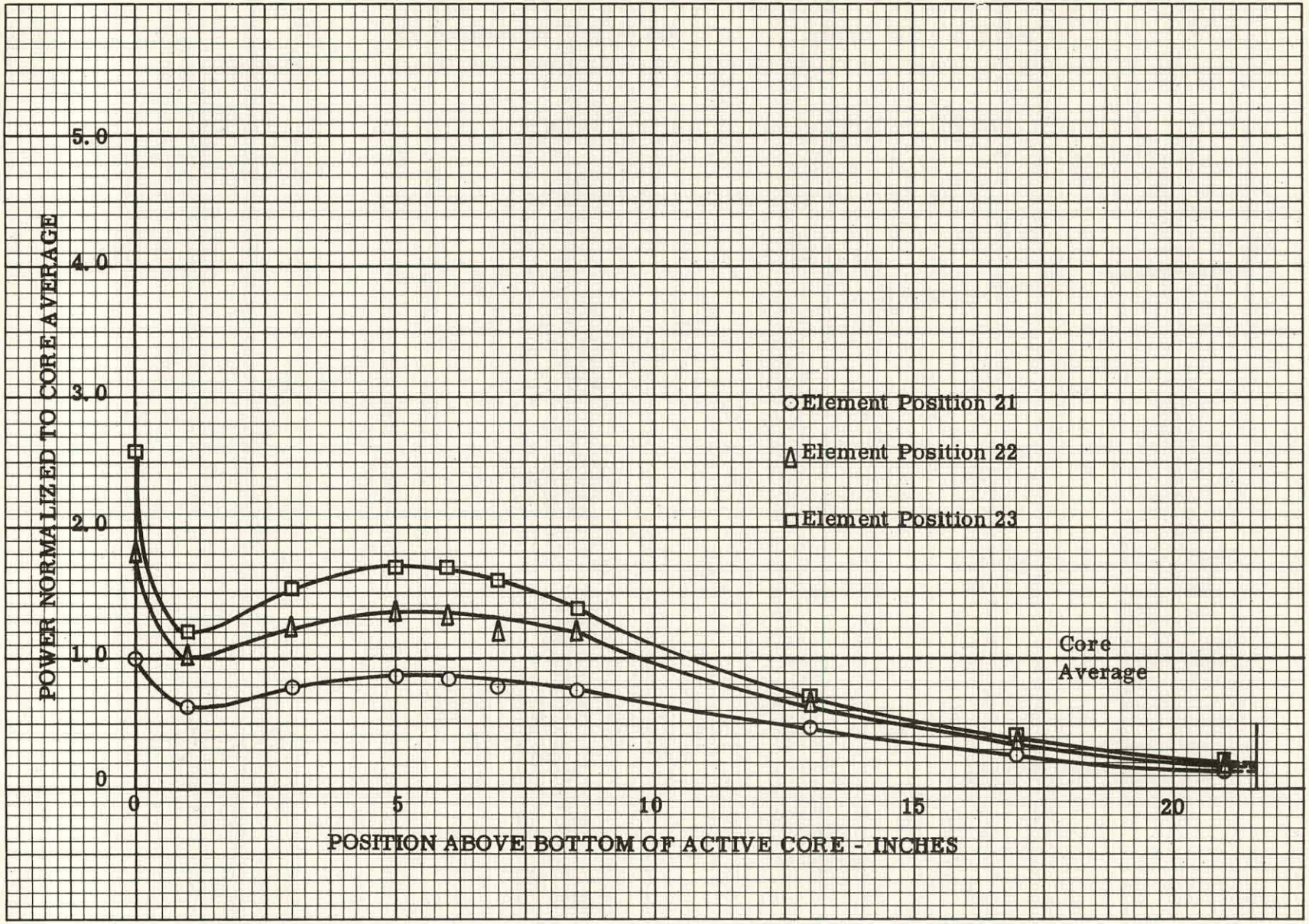

Figure 3.13 Relative Power Distribution Along Axial Traverse on Centerline of Fuel Plate "j", Elements in Positions 21, 22 and 23, SM-2 Final Mockup Core

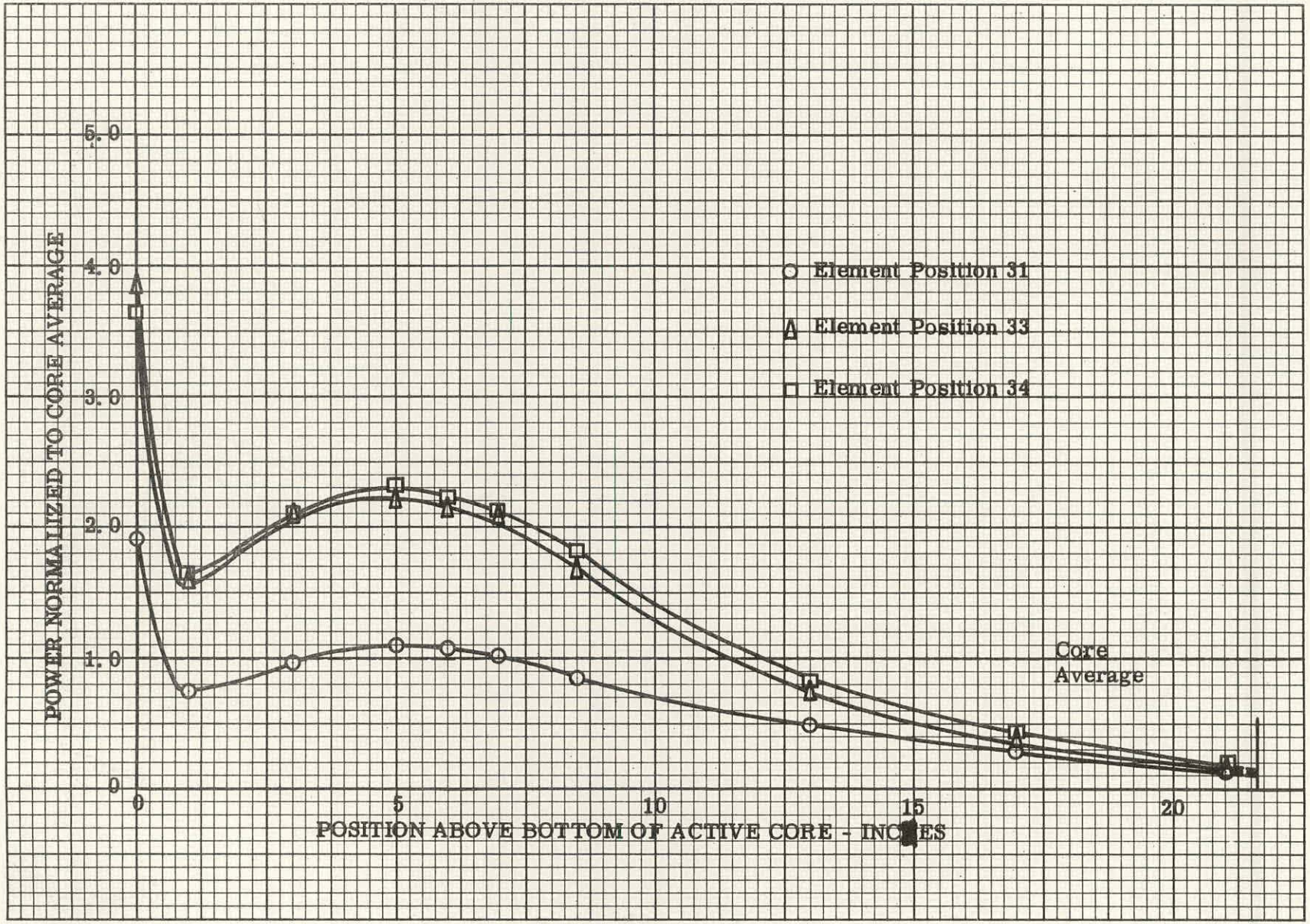

Figure 3.14 Relative Power Distribution Along Axial Traverse on Centerline of Fuel Plate "j", Elements in Positions 31, 33 and 34, SM-2 Final Mockup Core

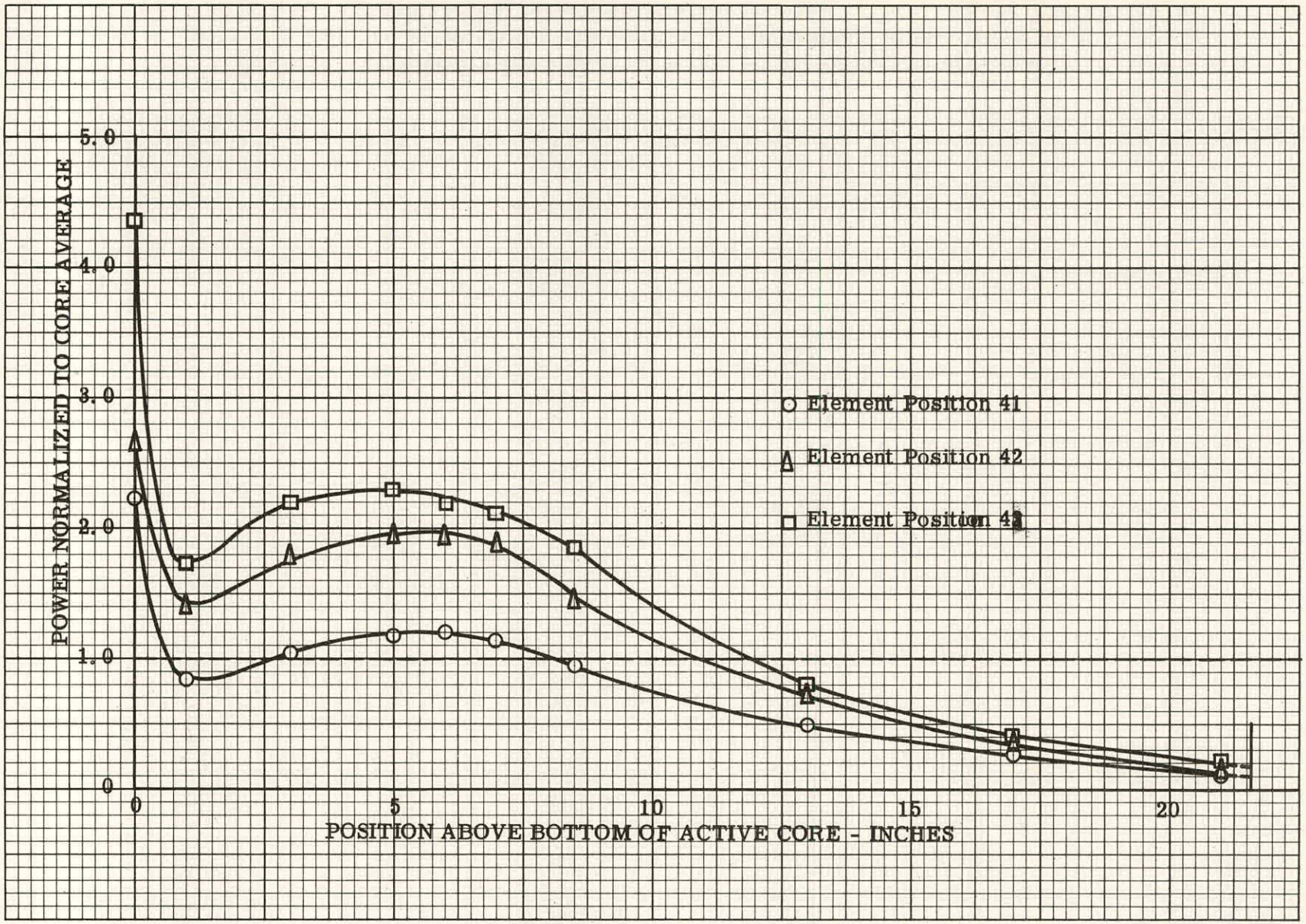

Figure 3.15 Relative Power Distribution Along Axial Traverse on Centerline of Fuel Plate "j", Elements in Positions 41, 42 and 43, SM-2 Final Mockup Core

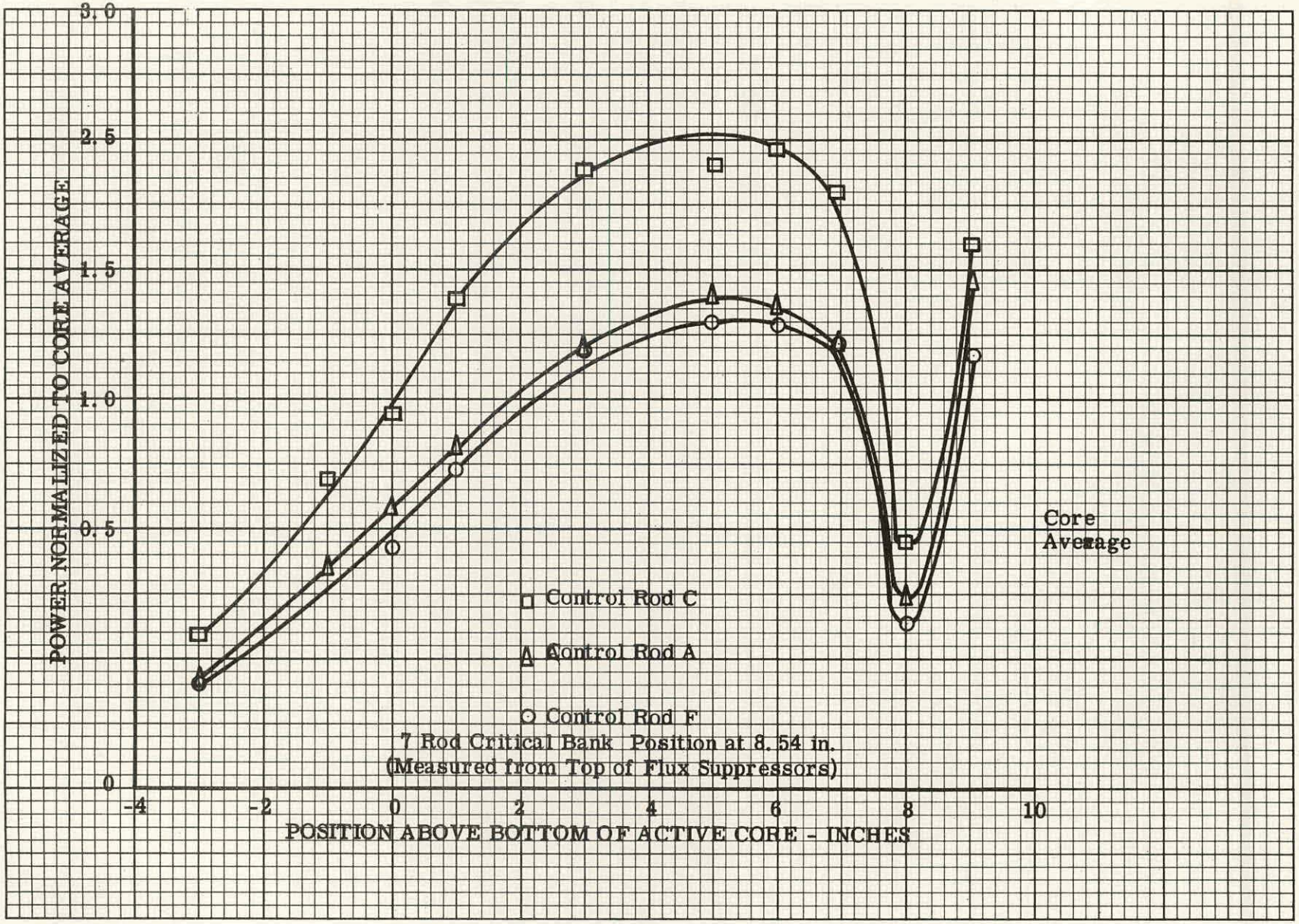

Figure 3.16 Relative Power Distribution Along Axial Traverse on Centerline of Fuel Plate "i" of Control Rods A, C and F, SM-2 Final Mockup Core

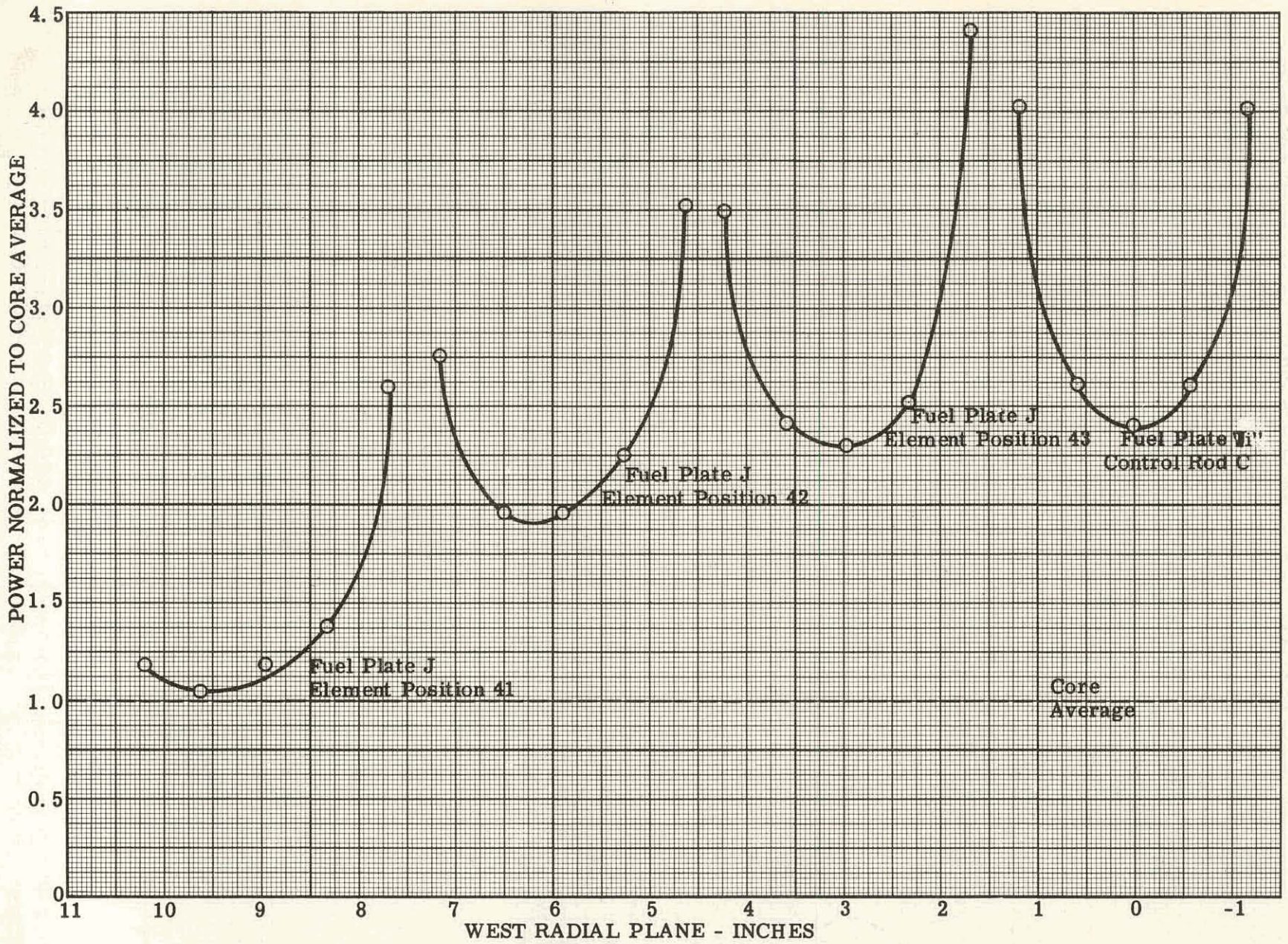

Figure 3.17 Relative Power Distribution Along Radial Traverse 5 In. Above Bottom of Active Core, SM-2 Final Mockup Core

center of the core is approached. Power minimas occur as expected along the centerline with maximas along the edges. The overall maximum-to-average power generation in the core is 4.74 to 1 occurring as a spike at the bottom of fuel element in position 43. The internal maximum of 4.62 to 1 occurs within the central control rod fuel element.

3.2.8 Conclusions

A survey of the power producing characteristics of the SM-2 core was obtained from activation measurements. The highest power density was in the region surrounding the center of the core, the lowest along the outer ring of elements. In stationary fuel elements power peaks occurred at the bottom of the active core and 4-7 in. above it in the vicinity of the critical bank position, with power gradually diminishing as the top of the active core was reached. In general, minimum power generation occurred along the centerline of fuel elements and maximum at the edges. The data of Fig. 3.4 and 3.11 differ from that previously reported[1] since these data include the control rods in the core average, include more detailed mapping and in the latter case include a flow divider mockup.

In control rod fuel elements without flux suppressors, the power exhibited a small gradual increase until near the critical position where a very sharp rise occurred corresponding on the average to more than a threefold increase in power. The addition of flux suppressors at the top of the active meat eliminated this peak in power, dropping the power by as much as 90%. Maximum suppressor effect of 9.2 to 1 occurred at the centerline of plate "i" of control rod F while it was 8.3 to 1 and 7.3 to 1 on the centerline of plate "i" of control rod C and A, respectively. This demonstrates the usefulness and effectiveness of suppressors in eliminating sharp power spikes, thus permitting maximum power to be generated within an appreciable volume of the fuel element.

Figure 3.18 shows the relative power distribution along an axial traverse on centerline of plate "i" of control rod C with and without suppressors. Figure 3.19 illustrates radial traverses at the top limit of the active meat for plate "i" of control rods A, C and F for the two mockups. Considerable reduction in power in the suppressor region is evident in the above two figures.

An examination of the power distribution in the vicinity of the flow divider and the resulting outward displacement of the outer ring of fuel elements indicates in general only a slight decline and a more even distribution of power in the flow divider region.

Among individual elements in the preliminary mockup core, a peak-to-average power density of 2.6 to 1 occurred within the portion of the central control rod in the active core while average-to-minimum power density of 1.7 to 1 occurred in element position 21 at the corner of the core. The use of flow divider and control rod flux suppressors in the final mockup slightly changed the overall power distribution in the core allowing for a more even distribution and lesser power spikes. Again, peak and minimum power densities occurred

THIS PAGE

WAS INTENTIONALLY

LEFT BLANK

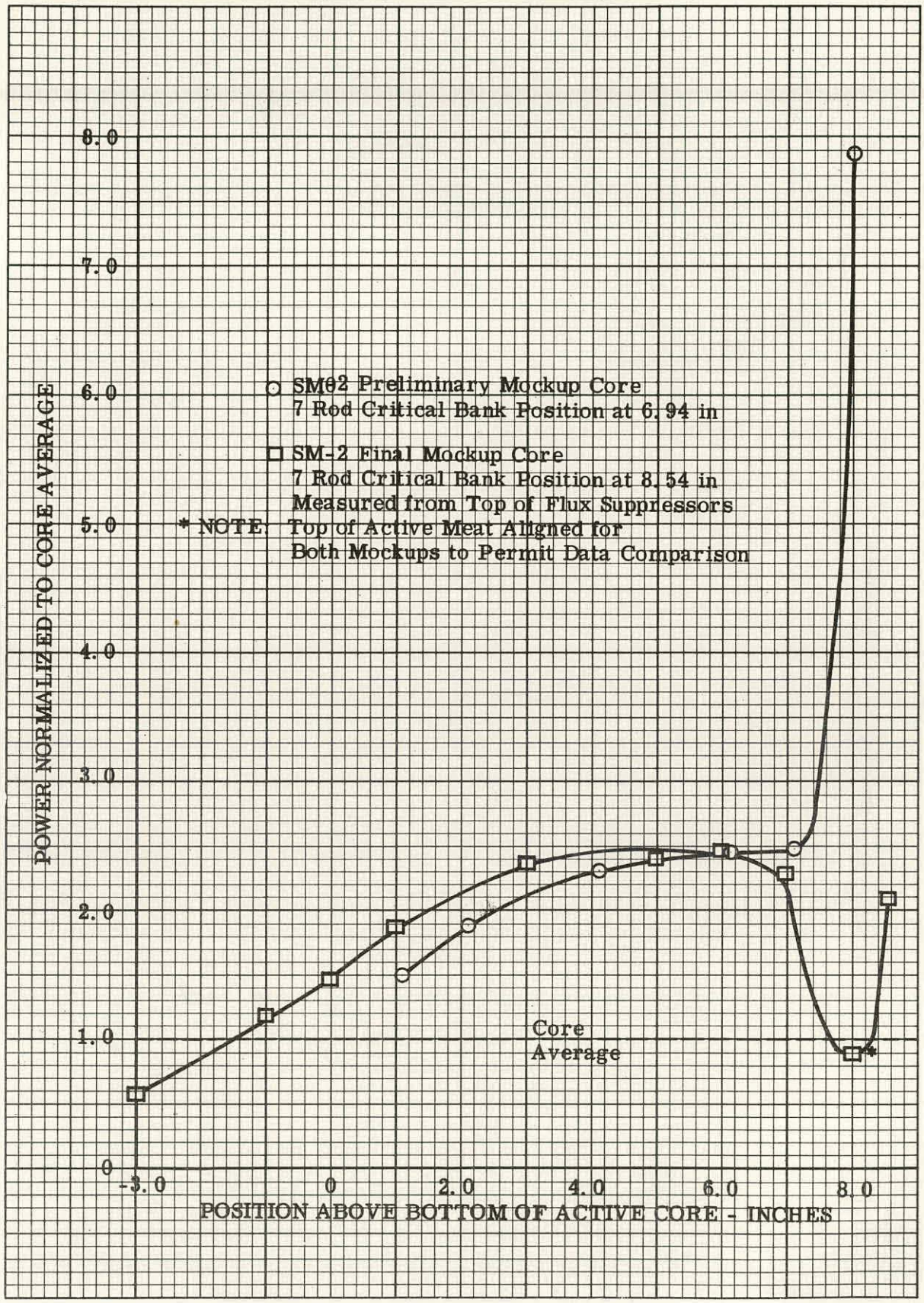

Figure 3.18 Relative Power Distribution Along Axial Traverse on Centerline of Fuel Plate "i" of Control Rod C, SM-2 Preliminary and Final Mockup Cores

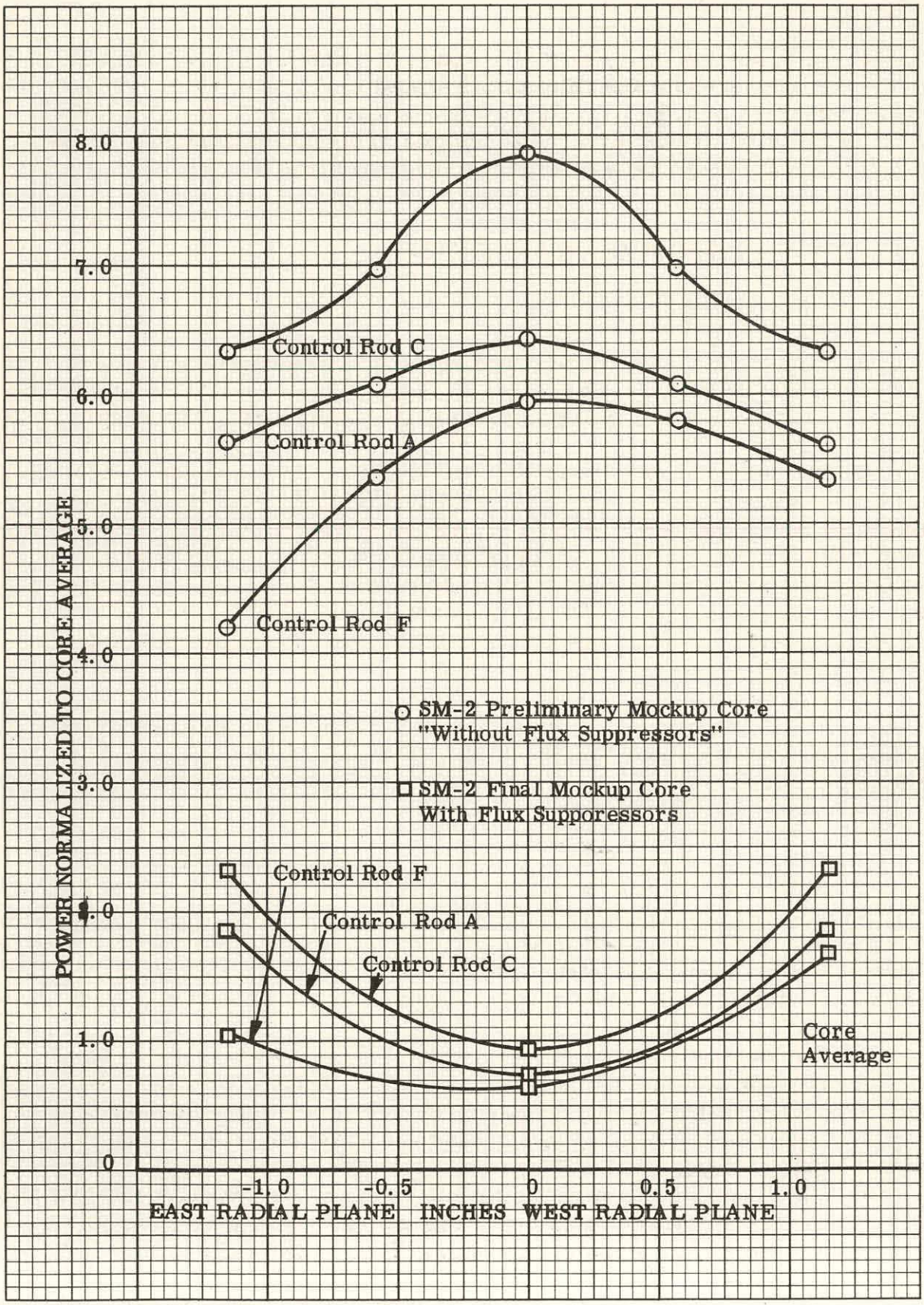

Figure 3.19 Relative Power Distribution Along Radial Traverse at Top of the Active Core of Fuel Plate "i" of Control Rods A, C and F, SM-2 Preliminary and Final Mockup Cores

within the active portion of the central control rod and the corner element in position 21; the peak-to-average ratio was reduced to 2.3 to 1 while average-to-minimum remained at 1.7 to 1. An indication of the overall change in power distribution is given by the changes in the normalization factor which increased from 2.18 for the preliminary to 2.31 for the final mockup.

3.3 FLUX SUPPRESSOR MEASUREMENTS

3.3.1 Introduction

The effectiveness of both mockup and integral suppressors located at the lower boundary of stationary fuel elements, was demonstrated in reducing the high power peaks occurring at the bottom of the active core. The relative power measured in these regions with flux suppressors was reduced to approximately 1/8 the value obtained without suppressors, bringing the local power well below the core average. Tables 3.31, 3.32, 3.33 and 3.34 summarize the measurements, made on elements 41, 42,and 43, respectively, using 1/2- and 3/4-in. long suppressors, normalized to a core average of unity. Comparison of foil activations with and without suppressors is given in Fig. 3.20, 3.21, and 3.22 through the centerline of plate "j" of elements 41, 42, and 43, respectively; Fig. 3.23 compares the effectiveness of mockup flux suppressors at the edge of fuel element 43 at plate "r".

The effectiveness of the suppressors extend up to an axial position of about 2 to 3 in. from the lower boundary of the active core.

3.3.2 Mockup Suppressors

The mockup flux suppressors consist of multi-layers of Mylar film impregnated with boron. The Mylar film was applied to both sides of the fuel plates to an aerial density of 0.0045 gm B-10 per cm^2 on each side. This B-10 density was equivalent to the europium density of 1.529 gm Eu/cc in the design europium flux suppressors. The width of the mockup suppressors was identical to the specified fuel matrix width and the upper suppressors boundary was at the lower active core limit.

The use of Mylar tape on the plate surface to mockup the suppressor fills 50% of the coolant channel between the plates. This would presuppose a reduction in neutron flux, thus tending to improve the apparent neutron absorption efficiency of the mockup suppressors over equivalent integral suppressors. However, subsequent data obtained with integral europium suppressors indicated that this effect was more apparent than real, and the foil activations with both types of suppressors were approximately the same (Fig. 3.22).

A comparison of runs using a "blank" suppressor, i.e., Mylar tape without boron impregnation, with those in which no tape at all was used, produced little differences in relative foil activations (Fig. 3.20-3.22). This indicates that the effect of placing the uranium foils farther out in the water gap is not readily discernable in the region directly below the active core boundary.

3.3.3 Flux Suppressor Effectiveness

The use of 1/2 in. long suppressors reduces the flux peaks near the bottom of the active core by a factor of approximately eight. However the 50% increase in suppressor length to 3/4 in. did not produce a further flux suppression above the bottom of the active core nor extend the range of flux suppression beyond the 2 in. to 3 in. axial position, thus demonstrating essentially an equivalence between 1/2- and 3/4-in. long flux suppressors.

3.3.4 Integral Suppressors

Subsequent to the mockup suppressor tests, 18 SM-2 fuel plates containing integral suppressors were made available for testing. These fuel plates had an average Eu_2O_3 loading in the suppressor region of 0.780 gm. This was about 33% less europium than the design loading of 1 gm of europium per plate or 1.529 gm Eu/cc. The integral suppressors had an average length of 0.549 in. and an average width of 2.686 in.

Since only 18 plates containing flux suppressors were available, flux measurements could be made only with a single fuel element containing the suppressors. Hence, the environment was not quite identical to that obtained using Mylar tape mockups where the fuel elements surrounding the foil instrumented element all contained suppressors. Nevertheless, reasonable agreement between the mockup and integral suppressor measurements was obtained. Figure 3.22 shows that the integral flux suppressors were only slightly less effective than the 1/2-in. long mockup suppressors. This is probably due to the combination of effects resulting from the slightly lower effective loading of the integral suppressors and the fact that integral suppressors did not extend into the coolant passage as the mockup suppressors did.

3.4 BLOCKED CHANNEL MEASUREMENTS

3.4.1 Introduction

The objective of these survey experiments was to determine the effects on local power generation that result from blocking a fuel element coolant channel with various filler materials. The blocked channel method is used for installation of thermocouples for fuel plate temperature profile measurements during reactor power operation. The experimental runs consisted of measuring the foil activations when blocking the central channel of element position No. 42 with a metal filler.

Measurements were made in the SM-2 core mockup both with a water reflector and with a stainless steel reflector. Stainless steel and aluminum fillers were used in the experiment.

Table 3.31
Relative Power Distribution Along Axial Traverses For Element in Position 41;
SM-2 Preliminary Mockup Core with Suppressor Mockups

Position	Plate "a"			Plate "j"			Plate "r"		
	9.97 WRP	8.81 WRP	7.65 WRP	9.97 WRP	8.81 WRP	7.65 WRP	9.97 WRP	8.81 WRP	7.65 WRP
Operation With Blank Flux Suppressors									
-1/2	1.96	3.47	3.86	2.33	3.60	4.58	1.98	3.30	3.98
0	1.28	2.33	3.05	1.34	1.85	2.82	1.27	1.92	2.33
1	0.83	0.93	1.65	0.76	0.85	1.69	0.81	0.91	1.48
3	1.02	1.18	2.06	1.00	1.09	1.96	1.02	1.13	2.02
Operation With Half Inch Flux Suppressors									
-1/2	0.50	0.66	1.00	0.39	0.49	0.81	0.43	0.53	0.56
0	0.33	0.30	0.58	0.27	0.26	0.36	0.22	0.26	0.41
1	0.56	0.74	1.24	0.60	0.65	1.23	0.64	0.74	1.21
3	0.91	1.08	1.71	0.84	0.95	1.77	0.94	1.03	1.58
Operation With Three Quarter Inch Flux Suppressors									
-1/2	0.25	0.25	0.41	0.22	0.21	0.43	0.21	-	0.34
0	0.27	0.27	0.52	0.26	0.26	0.46	0.29	0.26	0.47
1	0.65	0.77	1.30	0.71	0.76	1.34	0.75	0.78	1.33
3	0.92	1.06	1.71	0.95	0.99	1.96	1.02	1.01	1.72
Operation Without Flux Suppressors									
0		2.24			2.31			2.35	
1		0.91			0.93			0.97	
3		1.22			1.20			1.27	

Table 3.32
Relative Power Distribution Along Axial Traverses For Element in Position 42
SM-2 Preliminary Mockup Core With Suppressor Mockups

Position	Plate "a"			Plate "j"			Plate "r"		
	7.04 WRP	5.88 WRP	4.72 WRP	7.04 WRP	5.88 WRP	4.72 WRP	7.04 WRP	5.88 WRP	4.72 WRP
Operation With Blank Flux Suppressors									
-1/2	3.72	3.81	4.69	5.13	5.57	6.56	3.58	3.58	5.04
0	2.61	2.76	3.70	3.10	2.65	4.30	2.68	2.61	3.24
1	1.92	1.65	2.43	1.71	1.39	2.15	1.76	1.52	2.22
3	2.31	2.08	2.93	2.08	1.74	2.20	2.22	1.99	2.78
Operation With Half Inch Flux Suppressors									
-1/2	1.14	0.56	0.78	0.36	0.80	0.74	1.08	1.22	1.46
0	0.72	0.67	0.97	0.45	0.39	0.65	0.73	0.46	0.67
1	1.52	1.36	1.94	1.28	1.02	1.53	1.38	1.23	1.83
3	2.09	1.99	2.70	1.80	1.48	2.30	1.95	1.77	2.53
Operation With Three Quarter Inch Flux Suppressors									
-1/2	0.65	0.56	0.78	0.36	0.34	0.55	0.36	0.29	0.47
0	0.72	0.67	0.97	0.45	0.35	0.68	0.48	0.45	0.58
1	1.52	1.36	1.94	1.28	1.04	1.66	1.40	1.28	1.80
3	2.09	1.99	2.70	1.80	1.49	2.36	2.02	1.79	2.54
Operation Without Flux Suppressors									
0					3.49			3.30	
1					1.41			1.69	
3					1.80			2.24	

Table 3.33
Relative Power Distribution Along Axial Traverses For Element in Position 43
SM-2 Preliminary Mockup Core With Suppressor Mockups

Position Above Bottom of Active Core-Inches	Plate "a" 4.10" WRP	Plate "a" 2.94" WRP	Plate "a" 1.78" WRP	Plate "j" 4.10" WRP	Plate "j" 2.94" WRP	Plate "j" 1.78" WRP	Plate "r" 4.10" WRP	Plate "r" 2.94" WRP	Plate "r" 1.78" WRP
Operation With Blank Flux Suppressors									
-1/2	5.33	6.33	5.67	6.71	7.07	6.65	6.01	6.63	5.96
0	3.98	4.26	4.11	4.19	4.50	4.63	3.89	4.19	4.37
1	2.41	1.80	2.45	2.24	1.57	2.36	2.13	1.69	2.33
3	2.82	2.24	2.89	2.89	2.02	3.05	2.52	2.24	2.96
Operation With Half Inch Flux Suppressors									
-1/2	1.96	1.38	1.47	1.39	1.67	1.43	1.75	1.53	2.04
0	0.85	0.63	0.95	0.60	0.57	0.97	0.55	0.43	0.72
1	1.93	1.46	2.03	1.64	1.37	2.03	1.70	1.41	2.06
3	2.60	2.15	2.96	2.39	1.92	2.82	2.39	1.95	2.81
Operation With Three Quarter Inch Flux Suppressors									
-1/2	0.67	0.54	0.78	0.46	0.38	0.67	0.39	0.26	0.48
0	0.77	0.53	0.76	0.57	0.44	0.84	0.52	0.44	0.64
1	1.93	1.56	2.08	1.72	1.32	2.00	1.66	1.34	2.06
3	2.71	2.20	2.88	2.41	1.85	2.74	2.22	1.92	-
Operation Without Flux Suppressors									
0					4.54			4.44	
1					1.64			1.65	
3					2.13			2.70	

Table 3.34
Relative Power Distribution Along Axial Traverses For Element in Position 43;
SM-2 Preliminary Mockup Core With Integral Suppressors in Element Position 43

	Plate "a"			Plate "f"			Plate "j"			Plate "n"			Plate "r"		
Position	4.27" WRP	2.94" WRP	1.61" WRP	4.27" WRP	2.94" WRP	1.61" WRP	4.27" WRP	2.94" WRP	1.61" WRP	4.27" WRP	2.94" WRP	1.61" WRP	4.27" WRP	2.94" WRP	1.61" WRP
							Operation With Integral Suppressors								
-1/2	2.67	3.10	3.60	2.07	1.41	2.13	3.11	2.26	2.43	2.33	1.87	1.68	2.74	2.74	3.11
0	1.79	1.47	1.86	1.64	0.78	1.53	1.41	0.63	1.25	1.44	1.17	1.65	1.68	1.08	1.90
1	2.12	1.62	2.41	1.94	1.44	2.27	1.99	1.51	2.32	2.02	1.57	2.51	1.97	1.60	2.54
3	2.73	2.26	3.23	2.70	1.83	3.24	2.69	2.08	3.07	2.67	2.20	3.34	2.72	2.12	3.58
5		2.37			2.15			2.22			2.26			2.32	
7		2.12			1.98			1.97			2.00			1.97	

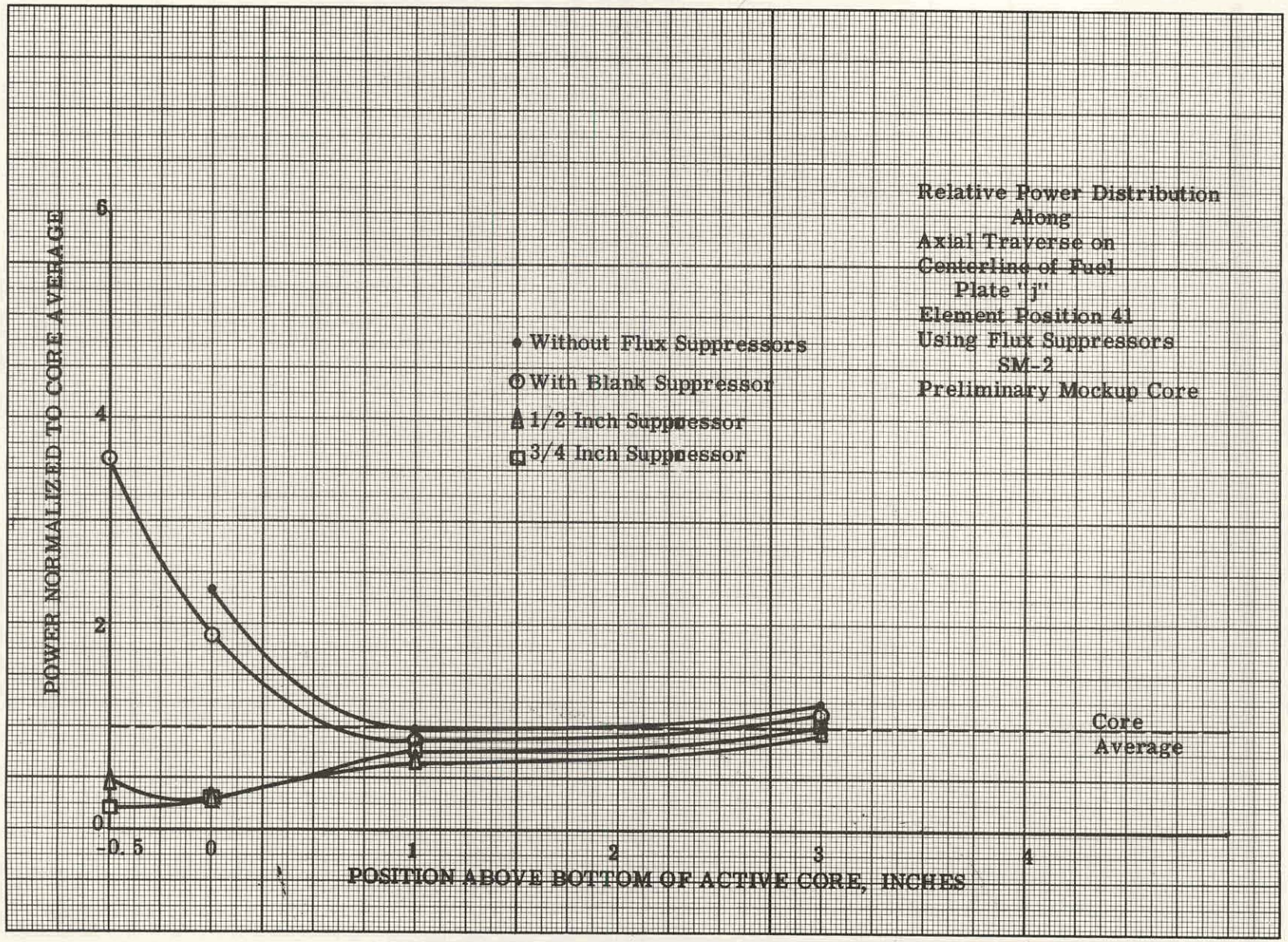

Figure 3.20 Relative Power Distribution Along Axial Traverse of Fuel Plate "j", Element in Position 41 Using Flux Suppressors, SM-2 Preliminary Mockup Core

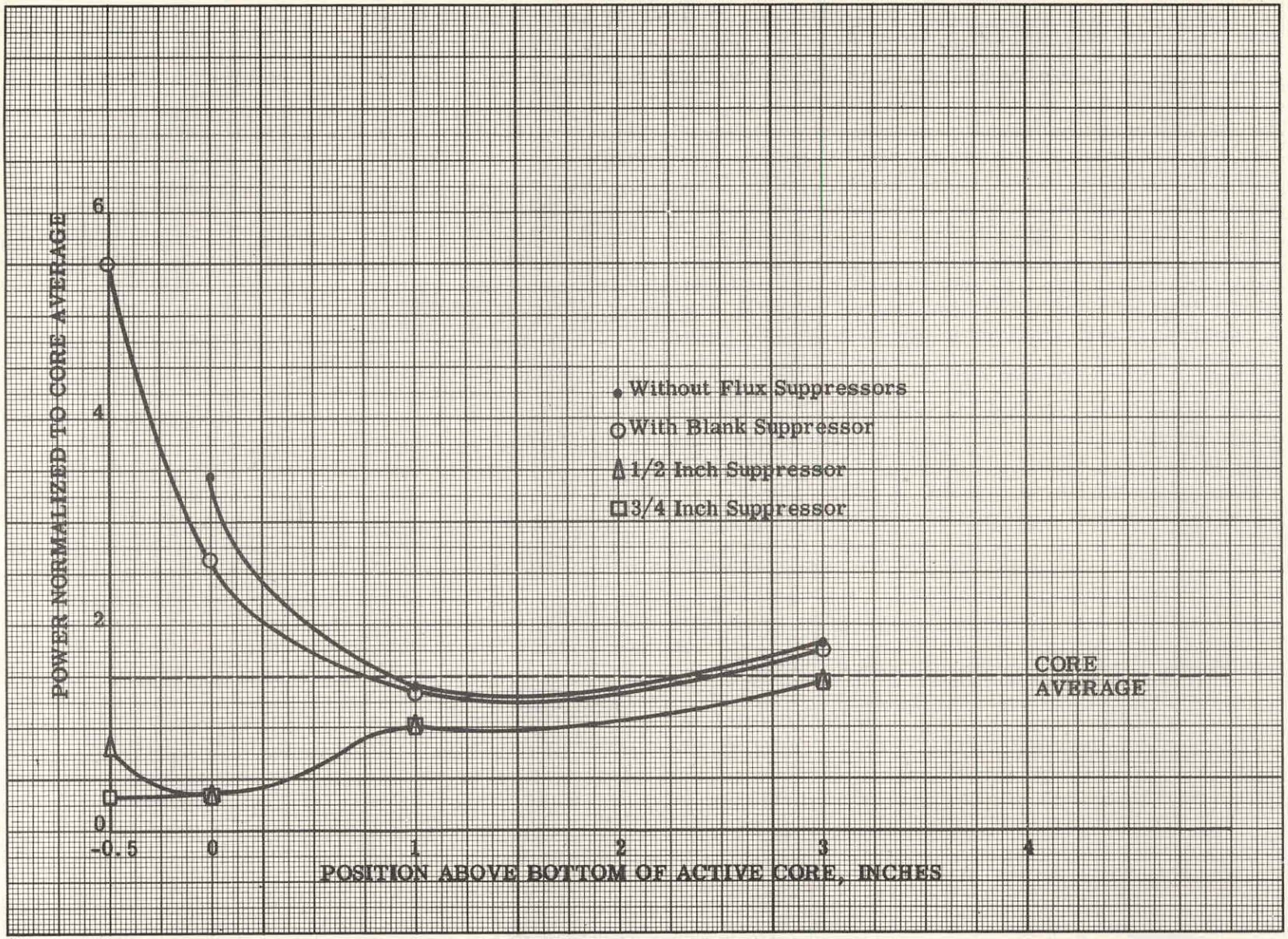

Figure 3.21 Relative Power Distribution Along Axial Traverse of Fuel Plate "j", Element in Position 42 Using Flux Suppressors, SM-2 Preliminary Mockup Core

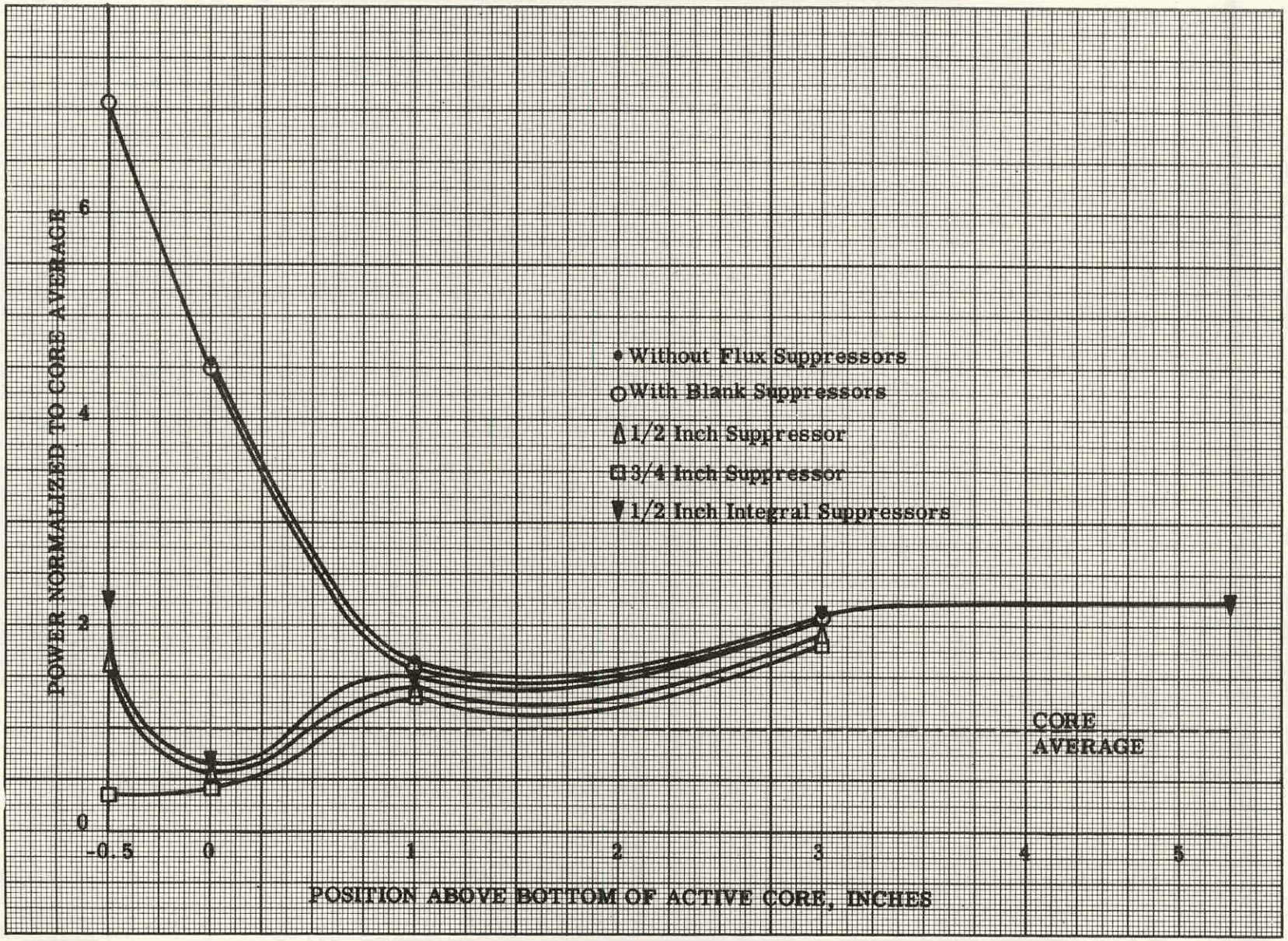

Figure 3.22 Relative Power Distribution Along Axial Traverse of Fuel Plate "j", Element in Position 43 Using Flux Suppressors, SM-2 Preliminary Mockup Core

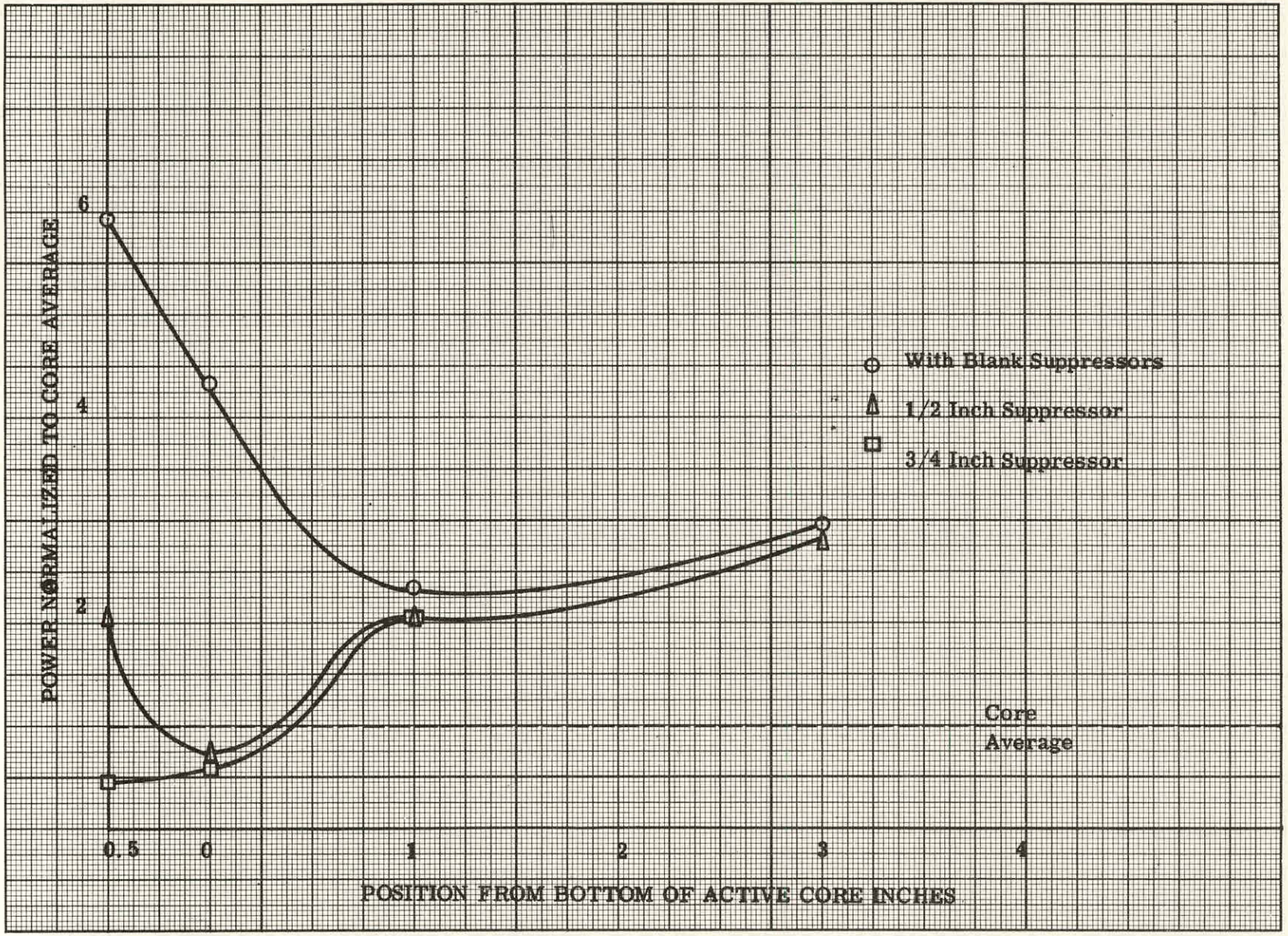

Figure 3.23 Relative Power Distribution Along Axial Traverse at 1.78 In. W.R.P. of Fuel Plate "r", Element in Position 43 Using Flux Suppressors, SM-2 Preliminary Mockup Core

3.4.2 Experimental Method

Two stainless steel or aluminum filler plates were used to block the water channel between fuel plates "i" and "j" of the element in position 42. Stainless steel sheathed chromelalumel thermocouples were inserted between the aluminum filler plates which were specially grooved for this purpose. It was felt that the cross section of the stainless steel filler satisfactorily approximated that of the thermocouples. The fillers were 0.063 in. thick and 22-15/16 in. long. Figure 3.24 is a drawing from which the fillers or thermocouple plates were made. Figure 3.25 shows the cross section of the central portion of the fuel element with and without the blocked channel.

The center of the blocked channel plus the south sides of fuel plates "n" and "r" were instrumented with uranium foils. The foils were activated, counted, and the data processed as described in AP Note 246. (5)

3.4.3 Water Reflected Core Measurements

Figure 3.26 shows that the blocked channel produces a flux suppressing effect. In addition, the relative foil activity measured in the run using stainless steel filler plates was less than the corresponding run with aluminum. It is estimated that a maximum flux reduction of 20% occurred between the unblocked and the aluminum blocked channel; the foil activity measured in the run with stainless steel filler was about 9% less than that obtained when using the aluminum filler plates. Because of time limitations, a zero run mapping the flux in a clear channel was not performed. However, data was available from previous experiments to establish the unperturbed flux distribution along plate "i". To facilitate data comparison, all measurements were normalized to a core average of unity. Table 3.35 lists the normalized foil activation for blocked channel measurements using aluminum and stainless steel filler material. It also presents earlier unblocked channel measurements.

3.4.4 Steel Reflected Core Measurements

The blocked channel measurements using stainless steel fillers were repeated using a steel reflected core. To offset any variances in bank positioning, foil counting, etc., which must be allowed for when different runs are compared, it was decided that element 46, symmetrical in core geometry to element 42 which contained the blocked channel, be also instrumented with uranium foils. This permitted flux measurements for the same clear and blocked channel to be made simultaneously. Tables 3.36, 3.37 and 3.38 present the data. Figure 3.27 shows the axial flux traverses with and without the stainless steel blocking plates. A comparison of Fig. 3.26 and 3.27 shows that the effect of blocking one channel is similar in the water and steel reflected cores. The largest difference in the ratio between clear and steel blocked channel measurements is about 1.38 at the 5 in. axial location above the bottom of the active core (refer to Table 3.38).

THIS PAGE

WAS INTENTIONALLY

LEFT BLANK

Table 3.35
Relative Power Distribution Along Axial Traverses For Element in Position 42 - Blocked Channel Measurements
SM-2 Mockup Core With Water Reflector Without Flow Divider

	Between Plates "i" and "j"					Plate "n"					Plate "r"				
Position	7.14 WRP	6.51 WRP	5.88 WRP	5.25 WRP	4.62 WRP	7.14 WRP	6.51 WRP	5.88 WRP	5.25 WRP	4.62 WRP	7.14 WRP	6.51 WRP	5.88 WRP	5.25 WRP	4.62 WRP
Blocking Material - Aluminum															
0	2.90		2.87		4.14	3.01		2.62		4.34	2.88		2.61		3.96
1	1.67		1.03		2.04	1.92		1.36		2.61	2.14		1.61		2.85
3	2.16		1.34		2.67	2.28		1.66		3.17	2.55		2.03		3.41
5	2.27	1.44	1.41	1.62	2.71	2.42	1.75	1.71	1.98	3.55	2.73	1.96	2.04	2.27	3.63
6	2.13		1.36		2.67	2.42		1.60		3.69	2.73		2.01		3.45
6.94	1.92	1.17	1.14	1.41	2.42	2.23	1.48	1.61	1.76	3.18	2.64	2.09	2.14	2.45	3.31
7.64	1.73		1.07		2.28	2.09		1.44		3.04	2.69		2.40		3.28
8.5	1.51		0.95		2.02	1.67		1.19		2.59	1.86		1.42		2.41
13	0.67		0.45		1.00	0.77		0.59		1.15	0.65		0.47		0.94
21	0.16		0.12		0.28	0.20		0.14		0.22	0.14		0.09		0.24
Blocking Material - Stainless Steel															
0	2.27		2.17		3.27	3.57		2.72		4.05	2.96		2.54		3.55
1	1.44		0.92		1.98	1.90		1.29		2.55	2.24		1.58		2.88
3	1.87		1.20		2.46	1.78		1.61		3.24	2.72		1.90		3.49
5	2.06	1.29	1.26	1.42	2.67	2.26	1.60	1.66	1.94	2.87	2.69	1.83	2.05	2.21	3.54
6	1.97		1.22		2.46	2.21		1.61		3.33	2.63		2.04		3.52
6.94	1.85	1.13	1.10	0.97	2.35	2.15	1.45	1.48	1.72	3.27	2.92	2.03	2.23	2.40	3.55
7.64	1.63		1.03		2.23	1.97		1.39		2.98	2.56		2.40		3.14
8.5	1.47		0.91		1.97	1.67		1.12		2.59	1.90		1.25		2.40
13	0.67		0.41		0.81	0.79		0.50		1.17	0.66		0.45		0.96
21	0.17		0.09		0.19	0.19		0.14		0.28	0.15		0.10		0.24
Blocking Material - None															
			Plate "i"												
0			2.87		3.81										
1			1.32		2.16										
3			1.69		3.05										
5			1.80	1.99	3.03										
7.15			1.59	1.76	2.44										
9			1.18	1.33	1.95										
13			0.60		0.97										
21			0.13		0.26										

Table 3.36
Relative Power Distribution Along Axial Traverses For Element in Position 42 - Blocked Channel Measurements
SM-2 Preliminary Mockup Core
Blocking Material Stainless Steel

	Between Plate "i" and "j"					Plate "n"					Plate "r"				
Position	7.14 WRP	6.51 WRP	5.88 WRP	5.25 WRP	4.62 WRP	7.14 WRP	6.51 WRP	5.86 WRP	5.25 WRP	4.62 WRP	7.14 WRP	6.51 WRP	5.88 WRP	5.25 WRP	4.62 WRP
0	2.53		2.39		3.27			2.53					5.10		
1	1.58		1.00		2.16			1.25					1.59		
3	1.97		1.20		2.60	2.30		1.62		3.38	2.58		2.06		3.43
5	2.05	1.28	1.29	1.50	2.79	2.45	1.71	1.71	1.89	3.38	2.68	2.06	2.20	2.48	3.68
6	1.88		1.19		2.52			1.65					2.17		
6.94	1.76	1.14	1.20	1.29	2.42	2.26	1.50	1.53	1.67	3.04	2.72	5.03	2.18	2.52	3.61
7.64	1.71		1.05		2.23			1.43					2.51		
8.5	1.47		0.94		1.93								1.42		
13	0.73		0.44		0.93			0.53					0.41		
21	0.16		0.10		0.20			0.11					0.11		

Table 3.37
Relative Power Distribution Along Axial Traverses For Element in Position 46 - Clear Channel Measurements
SM-2 Preliminary Mockup Core

	Plate "j"					Between Pl. "i" & "j"	Plate "n"					Plate "r"				
	7.14 ERP	6.51 ERP	5.88 ERP	5.25 ERP	4.62 ERP	5.88 WRP	7.14 ERP	6.51 ERP	5.88 ERP	5.25 ERP	4.62 ERP	7.14 ERP	6.51 ERP	5.88 ERP	5.25 ERP	4.62 ERP
0	3.23		2.65		4.26				2.91					2.88		
1	1 99		1.34		2.71				1.33					1.52		
2						1.64										
3	2.55		1.71		3.25		2.46		1.80		3.23	2.68		2.02		3.34
4						1.96										
5	2.77	1.85	1.78	2.05	3.52		2.50	1.81	1.77	2.05	3.35	2.28	2.09	1.97	2.34	3.54
6	2.64				3.46	1.80			1.70					2.06		
6.94	2.54	1.62	1.65	1.81	3.20		2.35	1.62	1.71	1.81	3.00	2.95	2.14	2.26	2.39	3.51
7.64	2.33				2.81	1.61			1.56					2.45		
8.5	1.94		1.27						1.34					1.37		
10						1.09										
13	0.95		0.65		1.27				0.62					0.45		
15						0.46										
20						0.21										
21	0.24		0.17		0.32				0.15					0.16		

Table 3.38
Ratios of Clear Channel to Blocked Channel Relative Power Measurements for Elements in Positions 46 and 42
SM-2 Preliminary Mockup Core
Blocking Material - Stainless Steel

	Plate "j" and Between plates "i" and "j"					Plate "n"					Plate "r"				
Position	7.14 ERP to 7.14 WRP	6.51 ERP to 6.51 WRP	5.88 ERP to 5.88 WRP	5.25 ERP to 5.25 WRP	4.62 ERP to 4.62 WRP	7.14 ERP to 7.14 WRP	6.51 ERP to 6.51 WRP	5.88 ERP to 5.88 WRP	5.25 ERP to 5.25 WRP	4.62 ERP to 4.62 WRP	7.14 ERP to 7.14 WRP	6.51 ERP to 6.51 WRP	5.88 ERP to 5.88 WRP	5.25 ERP to 5.25 WRP	4.62 ERP to 4.62 WRP
0	1.27		1.11		1.30			1.15					0.56		
1	1.26		1.35		1.25			1.06					0.96		
3	1.30		1.42		1.25	1.07		1.11		0.95	1.04		0.98		0.97
5	1.35	1.45	1.38	1.37	1.26	1.02	1.06	1.03	1.08	0.99	0.85	1.02	0.90	0.95	0.96
6	1.40				1.37			1.03					0.95		
6.94	1.45	1.42	1.37	1.41	1.32	1.04	1.08	1.12	1.08	1.10	1.08		1.04	0.95	0.97
7.64	1.36				1.53			1.09					0.98		
8.5	1.32		1.35										0.96		
13	1.31		1.49		1.36			1.17					1.03		
21	1.50		1.67		1.61			1.30					1.40		

THIS PAGE

WAS INTENTIONALLY

LEFT BLANK

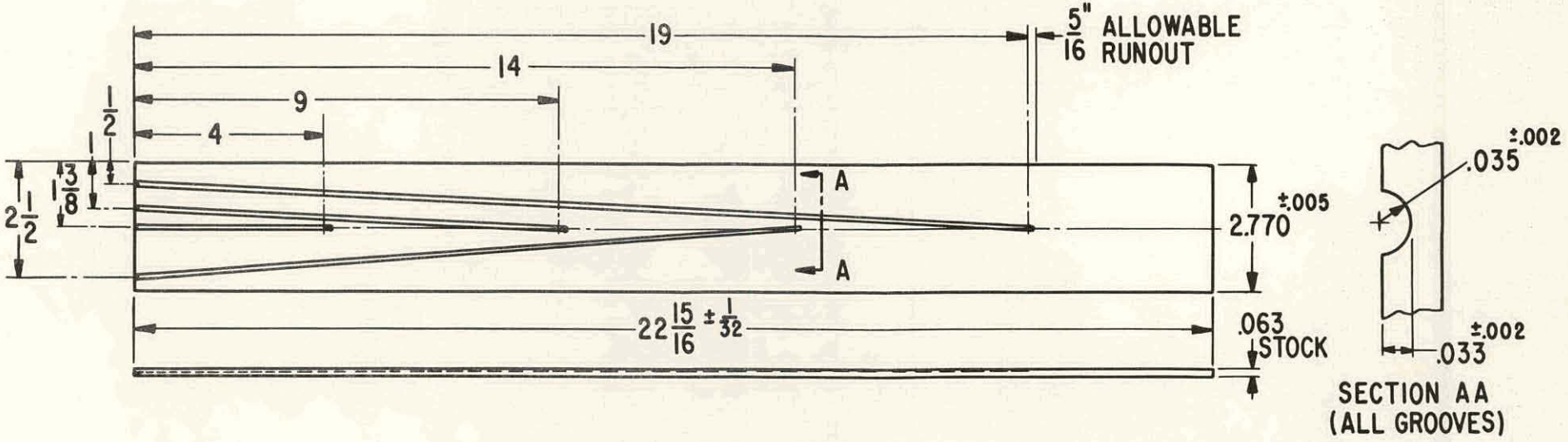

Figure 3.24 Thermocouple Plate, SM-2 Critical Facility Test

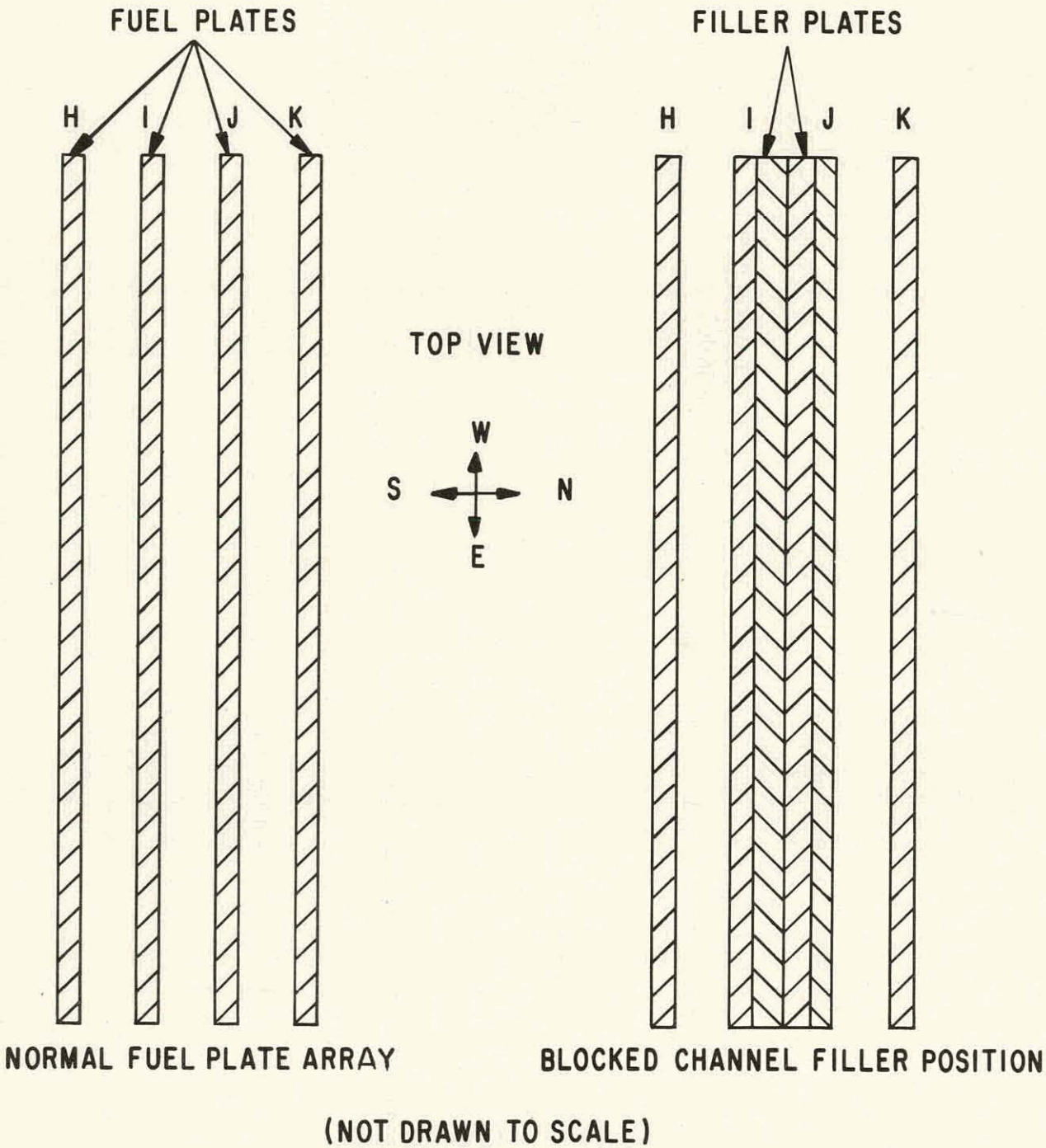

Figure 3.25 Blocked Channel Filler Position and Normal Fuel Plate Array

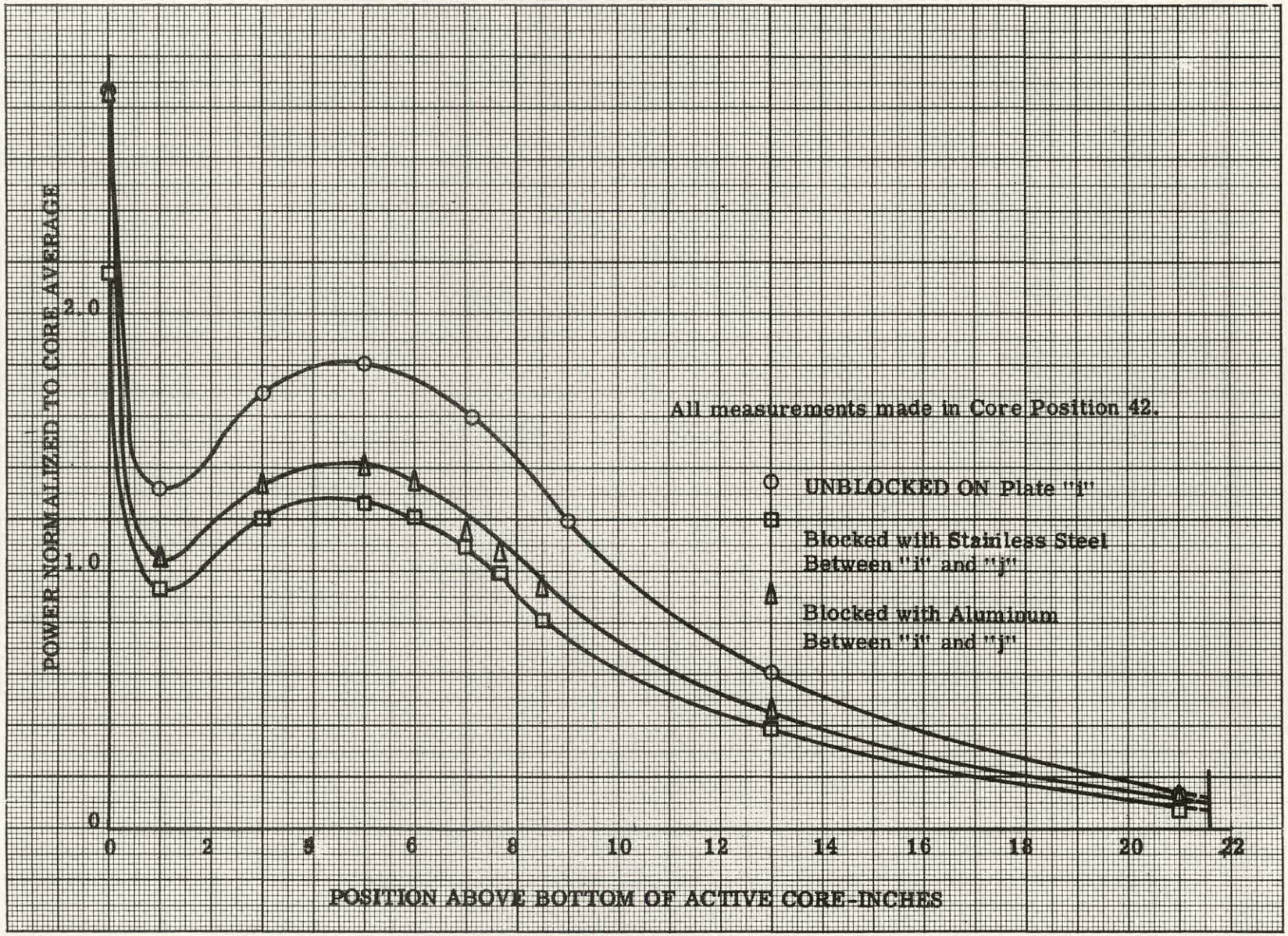

Figure 3.26 Relative Power Distribution Along Axial Traverse on Centerline of Fuel Plates "i" and "j" Blocked Channel Measurements Made in SM-2 Core Mockup with Water Reflector, Without Flow Divider

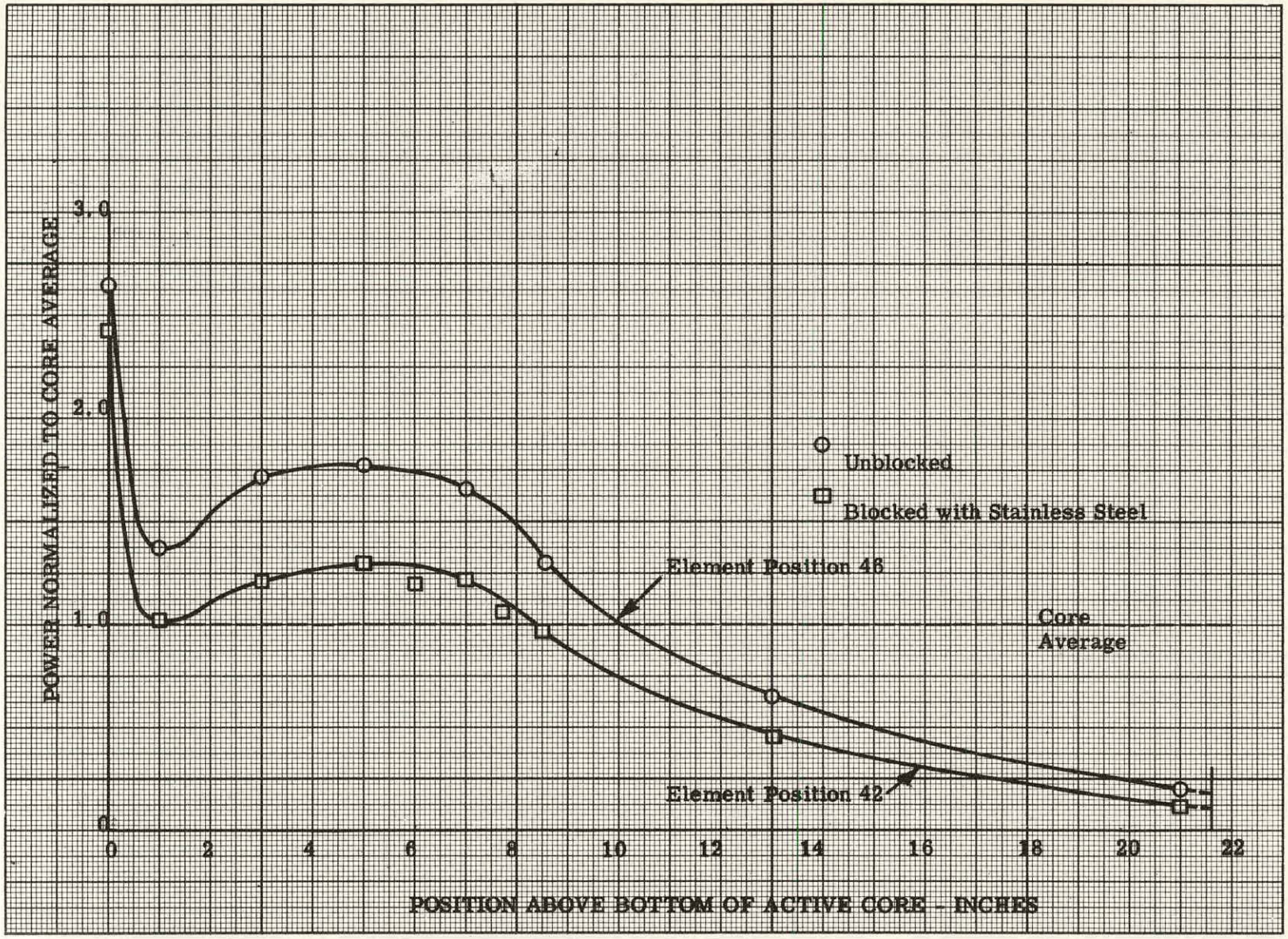

Figure 3.27 Relative Power Distribution Along Axial Traverse on Centerline Between Fuel Plates "i" and "j", Elements in Positions 42 and 46, Blocked Channel Measurements Made in SM-2 Core Mockup With Steel Reflector Without Flow Divider

4.0 MISCELLANEOUS MEASUREMENTS

4.1 GAMMA RAY DOSE MEASUREMENTS

An indication of the gamma heating distribution expected in the SM-2 core and vessel was obtained by a survey using film badges as radiation dosimeters. The location of these film badges is shown in Fig. 4.1 and 4.2 and Table 4.1 and 4.2. The reactor was operated for 10 minutes at a power level estimated at 10 watts and the badges removed within 30 minutes after shutdown. The integrated gamma dosage is given in Tables 4.1 and 4.2 and plotted in Fig. 4.3, 4.4 and 4.5. As expected, the maximum gamma heating occurred in the steel reflector adjacent to the core with the flux dropping rapidly toward the outer edge of the reflector.

4.1.1 Experimental Techniques

The film badges were located so that symmetry would give duplication of data. Each film was encased in Mylar tape to prevent water contact, and attached in the following locations:

1. Radially along the steel reflector midway between the top and core support plates.

2. Radially on the upper edge of elements 14, 34, 41, 42 and 43 just below the top plate.

3. Axially along the rod guide of control rod "C" which was kept fully withdrawn.

4. Radially in the water channels of the perforated core support plate just below elements 41, 42, 43, 54, 74 and the reflector.

5. Other miscellaneous locations on the core support plate.

Tables 4.1 and 4.2 present the radiation dose rate in terms of R/hr/watt for the run. These results are merely estimates and should be treated as such. For instance, the relationship between radiation dosage and power level could not be ascertained since absolute reactor power measurements had not been made. Hence, the estimate of 10 watt power operating level may have a rather large uncertainty factor. Secondly, each of the film badges received additional radiation after reactor shutdown, which, while of lesser magnitude, would still contribute to the total reported gamma dosage. Furthermore, it should be appreciated that the film badge cannot differentiate between the types of radiation it receives — the presence of other types of radiation which affect film exposure but whose

THIS PAGE

WAS INTENTIONALLY

LEFT BLANK

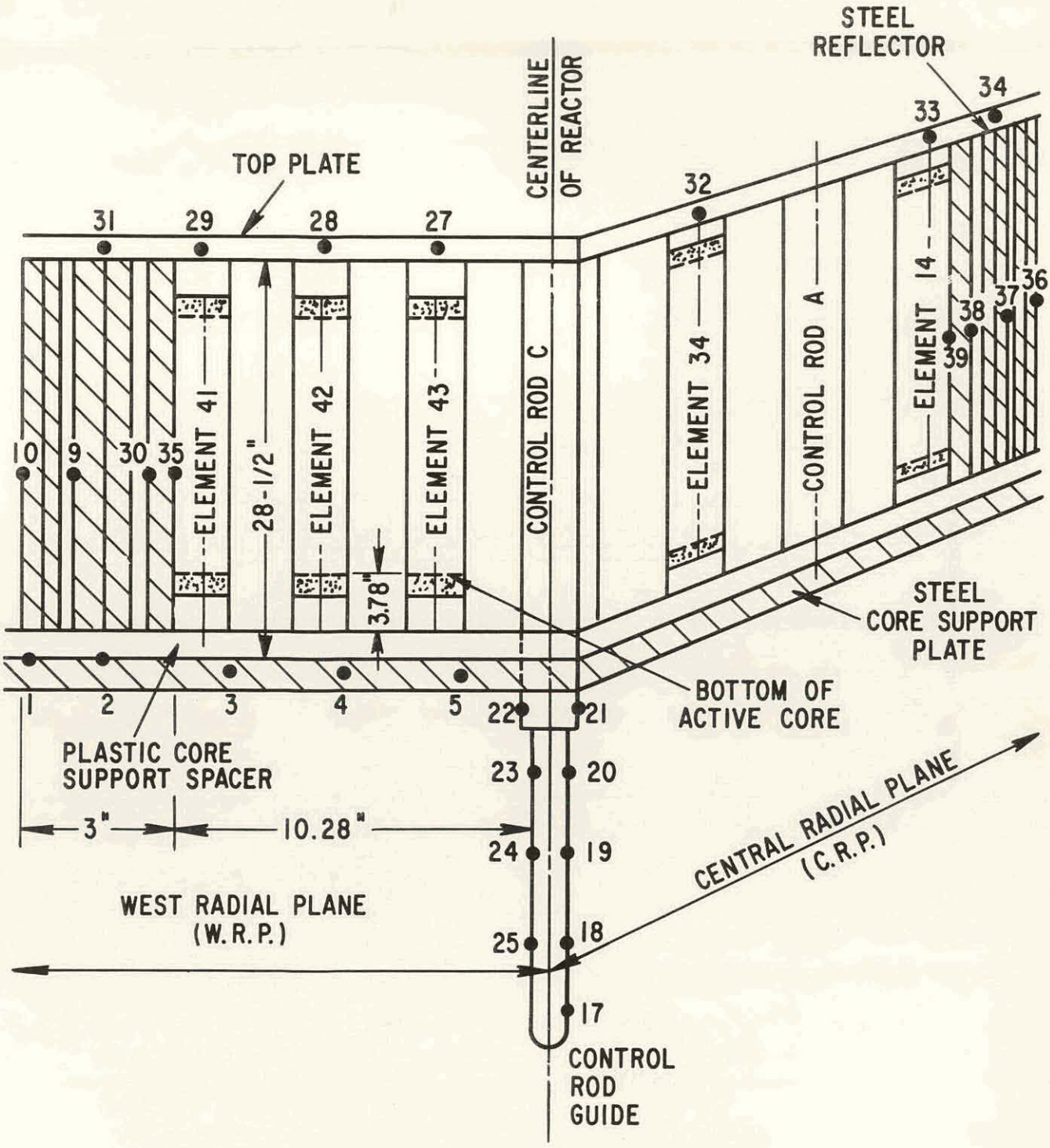

Figure 4.1 Location of Film Badges on Fuel Elements and Steel Reflector for Gamma Ray Dose Measurements

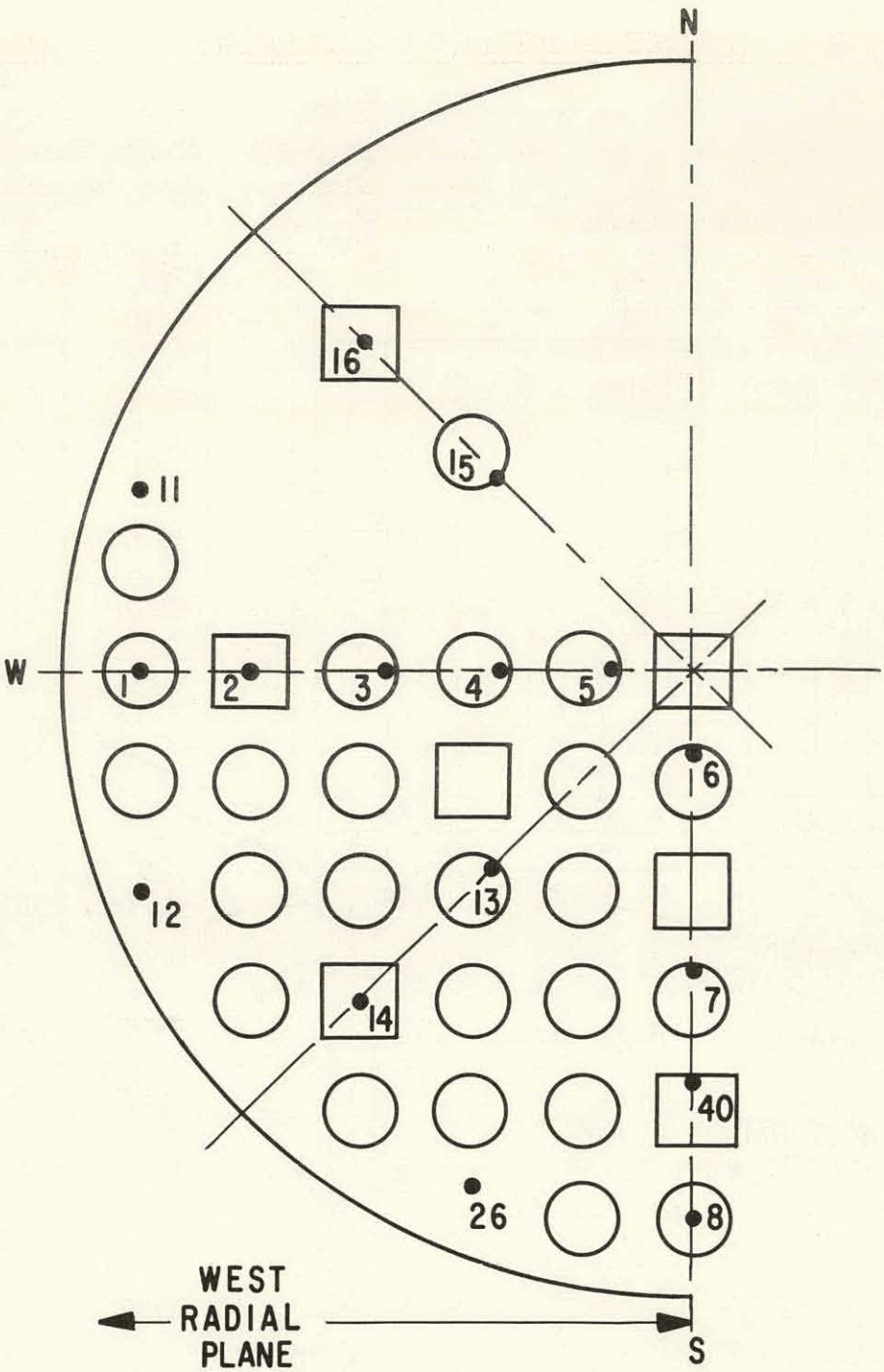

Figure 4.2 Location of Film Badges on Core Support Plate for Gamma Ray Dose Measurements

TABLE 4.1

GAMMA RAY DOSE MEASUREMENTS AND FILM BADGE* LOCATIONS

Location Number	Reported Dosage, R	Dosage R/hr/watt	Axial Location from bottom of active core, in.	Radial Location from Reactor Center, in.		
				West	North	South
1	0.185	0.11	-4.78	14.69		
2	1.4	0.84	-4.78	11.75		
3	3.8	2.3	-5.53	7.57		
4	6.0	3.6	-5.53	4.63		
5	5.0	3.0	-5.53	1.69		
6	6.0	3.6	-5.53			1.69
7	4.0	2.4	-5.53			7.57
8	0.85	0.51	-4.78			14.69
11	0.60	0.36	-6.28	14.69	5.88	
12	0.48	0.29	-6.28	14.69		5.88
13	4.8	2.88	-5.53	4.63		4.63
14	1.3	0.78	-4.78	8.82		8.82
15	4.6	2.76	-5.53	4.63	4.63	
16	0.308	0.18	-4.78	8.82	8.82	
26	0.50	0.30	-6.28	5.88		14.69
40	3.2	1.92	-5.53			10.50

* Exposed at estimated 10 watt power level for 10 minutes.

TABLE 4.2

GAMMA RAY DOSE MEASUREMENTS AND FILM BADGE* LOCATIONS

Location Number	Reported Dosage, R	Dosage R/hr/watt	Axial Location from bottom of active core, in.	Radial Location from Reactor Center, in.		
				West	North	South
9	4.6	2.76	9.22	12.03		
10	3.2	1.92	9.22	13.28		
17	0.058	0.035	-26.78			0.63
18	0.36	0.216	-21.28			0.63
19	0.75	0.450	-14.28			0.63
20	1.2	0.72	-10.28			0.63
21	3.4	2.04	- 7.28			1.4
22	3.4	2.04	- 7.28		1.4	
23	0.91	0.55	-10.28		0.63	
24	0.48	0.29	-14.28		0.63	
25	0.30	0.18	-21.28		0.63	
27	5.00	3.0	22.25	2.94		
28	4.00	2.4	22.25	5.88		
29	3.20	1.92	22.25	8.81		
30	8.50	5.10	9.22	10.78		
31	0.70	0.42	22.25	11.75		
32	5.50	3.30	22.25		2.94	
33	3.40	2.04	22.25		8.81	
34	0.80	0.48	22.25		11.75	
35	10.00	6.00	9.22	10.28		
36	3.60	2.16	9.22		13.28	
37	4.80	2.88	9.22		12.03	
38	8.50	5.10	9.22		10.78	
39	13.00	7.80	9.22		10.28	

* Exposed at estimated 10 watt power level for 10 minutes.

contribution to the reported dosage cannot be distinguished from that produced solely by gamma rays. Thus, the results obtained in these measurements should be interpreted merely as an indication of the trend and order of magnitude of the gamma flux expected without attaching quantitative importance to the reported dosage values.

4.1.2 Experimental Results

The experimental results have been plotted on Fig. 4.3, 4.4 and 4.5 with the appropriate film badge location numbered for convenience. From the data it can be seen that the gamma dosage in the center of the reflector drops rapidly from a high of 13 R/hr/watt to a low of 2 R/hr/watt at its outer edge and that the axial measurements along the guide of control rod C showed the expected decrease in gamma flux as the distance from the bottom of the active core increased. The flux along the core support plate decreased from 3.6 R/hr/watt to 0.1 R/hr/watt on a center to core edge traverse. Dosage measurements made at either end of the stationary fuel plates appear to have the same gamma field, reading a maximum of 3 R/hr/watt on element No. 43.

4.2 SEVEN ROD BANK CALIBRATION AT SIMULATED ELEVATED TEMPERATURE AND PRESSURE

4.2.1 Introduction

Since it is not possible to operate the ALCO Critical Facility at the design operating conditions of the SM-2 reactor, it was necessary to simulate these effects in order to obtain an estimate of the characteristics of the control rod bank in this region. Operation at 2000 psi and 510°F causes a loss of reactivity from operation at room conditions due to differences in moderator density; this results in a larger withdrawal of the control rod bank to achieve criticality. The experiments described below were run in order to calibrate the control rod bank in the desired SM-2 operating range with the flow divider in place. The calibration curve obtained is presented in Fig. 4.6. The data were corrected by 1 in. dial displacement incurred due to use of a plastic core support plate required for mockup operation with flow divider.

4.2.2 Calibration Technique

Operation of 2000 psi and 510°F causes a change in the density of water from 62.3 lbs/ft^3 at 70°F and 1 atmosphere to 48.9 lbs/ft^3. To simulate the loss in moderator density, it was calculated that 40 aluminum strips were required to be placed in each stationary fuel element and 38 in each control rod fuel section to displace the proper amount of water. The resulting reactivity measurements indicated approximately a 5 in. shift in bank position. In order to obtain a complete calibration of the bank as a function of bank location, some of the fuel plates were removed and stainless steel strips of equal thickness substituted. These strips were covered with 2 layers of #1-2 boron tape to replace the boron loading. These substitutions caused a further loss of reactivity; the effects of these additions to the mockup are given in Table 4.3.

THIS PAGE

WAS INTENTIONALLY

LEFT BLANK

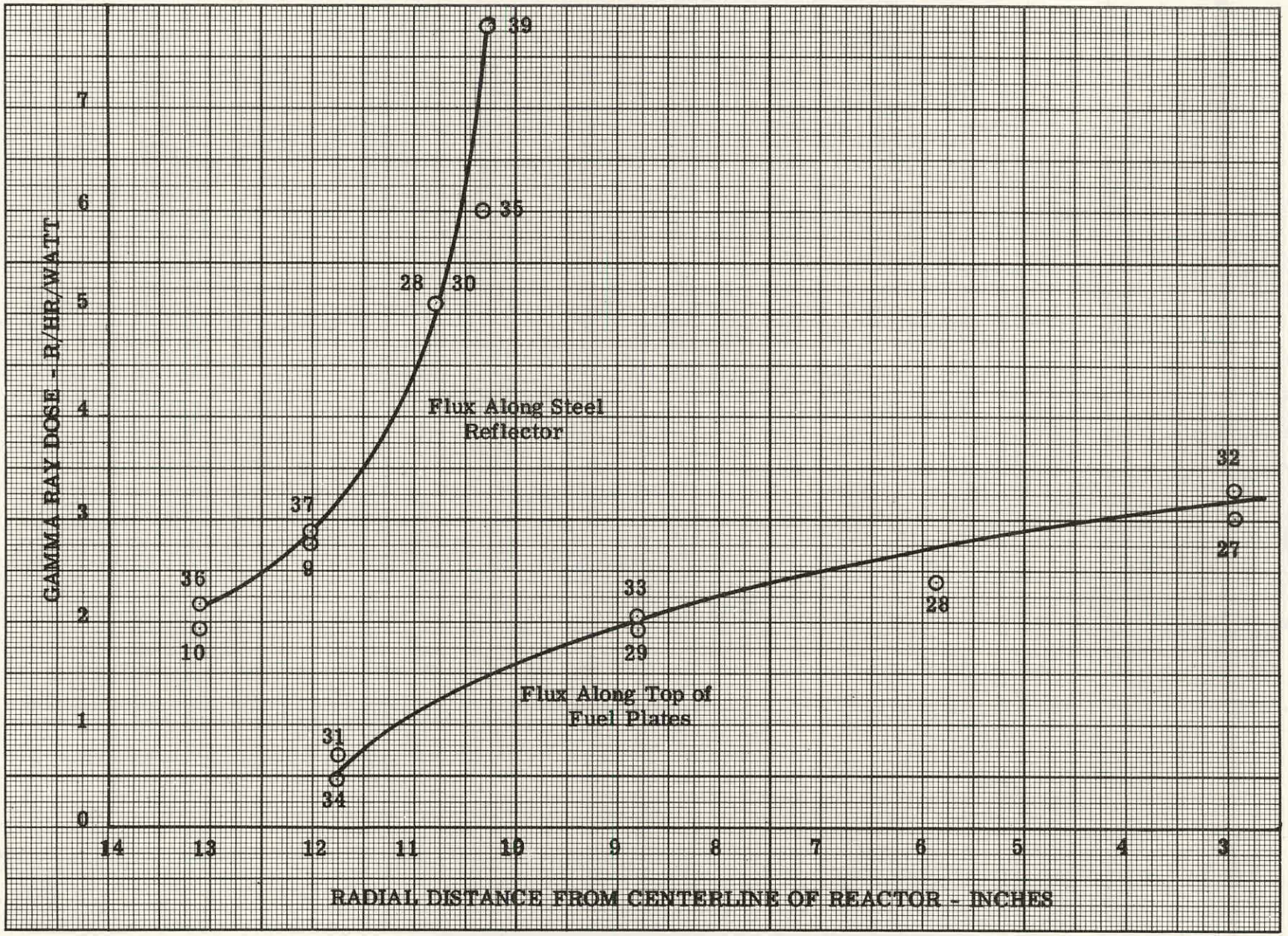

Figure 4.3 Gamma Ray Dose Measurements, SM-2 Preliminary Mockup Core

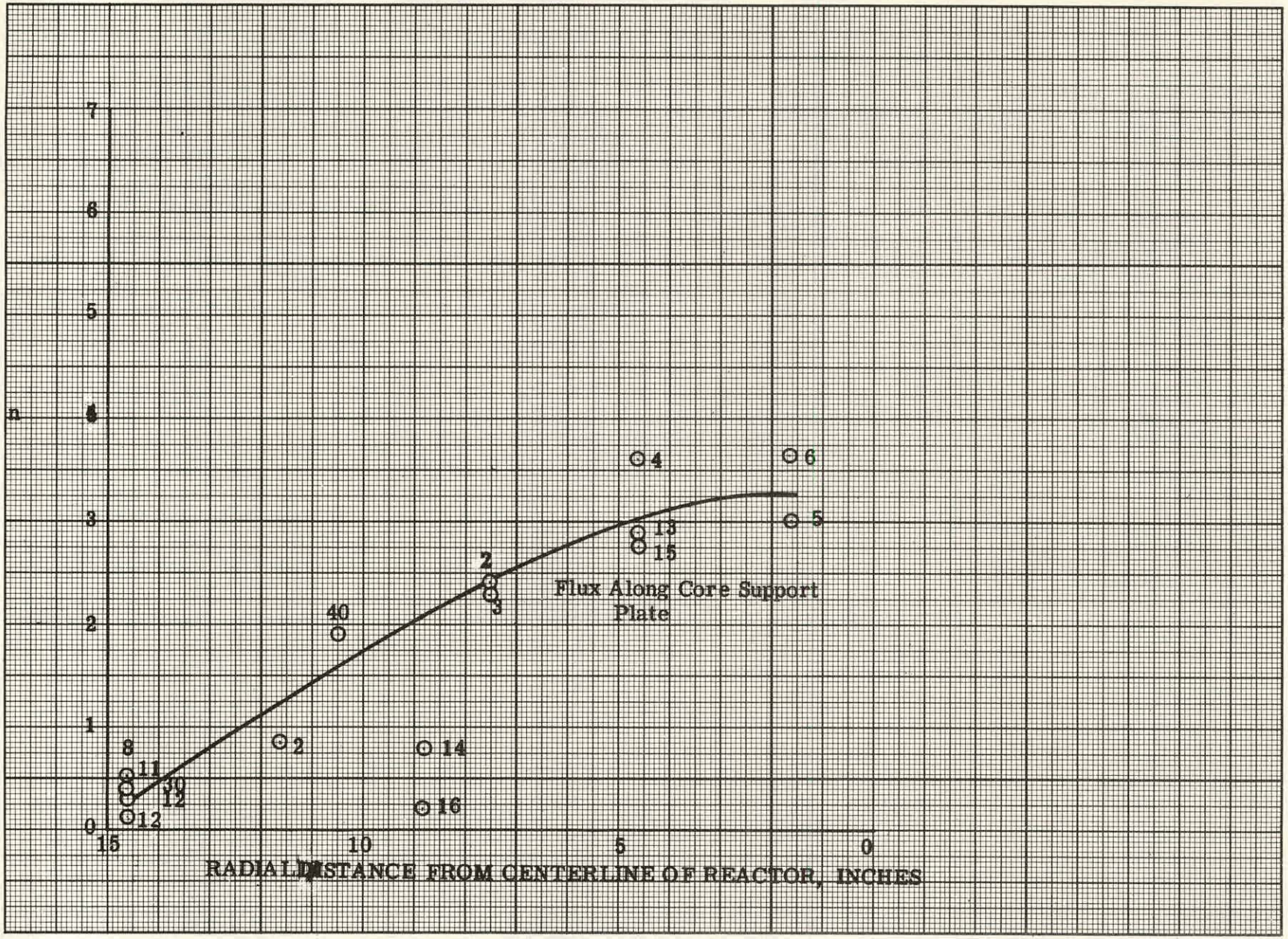

Figure 4.4 Gamma Ray Dose Measurements, SM-2 Preliminary Mockup Core

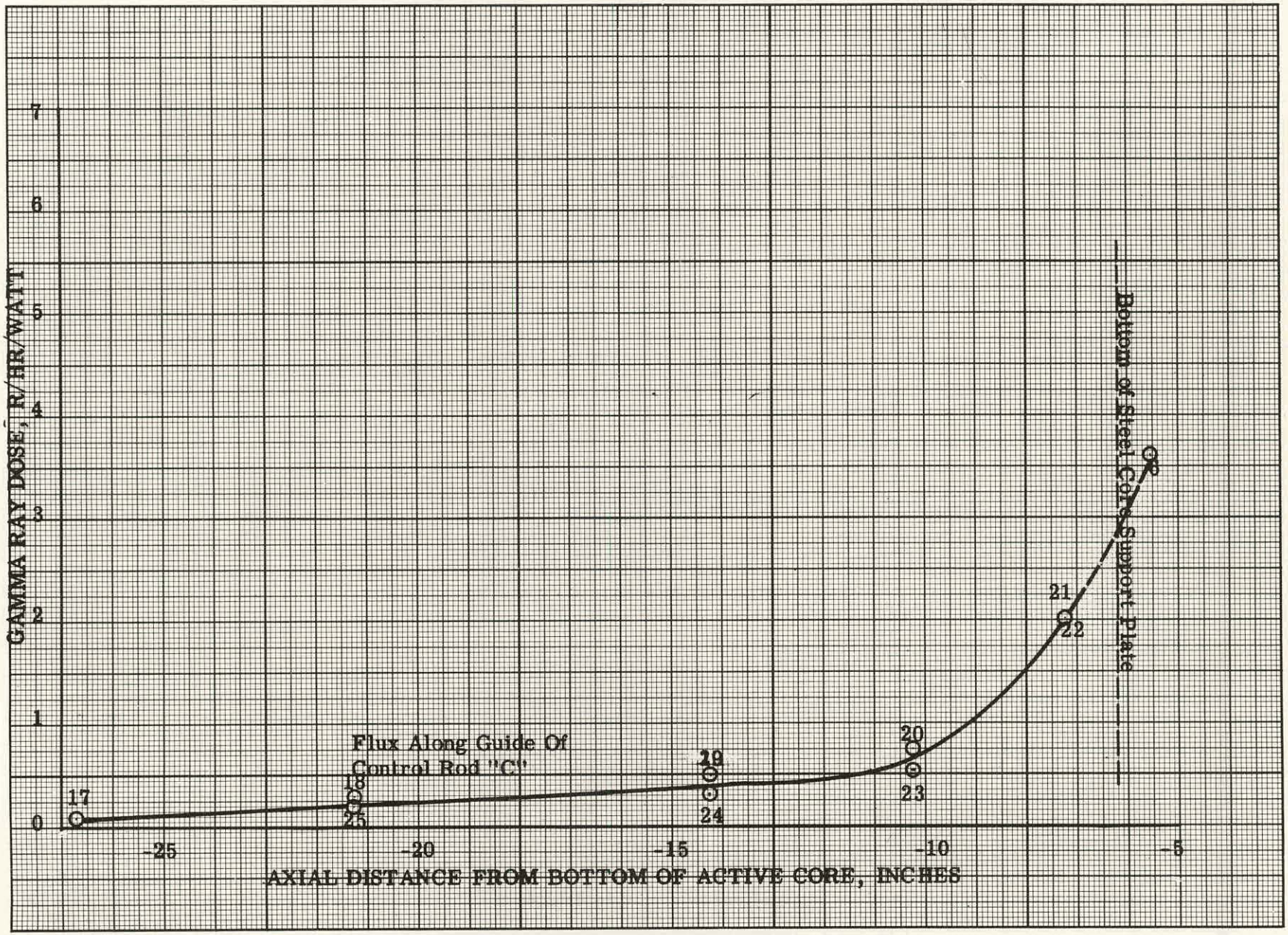

Figure 4.5 Gamma Ray Dose Measurements, SM-2 Preliminary Mockup Core

THIS PAGE

WAS INTENTIONALLY

LEFT BLANK

TABLE 4.3
CALIBRATION OF CONTROL ROD BANK UNDER
SIMULATED OPERATING CONDITIONS
OF 2000 Psi and 510°F

	Simulation Technique	Average 7 Rod Bank Critical Position Dial Reading, Inches
(1)	Initial Zero Run	8.725
(2)	Addition of 40 strips of 15-mil thick aluminum to each stationary fuel element and 38 strips to each control rod fuel section.	13.540
(3)	Same as (2) but with the addition of 23 aluminum strips per reflector water gap for a total of 92 strips in the reflector region.	13.472
(4)	Substitution of bundles of four 10-mil thick stainless steel strips in plate position a, j, and r of elements 34, 43, 45 and 54 with appropriate boron loadings.	15.216
(5)	Same as (4) above except that stainless steel bundles were also substituted in plates e and n in addition.	16.458
(6)	Same as (4) above except that stainless steel bundles were also substituted in elements 33, 35, 53 and 55 in addition.	17.140
(7)	Same as (6) above except that stainless steel bundles were also substituted in elements 23, 25, 63 and 65 in addition.	19.467
(8)	Same as (7) above except that stainless steel bundles were also substituted in element 46 in addition.	19.930
(9)	Same as (8) above except that stainless steel bundles were also substituted in element 42 in addition.	21.867

4. 2. 3 Simulation of Operating Conditions

The relationship of moderator temperatures vs density is presented in Fig. 4. 7. The number of aluminum strips required to displace an amount of water equal to the moderation loss incurred at the operating conditions due to density difference was calculated from the following:

$$N = \left(\frac{\rho_o - \rho}{\rho_o}\right) \quad \left(\frac{A_1}{A_2}\right) \; F$$

where N = No. of aluminum strips required

ρ_o = density at 70°F and 1 atmosphere

ρ = density at the desired conditions

A_1 = Cross-sectional area of fuel cell

A_2 = Cross-sectional area of aluminum strip

F = Fraction of fuel cell cross section filled with water.

Using data presented in APAE No. 54 and Fig. 4. 7, calculations were performed to relate the number of aluminum strips to the water temperature as shown in Fig. 4. 8.

To illustrate the calculation at 510°F, the number of strips "N" required for a stationary element:

$$\frac{\rho_o - \rho}{\rho_o} = \frac{62.3 - 48.9}{62.3} = 0.215$$

$$A_1 = (2.9375 \text{ in})^2 = 8.629 \text{ in}^2$$

$$A_2 = (0.0154)\,(2.266) = 0.0349 \text{ in}^2$$

$$F = \frac{A_1 - (18 \times \text{plate area} + 2 \times \text{side plate area})}{A_1}$$

$$= \frac{8.629 - (18 \times 2.77 \times 0.0408 + 2 \times 2.863 \times 0.0327)}{8.629}$$

$$= 0.742$$

$$N = \frac{(0.215)\,(8.629)\,(0.742)}{(0.0349)} = 39.4 \text{ or } 40 \text{ strips}$$

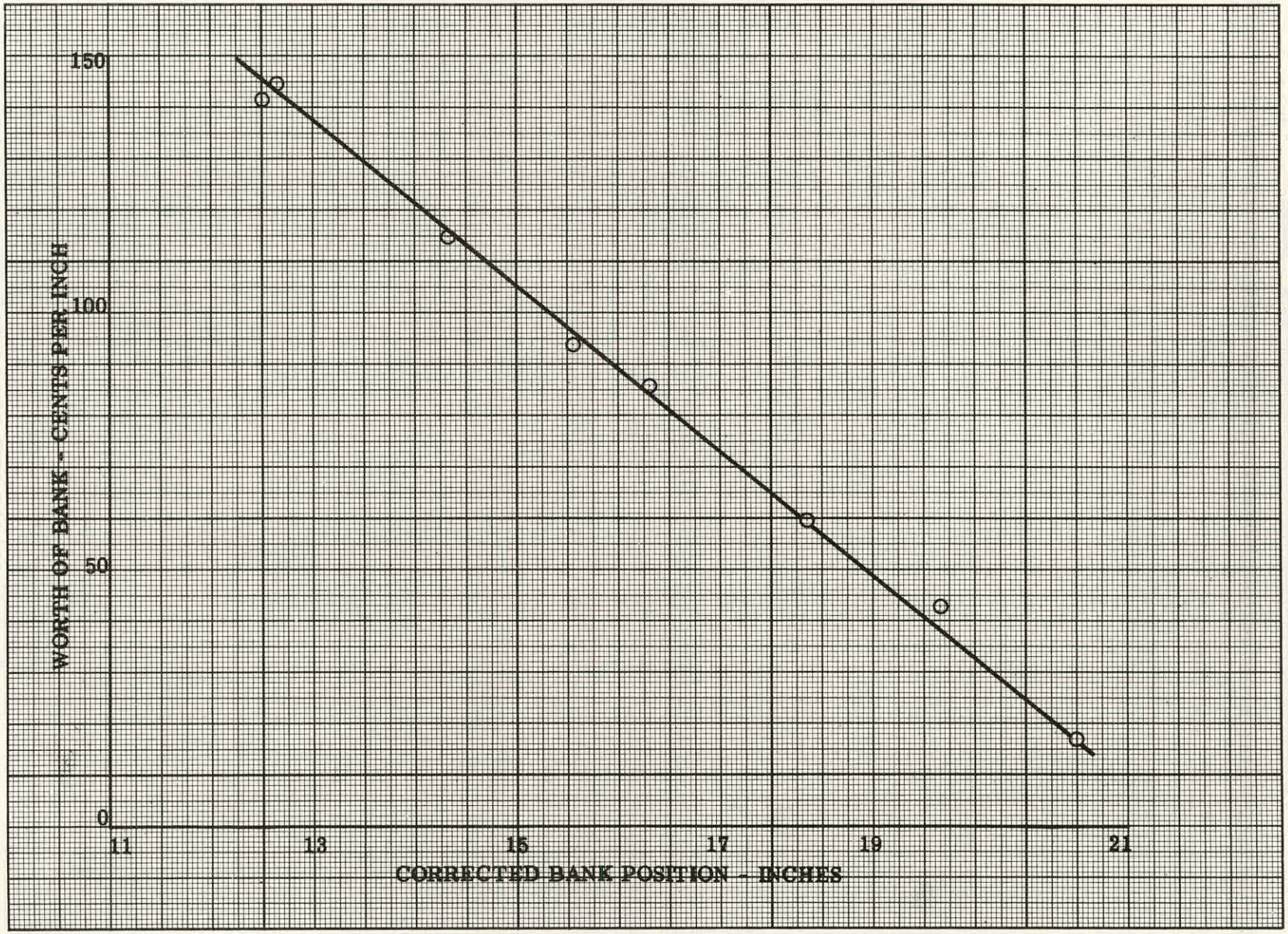

Figure 4.6 Seven Rod Bank Calibration Curve at Simulated 510°F and 2000 psi Conditions, SM-2 Mockup Core with Steel Reflector and Flow Divider

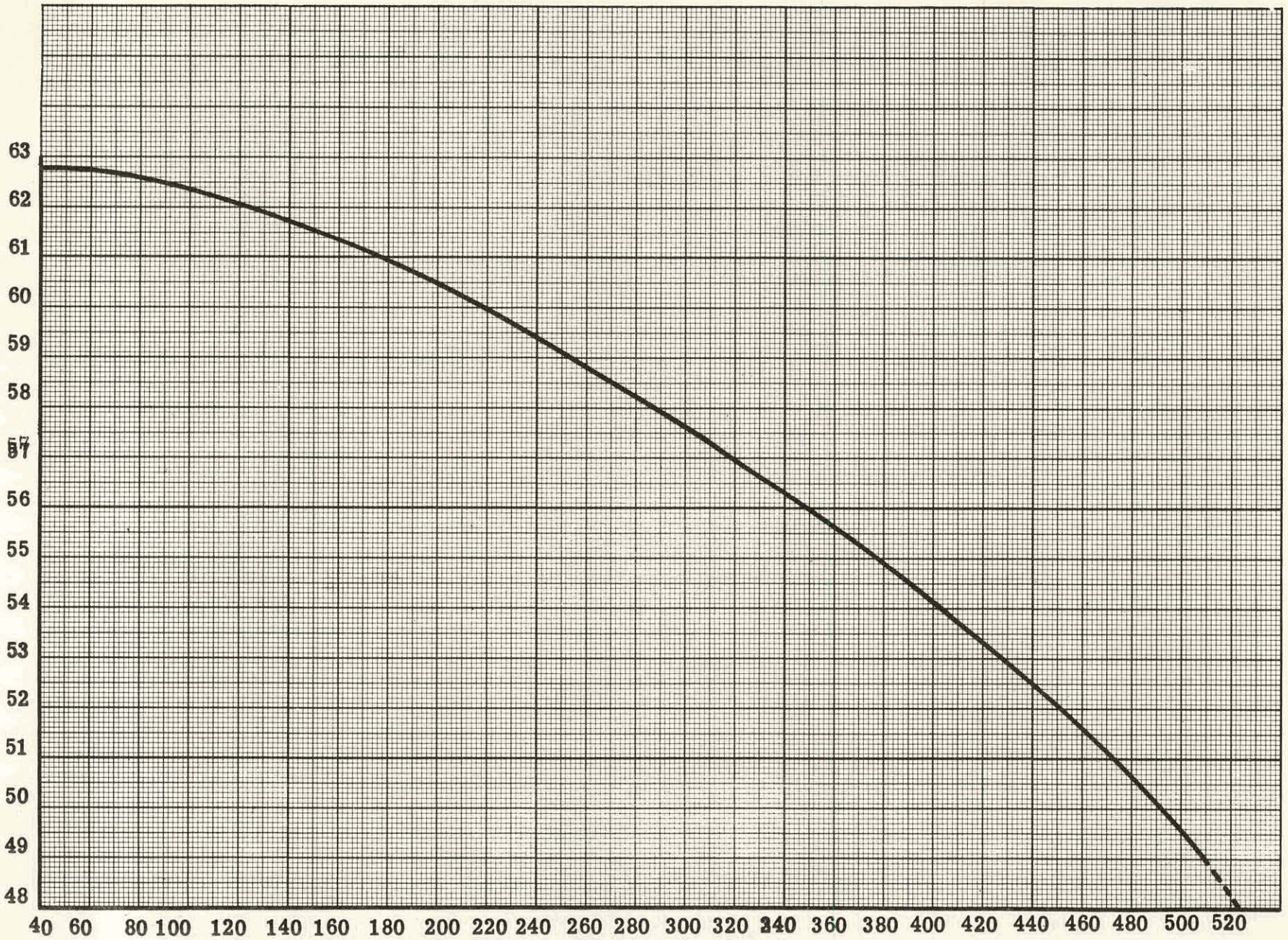

Figure 4.7 Density of Water Vs. Temperature at 2000 psi

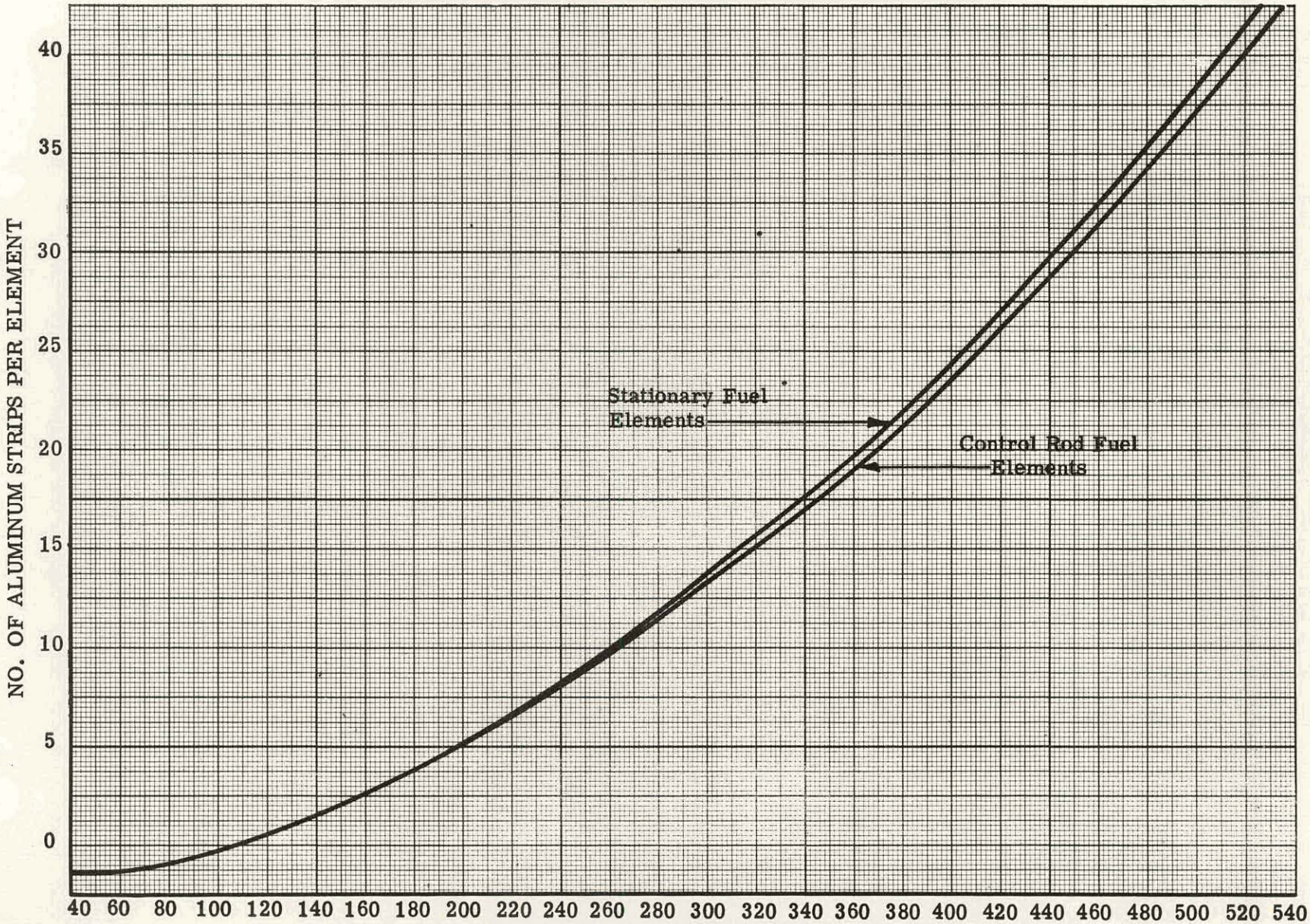

Figure 4.8 No. of Aluminum Strips per Fuel Element Required to Simulate Operating Temperature of the SM-2 Reactor at 2000 psi

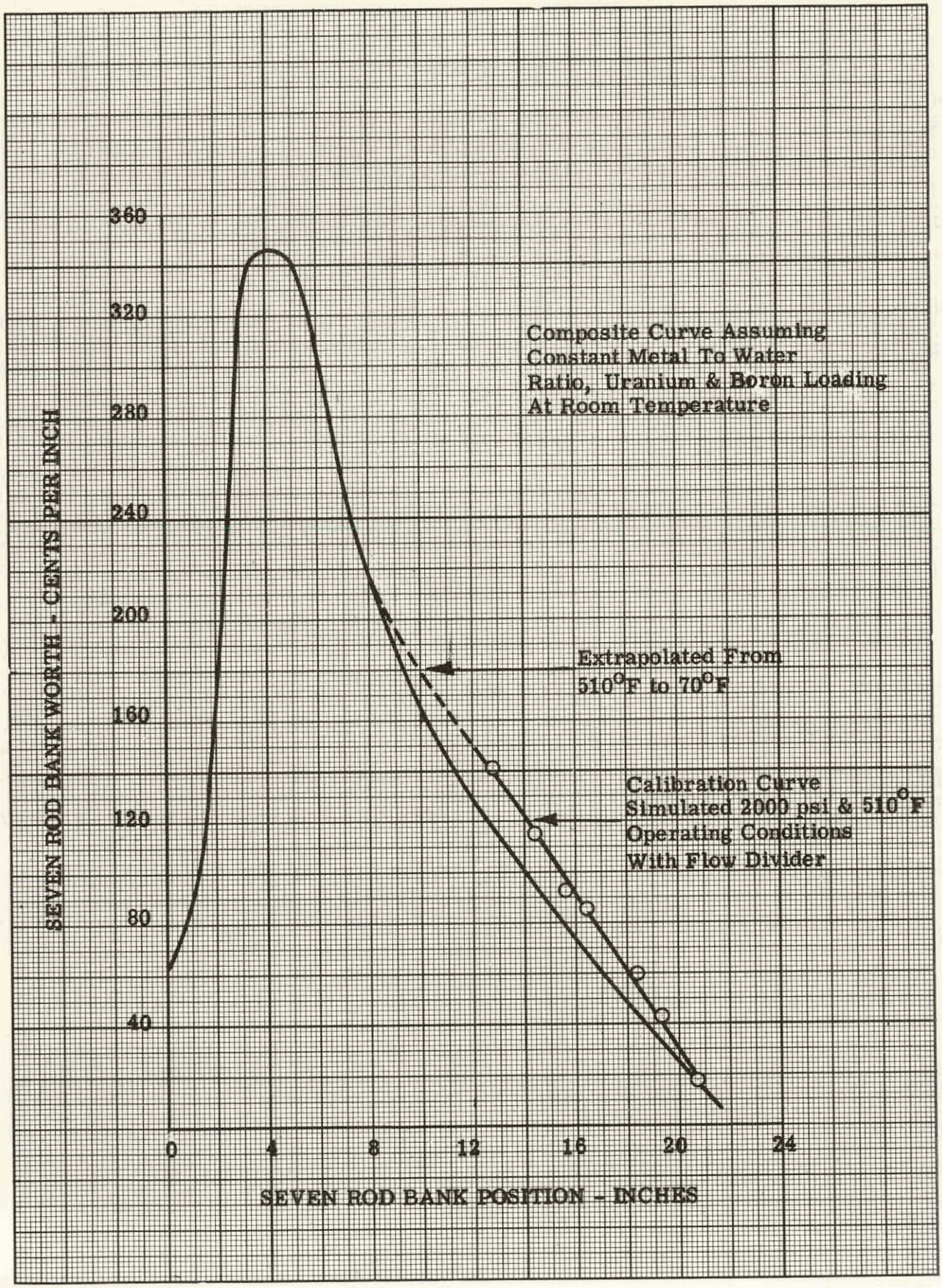

Figure 4.9 Composite Seven Rod Bank Calibration Showing Calibration at 2000 psi and 510°F

4.2.4 Reactivity Change Due to Operation at 510°F and 2000 Psi

The dashed portion of the seven rod bank position curve in Fig. 4.9 represents the bank worth from 70°F to 510°F, extrapolated to slope similarly to Fig. 4.3 in APAE No. 54.[1] Although no measurements were taken in this region, integration by Simpson's rule produced an average bank worth of 162 cents per inch at 11.1 in. Thus, the determined ΔK_E due to increasing the core temperature is calculated from Table 4.3 as:

$$\Delta K_E = 162\,(8.725 - 13.472) = -769 \text{ cents}$$

4.3 STUCK ROD MEASUREMENTS

Stuck rod measurements were made using the open seven control rod array SM-2 final mockup core, utilizing a 2.5-in. laminated stainless steel reflector, and a 0.125-in. stainless steel flow divider as shown in Fig. 1.2 and 1.7. Table 4.4 presents the critical control rod configurations and rod worth for various cases tested. Rods omitted in table were fully inserted and the reactor was brought critical on the critical rod(s) indicated for each case.

TABLE 4.4
CRITICAL ROD CONFIGURATIONS

Case	Rod (s) Fully Withdrawn	Critical Rod(s)	Critical Position(in.)	Worth cents/in.
1	C	A, D	15.616	42.4 @ 15.809 in.
2	C	A, F	13.443	68.2 @ 13.587 in.
3	C	A, G	17.282	30.0 @ 17.504 in.
4	C	E, F	14.778	55.5 @ 14.964 in.
5	C	B, D, F	12.481	75.9 @ 12.609 in.
6	A, D	C	14.891	37.4 @ 15.155 in.
7	A, E	F	18.482	11.9 @ 19.319 in.
8	A, D, E	B	13.704	19.1 @ 14.087 in.
9	B, C, E	D	4.959	32.7 @ 5.263 in.
10	B, D, E	F	12.440	25.9 @ 12.781 in.
11	B, E, F, G	C	1.088	18.8 @ 1.775 in.

The critical rod configurations reported above are much different from those in APAE No. 54[1] because of increase in B-10 loading and addition of flow divider and reflector. The following rod combinations were found to be subcritical when fully withdrawn: any two rods; three rod arrays ADE, BCE, BCF, BDE, EFG; and four rod array, BEFG.

REFERENCES

1. Noaks, J. W., et al, "SM-2 Critical Experiments - CE-1," APAE No. 54, November 30, 1959.

2. Noaks, J. W., "The Alco Products, Inc., Criticality Facility - Description and Operation," APAE No. 36, July 16, 1958.

3. Noaks, J. W., "Hazards Summary Report for SM-2 Critical Experiments," APAE No. 36 Supplement 1, January, 1959.

4. Meem, J. L., "Hazards Summary Report on the Zero Power Experiments for the Army Package Power Reactor," APAE No. 5, January 27, 1956.

5. McCool, W. J., et al, "Description of Fission Foil Counting and Data Processing Techniques Employed at Alco Criticality Facility," AP Note 246, April 22, 1960.

6. Hoover, H. L., Project Engineer, "SM-2 Reactor Core and Vessel Review Report, December 15, 1959 to March 18, 1960," APAE Memo No. 250, March 30, 1960.

APPENDICES

APPENDIX A

CALCULATION PROCEDURES USED TO DETERMINE B-10 LOADINGS

A. 1 CALIBRATION OF BORON STANDARDS

The repositioning of control rod E with the insertion of a standard sample in place of a "blank" establishes a method of relating boron loading to core reactivity change. The following presents a typical calculation used to calibrate standard samples in terms of reactivity.

$$\text{Reactivity, } ¢ = \left[1/2\,(W_1 + W_2)\right]\ (P_1 - P_2) \qquad (1)$$

where P_1 = Position of control rod E with standard No. 1 placed in plate i of element No. 22, i. e., measuring position

P_2 = Position of control rod E with blank standard placed in plate i of element No. 22 i. e., zero position.

W_1 = Worth of the rod E at P_1, in ¢/in.

W_2 = Worth of rod E at P_2 in ¢/in.

In the following computations several Rod E calibration curves were used because of change in the bank position for the different measurements. A typical curve is shown in Fig. A. 1 which represents a "least squares" average taken from data points obtained by period measurements. Figure A. 3 was used in period computations.

From Reactor Log Data Book, for runs No. 147 and 148:

Rod E Position	B-10 Content of Tape mg/cm^2	Rod E Worth
P_1 = 13. 395 in.	0. 186	W_1 = 24. 14
P_2 = 13. 008 in.	0	W_2 = 25. 47

$$\text{B-10 Worth} = \left[1/2\,(24.14 + 25.47)\right]\,(13.395 - 13.008)$$

$$= (24.81)\,(0.387) = 9.60\ ¢$$

Repeating these measurements for the other standard samples, B-10 worth vs. B-10 loading is plotted in Fig. A-2.

A. 2 INTERCALIBRATION OF TAPES

The B-10 loading of tape 2-1 #6 (Ref. Table 2. 1), substituted in plate i of element No. 22, for example, was similarly obtained from equation (1) and Fig. A-2.

From the reactor log book, runs No. 149 and 150:

Rod E Position	Tape	Rod E Worth
P_1 = 13. 146	Tape 2-1 #6	W_1 = 24. 99
P_2 = 12. 994	Blank Tape	W_2 = 25. 52

$\therefore$ B-10 Worth = 3. 847 ¢

From Fig. A-2 a core reactivity change of 3. 847 ¢ under these test conditions corresponds to a boron loading of 0. 0717 mg B-10/cm^2. In this fashion, data for the other intercalibrated tapes was calculated which is given in Table 2. 1.

A. 3 INTERCALIBRATION OF SM-2 MOCKUP FUEL PLATES

The substitution of fuel plate 139-S-3 in plate i of element 22, with and without intercalibrated tape 1-2 #3 resulted in the following:

Runs No. 166, 167

Rod E Position	Tape	Rod E Worth
P_1 = 11. 201	With Tape 1-2 #3	W_1 = 31. 66
P_2 = 10. 861	No Boron on plate	W_2 = 32. 82

$\therefore$ Reactivity by equation (1) = 10. 962 ¢

B-10 Worth of tape on fuel plate, ¢/gm = $\frac{R}{AG}$

R = reactivity, cents from equation (1)

A = area of boron tape applied, cm^2

G = boron loading for tape, mg/cm^2

B-10 Worth = 10. 962/ (348. 4) (0. 1590) = 197. 9 ¢/gm

A similar calculation for the addition of tape 2-1 #12 produced a boron worth of 136.4 ¢/gm. The total loading on plate 139S-3 is 55.4 + 26.3 = 81.7 mg.

The substitution of fuel plate 156S-2 in place of reference plate 139S-3 (containing tapes 1-2 #3 and 2-1 #12) produced the following:

Runs No. 168, 169

Rod E Position	Plate No.	Rod E Worth
P_2=11.326	156S-2	W_1 = 31.23
P_1=11.315	139S-3	W_2 = 31.27

∴ Reactivity from equation (1) = - 0.344 ¢

The B-10 difference between plates 139S-3 and 156S-2 is found by:

B-10 Mass Difference -0.344/-136.4 = + 0.0025 gm

∴ Total loading on plate 156S-2 is then = 0.0817 + 0.0025 = 0.0842 gm.

The results of similar calculations for the other fuel plates of element 22 is given in Table 2.2.

A.4 INTERCALIBRATION OF ELEMENTS

A similar calculation was performed to obtain the boron loadings of other elements. Instead of using 136.4 ¢/gm, which is the boron worth of a single tape on a fuel plate in the center of an unloaded fuel element as described in paragraph 2.2.2.4, the value of 56.62 ¢/gm was determined by the addition of 5 calibrated tapes on element No. 22 as the worth of uniformly distributed boron in a fully assembled fuel element. For element 47, for example,

$$\text{Reactivity} = \left[1/2\,(W_1 + W_2)\right](P_1 - P_2) = (30.06\ (0.109) = 3.28\ ¢$$

Additional boron on element 47 over that on element 22:

Weight Diff. = 3.28 ¢/56.62 ¢/gm = + 0.0579 gm

Total loading of element 47 = 1.4905 gm + 0.0579 gm = 1.5484 gm. Results for other elements are given in Table 2.3.

A. 5 B-10 WORTH CALCULATION OF ASSEMBLED MOCKUP ELEMENT

Runs No. 195, 199, 200

Rod E Position		Rod E Worth
P_1 = 10. 492	Element 22 with 5 Tapes	W_1 = 35. 61
P_2 = 10. 284	Element 22 without these 5 Tapes	W_2 = 36. 35

total loading of 5 tapes = 0. 1321 gm B-10

Reactivity from equation (1) = 7. 48 ¢

∴ B-10 worth of tapes = 7. 48 ¢/0. 1321 gm = 56. 62 ¢/gm

A. 6 COMPARISON OF BMI REFERENCE AND MOCKUP ELEMENTS

Runs No. 195, 196, 199

Rod E Position		Rod E Worth
P_1 = 10. 701	BMI Element	W_1 = 34. 92
P_2 = 10. 284	Element 22	W_2 = 36. 35

Reactivity, from equation (1) = 14. 86 ¢

∴ B-10 Loading of BMI Element = $1.4905 + \frac{14.86\ ¢}{56.62\ ¢/gm} = 1.753$ gm

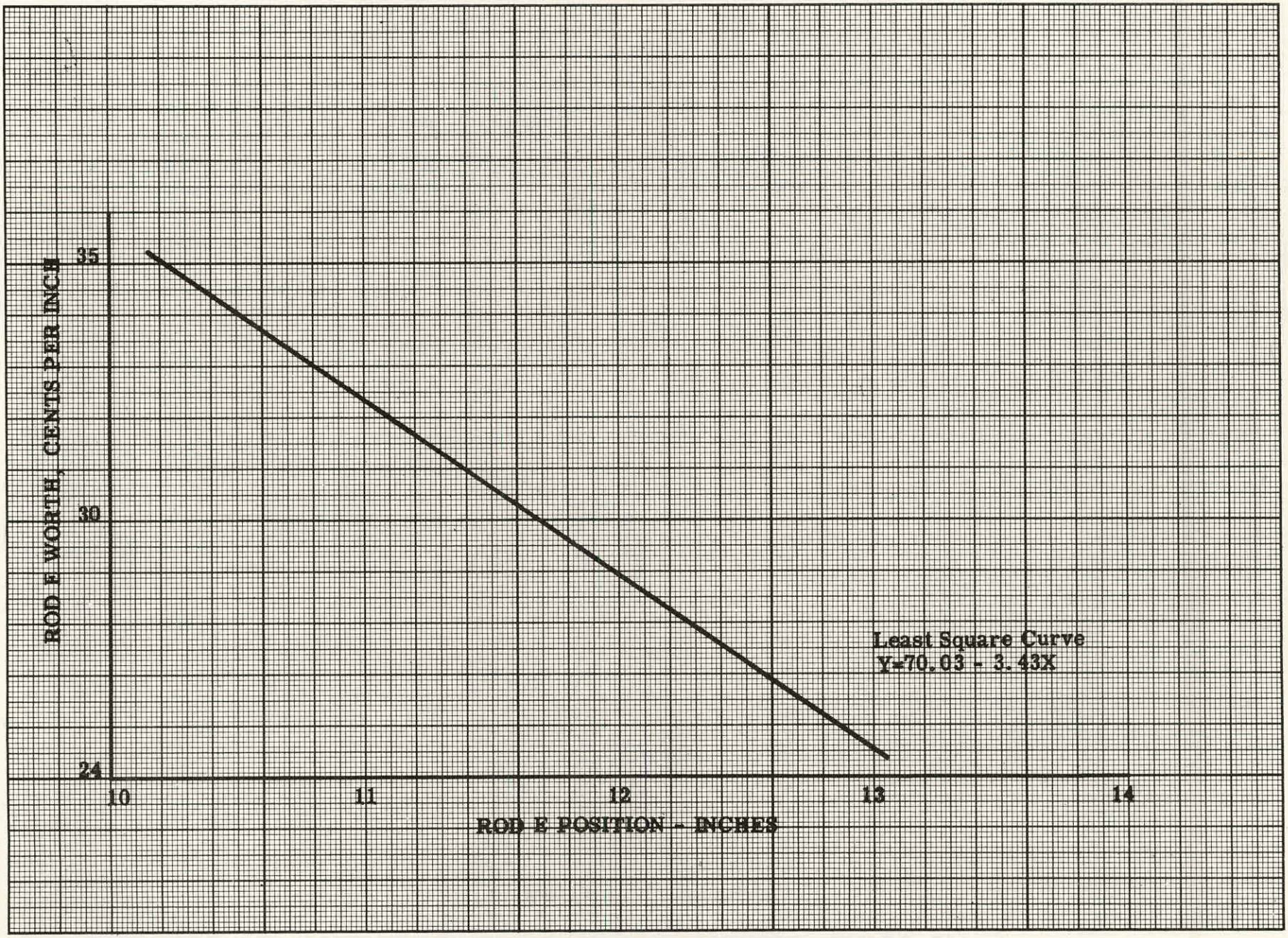

Figure A.1 Control Rod E Calibration Curve

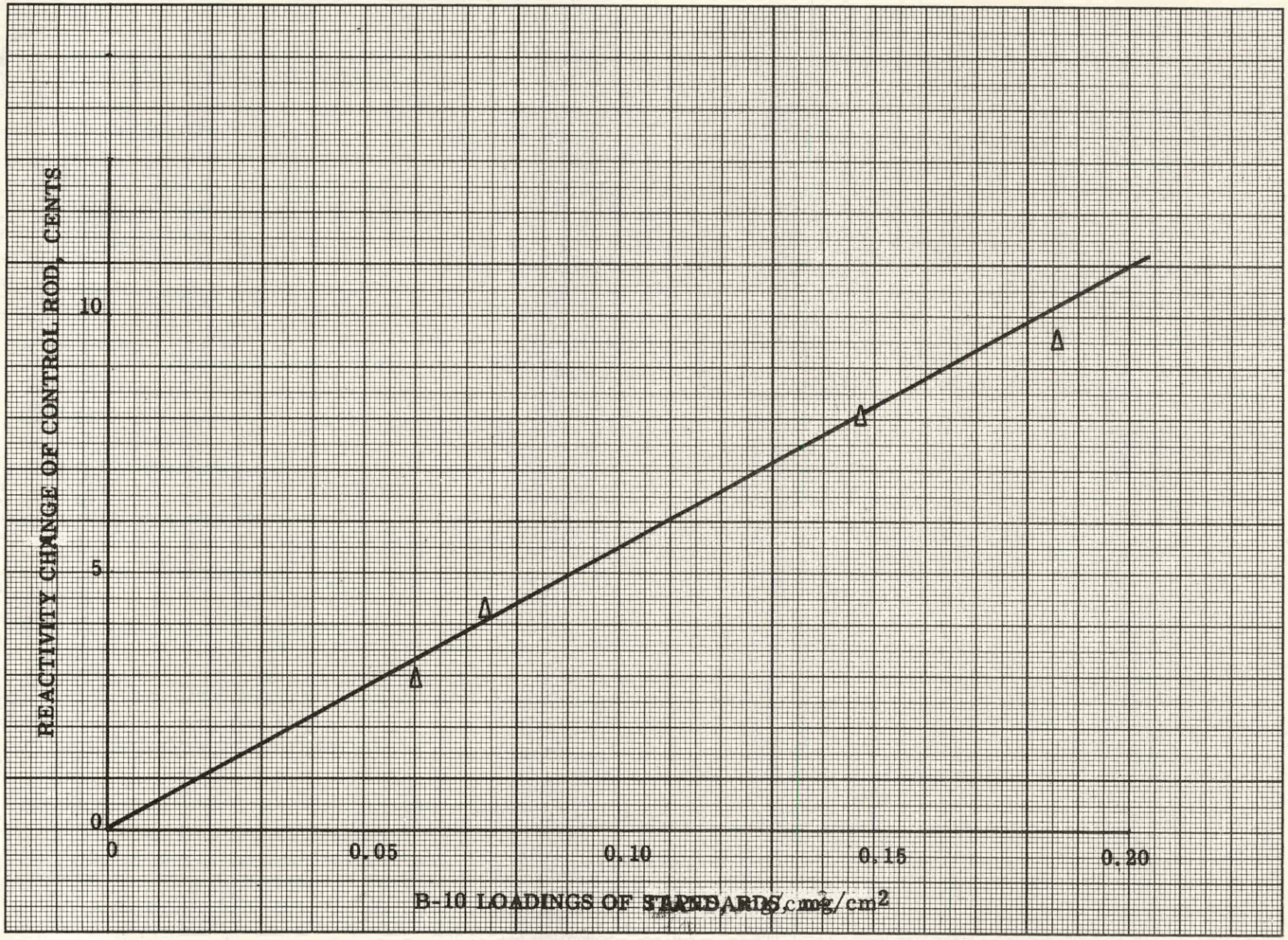

Figure A.2 B-10 Worth of Standards in Element Position 22 Plate "i"

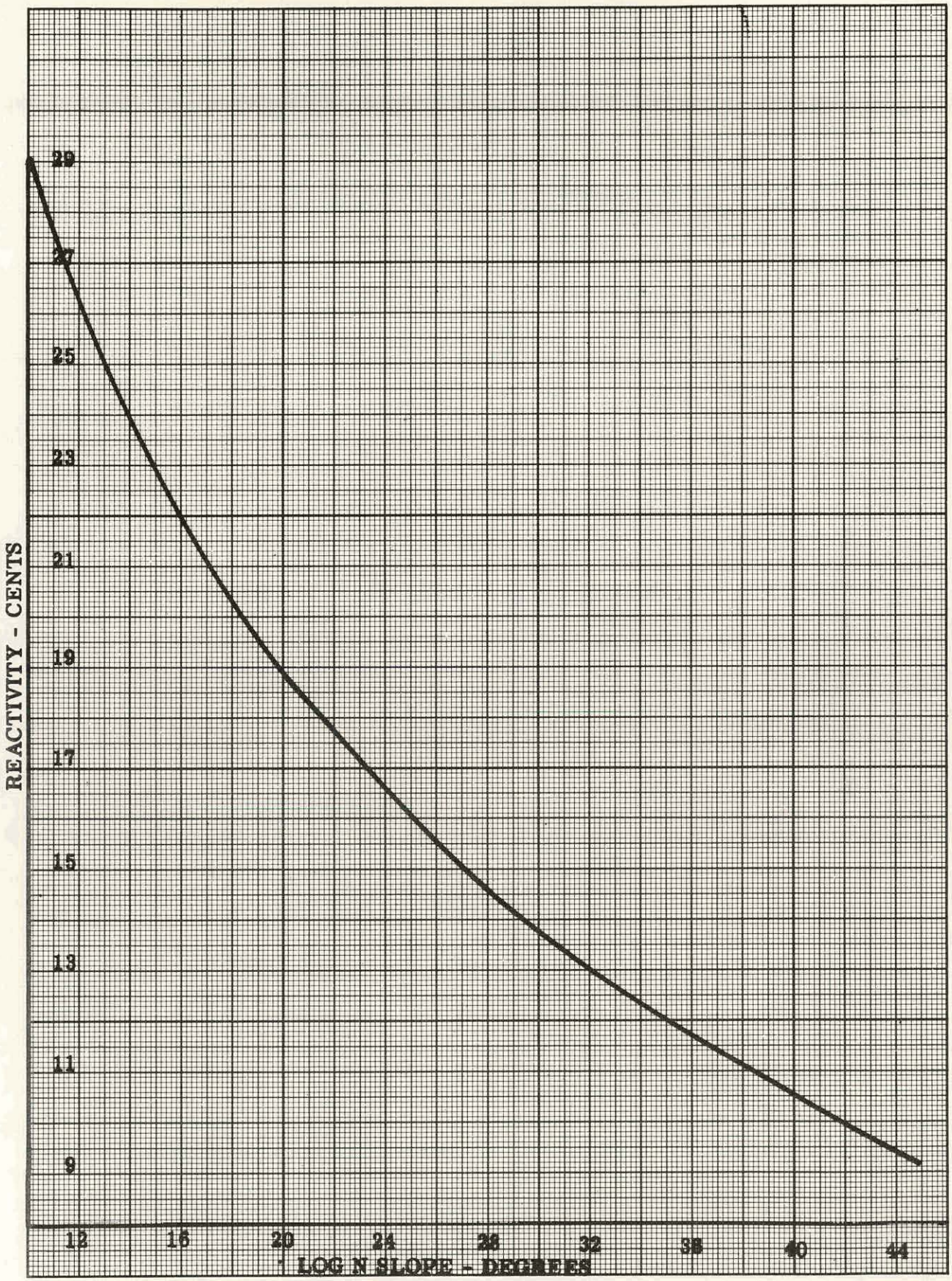

Figure A. 3 Log N Slope vs. Reactivity

APPENDIX B

TYPICAL CALCULATION PROCEDURE FOR OBTAINING THE CORE AVERAGE

B. 1 EXPERIMENTAL DATA OBTAINED USING PRELIMINARY MOCKUP AS AN EXAMPLE

The relative foil activation data for element 12, plate a is typical for these runs. Table B-1 below presents the relative flux data in raw form; these have been normalized by the procedure outlined below to form part of Table 3. 1.

TABLE B. 1
EXPERIMENTAL FOIL ACTIVATION DATA FOR ELEMENT 12

Axial Foil Location above bottom of active core, inches	Radial Foil Location from Center of Reactor, Inches				
	7. 13 WRP	6. 51 WRP	5. 88 WRP	5. 26 WRP	4. 64 WRP
	Relative Power Distribution on plate a*				
0	0. 656		0. 954		1. 111
1	0. 436		0. 430		0. 774
3	0. 559		0. 530		0. 965
5	0. 616	0. 574	0. 640	0. 684	1. 089
6. 94	0. 593	0. 556	0. 600	0. 673	1. 011
8. 50	0. 536		0. 530		0. 929
13. 0	0. 328		0. 300		0. 515
17. 0			0. 203		
21. 0	0. 0863		0. 0727		0. 125

* The relative power at a specific test point is established by the ratio of the induced activities of test foil to that of the reference foil (paragraph 3. 2. 1).

B. 2 CALCULATION OF AVERAGE POWER ACROSS PLATE "a" IN RADIAL DIRECTION USING SIMPSON'S RULE:

For axial positions 0, 1, 3, 8. 5, 13, and 21, the 3-point Simpson's rule was employed.

For axial positions 5 and 6. 94, the 5-point Simpson's rule was employed.

a. Using 3-point Simpson's rule of axial position 0 as a typical example of its application:

$$A = 1/3\ h\left[y_o + y_2 + 4\ y_1\right]$$

where

$$y_o = 0.656,\ y_2 = 1.111,\ y_1 = 0.954$$

$$1/3\ h = 1/3\left\{\frac{7.13\ WRP - 5.88\ WRP}{7.13\ WRP - 4.63\ WRP}\right\} = 1/3\left(\frac{1.25}{2.5}\right) = 0.1667$$

$$\therefore A = 0.931$$

b. Using 5-point Simpson's rule at 5-in. axial position as a typical example of its application:

$$A = 1/3\ h\left[y_o + y_4 + 4\ (y_1 + y_3) + 2\ y_2\right]$$

where

$$y_o = 0.616,\ y_4 = 1.089,\ y_1 = 0.574,\ y_3 = 0.684,\ y_2 = 0.640$$

$$1/3\ h = 1/3\left(\frac{7.13\ WRP - 6.51\ WRP}{7.13\ WRP - 4.63\ WRP}\right) = 1/3\left(\frac{0.62}{2.50}\right) = 0.0833$$

$$\therefore A = 0.67$$

In this fashion, the experimental data given in Table B-1 was reduced to the following:

Axial location above bottom of active core, inches	Average radial activity for plate a
0	0.94
1	0.49
3	0.64
5	0.67
6.94	0.64
8.5	0.59
13.0	0.34
17.0	0.23
21.0	0.08

B.3 CALCULATION OF AVERAGE POWER ALONG PLATE "a" IN AN AXIAL DIRECTION

A plot of the above data produced a curve shown in Fig. B-1. Using a planimeter, the area under the curve was obtained. This procedure was repeated for all the plates of element 12, giving the following:

Plate Position	Average Power Density
a	0.427
e	0.383
j	0.300
n	0.260
r	0.216

A similar procedure was employed for all the stationary elements. The control rod curves, however, were plotted up to 7 in. instead of 21.6 in., since only 7 in. extended into the active core.

B.4 CALCULATION OF CELL AVERAGE

The average power of element 12 was obtained by applying Simpson's 5-point rule to the above data across the element in a north-south direction. This gave a cell average of 0.313. However, the use of the Simpson formula is only an approximation; the use of graphical integrations produces a cell average of about 5% lower value. To compensate for the use of Simpson's approximation, all cell averages were multiplied by 0.946. These cell averages for all elements and control rods are given in Table B-2.

B. 5 CALCULATION OF CORE AVERAGE

The core average was obtained by weighting the cell average of each fuel element in the quadrant and dividing the sum of the weighted cell average by the weighting factor. The results, given in Table B-2, give a core average of 0. 459.

TABLE B-2
DATA FOR OBTAINING THE AVERAGE POWER OF THE SM-2 PRELIMINARY MOCKUP CORE

Element No.	Cell * Average	Weighting ** Factor	Weighted Cell Average	Fuel Element *** Averages Normalized to Core Average Equal to One (Relative Power)
12	0. 296	1	0. 296	0. 645
13	0. 373	1	0. 373	0. 812
14	0. 385	1/2	0. 192	0. 839
21	0. 267	1	0. 267	0. 581
22	0. 443	1	0. 443	0. 965
23	0. 548	1	0. 548	1. 193
31	0. 334	1	0. 334	0. 728
33	0. 587	1	0. 587	1. 278
34	0. 653	1/2	0. 326	1. 423
41	0. 376	1/2	0. 188	0. 818
42	0. 545	1/2	0. 272	1. 187
43	0. 621	1/2	0. 310	1. 353
Rod A	0. 948	1/2 x 0. 265	0. 126	0. 547
Rod F	0. 883	1 x 0. 265	0. 234	0. 509
Rod C	1. 177	1/4 x 0. 265	0. 078	0. 679
		9. 965	4. 574	

* Average foil activation in element obtained by a combination of Simpson's rule averaging and graphical integration.

** Symmetry factor for the elements in one core quadrant. For control rods, this value is reduced by the ratio of the volume of uranium in a control rod actually inserted in the active core (a depth of 7in.) to the volume of uranium in a stationary fuel element (length of 21. 6 in.).

$$\frac{V \text{ control rod}}{V \text{ fuel element}} = \frac{16 \text{ plates x } 2.32'' \text{ wide x } 0.03'' \text{ tk x } 7.0'' \text{ in active core}}{18 \text{ plates x } 2.52'' \text{ wide x } 0.03'' \text{ tk x } 21.6'' \text{ long}} = 0.265$$

*** The core average is obtained from the following:

$$\text{Core average} = \frac{\sum \text{Weighted cell averages}}{\sum \text{Weighting factor}} = \frac{4.574}{9.965} = 0.459$$

From this, the relative power of each element related to the core average is obtained by the following:

$$\text{Relative power of stationary element} = \frac{\text{cell average for stationary element}}{\text{core average}}$$

$$\text{Relative power of control rod} = \frac{\text{cell average for control rod x 0. 265}}{\text{core average}}$$

B. 6 NORMALIZATION OF DATA

Preliminary mockup data presented in this report have been normalized to this core average. Thus, for example, the activation data shown in Tables 3. 1 to 3. 15 are the raw data points divided by 0. 459 to permit intercomparison to a common reference.

Final mockup data presented in Tables 3. 16 to 3. 30 were normalized to a final mockup core average of 0. 432 obtained in a similar manner to that described in this Appendix.

THIS PAGE

WAS INTENTIONALLY

LEFT BLANK

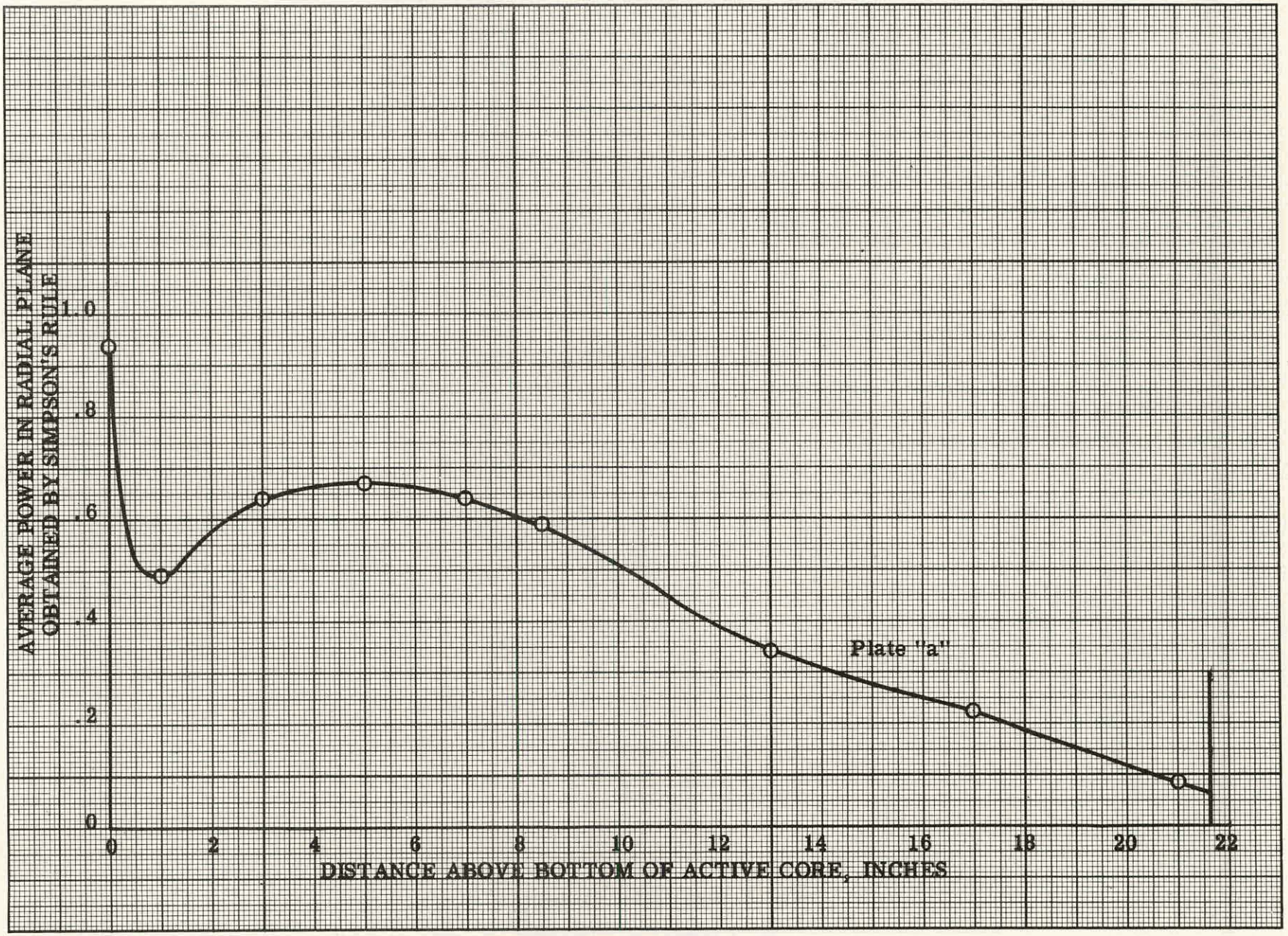

Figure B. 1 Relative Power Distribution of Average Radial Power For Plate "a", Element in Position 12

APPENDIX C

DETERMINATION OF B-10 CONTENT OF BORON TAPES

Table C. 1 lists the results of the B-10 determination obtained from reactivity measurements and from chemical analysis. The experiments and analysis were performed on two sets of boron impregnated Mylar tape, for reference: order one batch two (1-2), and order two batch one (2-1).

It should be noted that two separate chemical analyses were performed independently by Lucius Pitkin and by BMI.

TABLE C. 1
B-10 ANALYSIS

Method of B-10 Determination	B-10 Content Mg/cm^2 Tape (1-2)	Tape (2-1)
Reactivity measurements	0. 1578*	0. 0752**
Chemical Analysis Lucius Pitkin (1)	0. 1717	0. 0709
Chemical Analysis Lucius Pitkin (2)	0. 1591	0. 0574
Chemical Analysis BMI (1)	0. 1408	0. 0551
Chemical Analysis BMI (2)	0. 1417	0. 0559

* Average of 3 measurements
** Average of 9 measurements

It is apparent that no clear and definite result could be derived from the above measurements because of the large variation among them. Although results obtained from reactivity measurements are in close agreement among themselves, they differ considerably from those obtained by chemical analysis. The same is true for the BMI results; they are consistent among themselves but inconsistent with the others. The Lucius Pitkin results are neither consistent among themselves nor fully agree with the other two. The method of manufacture of the boron tape precludes such large discrepancies. The choice of the reactivity measurements as the basis for estimating the B-10 content of the SM-2 mockup core was made because of their reproducibility.